EXPERIMENTAL INVESTIGATION OF THE THERMAL PERFORMANCE OF VERTICAL AND ELBOW THERMOSYPHONS

EXPERIMENTAL INVESTIGATION OF THE THERMAL PERFORMANCE OF VERTICAL AND ELBOW THERMOSYPHONS

By MOHAMED HAMMOUDA, B.Sc.

A Thesis Submitted to the School of Graduate Studies in Partial Fulfilment of the Requirements for the Degree of Master of Applied Science in Mechanical Engineering

McMaster University M.A.Sc (2021) Hamilton, Ontario (Mechanical Engineering)

TITLE:	EXPERIMENTAL INVESTIGATION OF THE THERMAL PERFORMANCE OF VERTICAL AND ELBOW THERMOSYPHONS
AUTHOR:	Mohamed Hammouda, B.Sc.
SUPERVISOR:	Dr. Chan Y. Ching, Professor, Dept. of Mechanical Engineering
NUMBER OF PAGES:	103

Abstract

The thermal performance of two thermosyphons with different geometries was experimentally investigated in this study. The first thermosyphon utilized a 310 mm long vertical evaporator and a 385 mm long condenser section that was inclined at 5 degrees from the vertical. The second was an elbow configuration with a 140 mm long vertical evaporator and a 190 mm long condenser oriented 8 degrees from the horizontal. Both thermosyphons were made of internally grooved copper tubing with an outer diameter of 15.87 mm, wall thickness of 0.5 mm and a nominal groove height of 0.3 mm. Tests were performed over a range of input heat fluxes where the condenser was cooled by flowing water around the condenser with inlet temperature of 10°C, 20°C, and 35°C. The effects of incrementally increasing and decreasing heat flux was investigated for the elbow thermosyphon. Temperature measurements along the thermosyphon were taken when incrementally changing the heat flux from 0.5 to 11 W/m^2 for the first thermosyphon and 0.3 to 6 W/m^2 for the second thermosyphon.

Internal flow regimes were characterized using temperature transient profiles and compared to existing flow regime maps for closed thermosyphons suggested by Smith et al. (2018: Part a and Part b) and Terdoon et al. (1997). The temperature transients along the evaporator for the first thermosyphon settled to a more uniform profile as heat flux was increased. For the second thermosyphon the temperature profiles suggested a change to a more dynamic flow in the evaporator at heat flux of approximately 6 W/m^2. The elbow thermosyphon showed evidence of a significant hysteresis in the evaporator performance at moderate heat fluxes between 2 and 8 W/cm^2. Comparisons were made between the two thermosyphons to study the effects of inclination angle and the feasibility of angle corrections to the Nusselt film condensation model from Guichet and Jouhara

(2020). A modification to the Rohsenow condensation model from Guichet and Jouhara (2020) was recommended for the first thermosyphon showing good representation of the condenser performance. The evaporator performance results were compared to existing models from the literature.

Keywords: Thermosyphon; Evaporator; Condenser; Instabilities; Flow pattern

Acknowledgments

In the name of Allah, the Most Gracious and the Most Merciful, all praises to Allah for blessing me with patience, knowledge, and strength to complete this work.

I would like to express my deep and sincere gratitude to my supervisors Dr. Chan Ching and Dr. Daniel Ewing for giving me the opportunity to complete research under their supervision and providing me with invaluable guidance throughout the entirety of my of Masters. Thank you for your great amounts of assistance, motivation, and support. Your guidance helped me greatly in enhancing my knowledge in thermal management and helped improve my technical knowledge greatly.

Special thanks to Mohamed Hossam Zaher for your guidance and assistance with the experimental setups. My thanks to Nicole Mclean for helping me find this research opportunity. My thanks to the Mechanical Engineering staff, Mark Mackenzie, Rob Sluban, John Colenbrander, Justin Bernar, and Michael Lee. Your tips and support have helped me greatly in my experimental research.

I would like to express my warm thanks to my lab mates, Mohamed Abdelnabi, Saksham Gupta, Ahmed Ali Mahmoud, Saber Mohamed, Mohamed Fathalla, and Mahmoud Abdelfattah, you made my masters experience a memorable time filled with laughs and joy. My special thanks to my close colleagues Mohamed Abdelnabi and Sakhsam Gupta for endless motivation and support through the busiest schedules.

Finally, I would like to give my sincere thanks to my fiancé Leenah Abu Obeid for keeping me focused and motivated for the entirety of my research. You helped me greatly over the years, and I can’t express how glad I am that you are part of my life.

Table of Contents

List of Figures

List of Tables

Chapter 1: Introduction

Heat pipes are highly effective two-phase heat transport devices capable of transporting heat between two different temperature regions with buoyancy effects and gravity as the main driving force [7][8]. Over the years, many different types of heat pipes have been developed that are classified by their geometry. These include the conventional thermosyphons and wicked or grooved heat pipes, rotating or revolving heat pipes [7], capillary pumped loops and looped heat pipes [7], and oscillating heat pipes [8][9] as shown in Figure 1.1. The focus here is on thermosyphons which have the advantage of operating without the need of an internal wicked surface or pump which simplifies the construction and lowers the overall cost [7]. A typical thermosyphon is a straight closed long pipe partially filled with a working fluid. Thermosyphons are made up of three main sections; the section at the hotter region (the evaporator), the section at the colder region (the condenser) and the mid-section joining the two (the adiabatic section). During operation, heat from the evaporator is transferred into the working fluid that boils or evaporates into vapour. The vapour flows upwards in the direction of the colder region by buoyancy forces and is condensed back into liquid form. From the condenser section, the fluid returns to the evaporator section as liquid droplets or a liquid film by gravity. Gravity being the main driving force, the operation restricts the use of thermosyphons to where the condenser section is located at a higher elevation than the evaporator section.

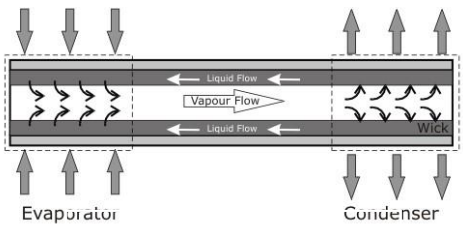

a) Wicked heat pipe

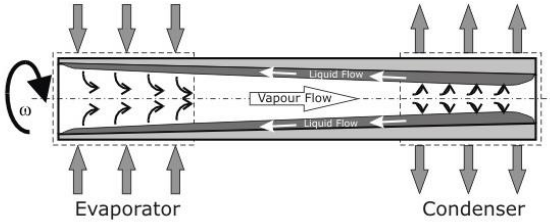

b) Rotating heat pipe

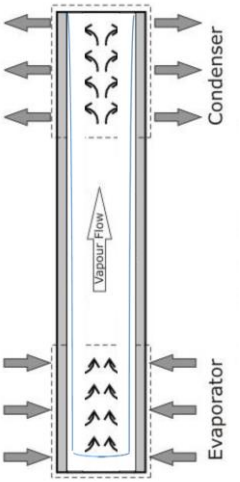

c) Thermosyphon

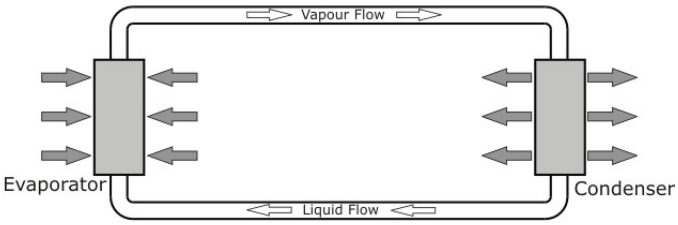

d) Capillary loop heat

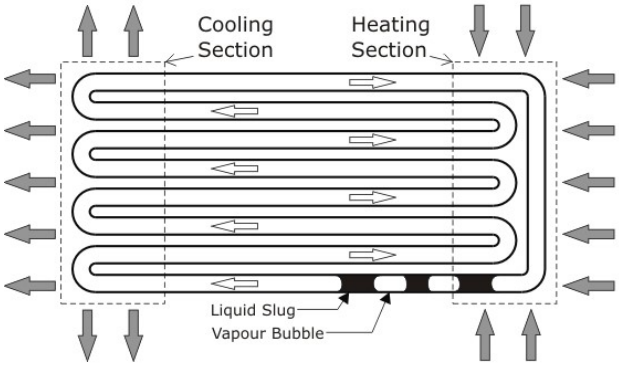

e) Oscillating heat

Figure 1.1 Schematic of different heat pipe configurations

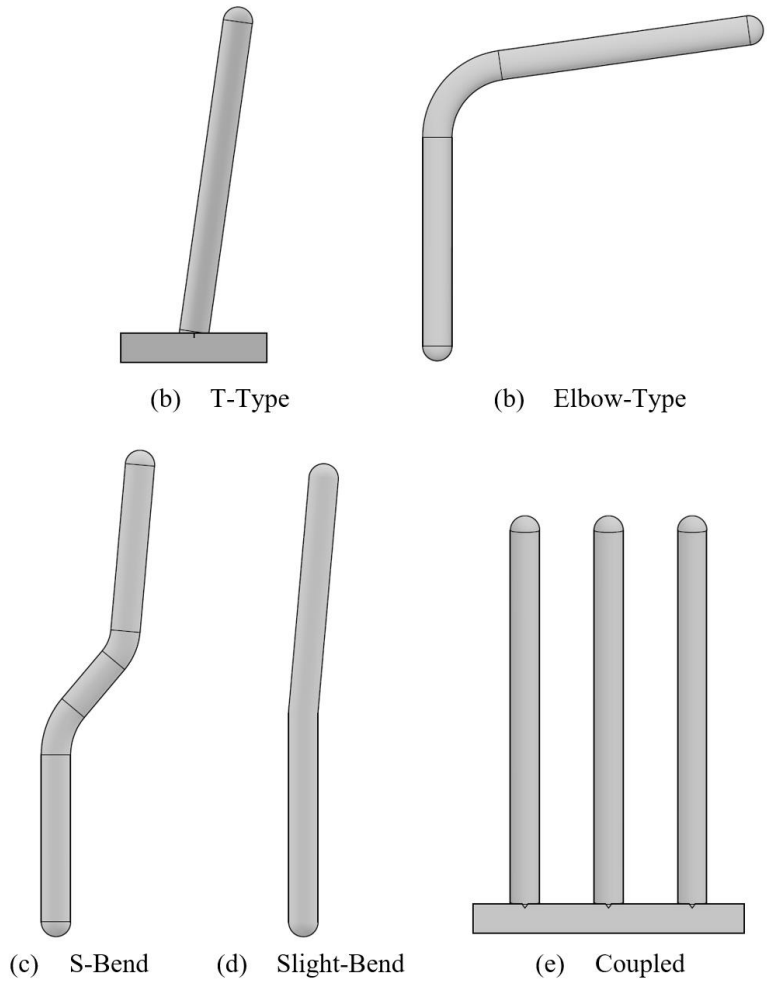

Figure 1.2 Non-linear thermosyphon configurations

The thermosyphons considered here are all closed-type thermosyphons allowing for fluid containment. In addition to the basic layout of a typical thermosyphon having the evaporator and condenser in a straight geometry, the orientation of the thermosyphon can be inclined. Negishi & Sawada [9] investigated the effects on the performance of varying condenser inclinations. Several thermosyphon geometries have been investigated to fit applications where a straight thermosyphon would not be feasible due to geometric constraints. For example, there are a number of applications that require the condenser and evaporator to be oriented at different inclinations. Different geometric shapes are shown in Figure 1.2, where only the condenser is inclined to keep the

evaporator straight (Figure 1.2d) having the evaporator and condenser oriented perpendicular to one another (Figure 1.2a), and others to have the condenser shifted away from the evaporator (Figure 1.2c)

Thermosyphons have been deployed to a wide variety of applications from stabilizing permafrost in the ground [10], and to remove excess heat from electronics [11]. Of the many applications, those of which have been previously investigated in literature include: thermoelectric devices (Kolenko and Verdiev [12]); internal cooling of gas turbine blades (Cohen and Bayley [13]), cooling of electric motor rotors (Finlay [14]), and cooling electric circuits (Larkin 1973[15]).

The objective of this thesis focuses on atypical thermosyphons used for electronic cooling. The investigation was completed on the performance of non-straight thermosyphons with two distinct geometries used for thermal management of high-power electronics mounted as a vertical heating source. Both thermosyphons utilize a vertical evaporator with the first thermosyphon having a condenser inclined at a shallow angle similar to (Figure 1.2d). The second thermosyphon utilizes a condenser inclined almost perpendicular to the evaporator as seen in Figure 1.2b.

1.1 Scope of this thesis

The motivation for this thesis stems from our collaboration with our industrial partner, MERSEN Canada Inc., which is a global provider, designer, and manufacturer of thermal management solutions for high-power electrical systems. Thermosyphons are one of the key components in the thermal management solutions provided by MERSEN. It typically consisting of heat spreader plates mounted to the heat source (power electronics), thermosyphons that transport the heat, and a heat exchanger mounted at the condenser to reject the heat to the ambient. MERSEN

uses many non-traditional geometrical designs as a result of the constraints and requirements of the application. These include elbow, S-shaped, and T-shaped thermosyphons as shown in

Figure 1.2. These non-traditional geometries have been less studied. In addition, many of MERSEN's applications employ high heat flux to be transported and/or operating under extreme environmental conditions. Thus, characterizing and predicting the performance and instabilities of these thermosyphons under variable operating conditions are crucial in the design of these systems.

The objective of this thesis is to investigate the performance of two thermosyphons with different geometries. The thermosyphons studied here are: (i) a vertical evaporator and condenser oriented at 5 degrees from the vertical also referred to as a slight bend thermosyphon and (ii) a vertical evaporator with the condenser oriented 8 degrees from the horizontal and commonly referred to as an elbow thermosyphon. The internal surface of both thermosyphons were grooved with a groove height of 0.3mm. Water was used as the working fluid and the fill ratios were 35% for the slight bend thermosyphon and 30% for the elbow thermosyphon. Fill ratio defined as ratio of working fluid to volume of evaporator. The specific objectives of these investigations were to examine: (i) evaporator heat transfer performance, (ii) evaporator two phase flow regimes, and (iii) condenser performance. The performance is characterized by examining the temperature transients and heat flux along the heating length. The experiments were performed for different cooling water temperatures that was circulated around the condenser section.

This study is presented as a sandwich thesis consisting of two publications that is preceded by an overview of the literature pertaining to this study. Each publication also contains a brief review of the literature to the study in addition to the general overview presented in this study. As such, there is some repetition although this has been minimized. In this thesis, the study of the

slight bend thermosyphon is presented in Chapter 3. This has been published in the International Journal of Thermofluids (https://doi.org/10.1016/j.ijft.2021.100107). The study of the elbow thermosyphon is presented in Chapter 4. This has been submitted to Thermal Science and Engineering Progress. Finally, the conclusions from this thesis are presented in Chapter 5, which includes recommendations for future studies.

1.2 References

[1] Smith K, Kempers R, Robinson AJ. Confinement and vapour production rate influences in closed two-phase reflux thermosyphons Part A: flow regimes. Int. J. Heat and Mass Transfer, 2018;119:907-21.

[2] Smith K, Robinson AJ, Kempers R. Confinement and vapour production rate influences in closed two-phase reflux thermosyphons Part B: Heat transfer. International Journal of Heat and Mass Transfer. 2018 May 1;120:1241-54.

[3] Terdtoon P, Chailungkar M, Ritthidej S, Shiraishi M. (1997) Effects of Bond numbers on internal flow patterns of an inclined, closed, two-phase thermosyphon at normal operating conditions, Experimental Heat Transfer, 1997, 10:4, 233-251.

[4] Guichet V, Jouhara H, Condensation, evaporation and boiling of falling films in wickless heat pipes (Two-phase closed thermosyphons): A critical review of correlations, Int. Journal of Thermofluids, 2020 (1-2) 100001.

[5] Rohsenow WM. A method of correlating heat transfer data for surface boiling of liquids. Cambridge, Mass. MIT Division of Industrial Cooperation, 1951.

[6] Kim Y, Shin DH, Kim JS, You SM, Lee J, Boiling and condensation heat transfer of inclined two-phase closed thermosyphon with various filling ratios, Applied Thermal Engineering, 2018 (145) 328-342.

[7] Faghri, A. (1995) *Heat pipe science and technology*, Taylor & Francis, Washington, DC.

[8] Peterson, G. P. (1994) *An introduction to heat pipes*, John Wiley & Sons,Inc.,New York.

[9] Negishi, K, Sawada, T. (1983) Heat transfer performance of an inclined two-phase closed thermosyphon, *International Journal of Heat and Mass Transfer*, **26**, 1207 – 1213.

[10] Wagner AM. Review of thermosyphon applications.

[11] Smith, K. Siedel, S. Robinson, A. J., Kempers, R. (2016) The effect of bend angle and filling ration on the performance of a naturally aspirated thermosyphon, *Applied Thermal Engineering*, **101**, 455-467.

[12] Kolenko EA, Verdiev MG. Utilization of thermosiphon in thermoelectric devices. Appl. Solar Energy (USSR)(Engl. Transl.);(United States). 1973 Jan 1;9(1).

[13] Cohen H, Bayley FJ. Heat-transfer problems of liquid-cooled gas-turbine blades. Proceedings of the Institution of Mechanical Engineers. 1955 Jun;169(1):1063-80.

[14] Finlay IC. Heat pipes and two-phase thermo-syphons. I. Mech. Eng. 1975 Mar:59-63.

[15] Larkin B.S. A computer cooling application for thermosyphons. Engineering Journal. 1973 Jan: 30-33

Chapter 2: Literature Review

The previous literature on the performance of thermosyphons is reviewed in this chapter. This review provides a broad overview while more focussed reviews pertinent to this study are provided in each of the manuscripts that are presented in Chapters 3 and 4. The performance of thermosyphons with varying geometries are discussed first, followed by the flow patterns in the evaporator and how it affects the heat transfer characteristics. The evaporator and condenser performance and predictive methods are presented along with limitations. Methods for improving the performance of thermosyphons are finally discussed.

2.1 Thermosyphon Geometry

The performance of a thermosyphon is typically characterized by the maximum heat transfer rate that can pass through the device and the temperature drop over the device for a given heat flux. Inclining a thermosyphon can reduce the thermal resistance of the device or enhance its heat transfer for a given temperature difference. Hahne & Gross [1] and Negishi & Sawada [2] found optimal inclination angles of 20 to 40 degrees from the horizontal for refrigerant and water with fill ratios of 40 to 50 percent. The inclination had more effect when the fluid charge was smaller with optimal inclination increasing as the fill ratio decreased for small fluid loading [2].

The performance of a thermosyphon is typically characterized by the maximum heat transfer rate through the device and thermal resistance or the temperature drop over the device for a given heat flux. In many instances, the geometry of the thermosyphon must be modified from a straight layout to accommodate system and environmental constraints. The performance of such

thermosyphons has received less attention than straight thermosyphons. Inclining a thermosyphon from the vertical can reduce the thermal resistance of the device or enhance its heat transfer for a given temperature difference. Hahne & Gross [1] and Negishi & Sawada [2] found optimal inclination angles of 20 to 40 degrees from the horizontal for refrigerant and water with fill ratios of 40 to 50 percent. The inclination had more effect when the fluid charge was smaller with optimal inclination increasing as the filling ratio decreased for small fluid loading [2].

Lock & Fu [3] investigated the performance of a smooth-walled 90-degree elbow thermosyphon oriented with a vertical evaporator and a horizontal condenser as well as horizontal evaporator and vertical condenser. The results revealed the performance of the vertical evaporator and horizontal condenser performed better of the two, though neither performed as well as a straight vertical thermosyphon with similar specifications. The thermosyphon oriented with the vertical evaporator failed due to flooding while the other orientation failed due to dry-out. Fu [4] investigated elbow thermosyphons oriented at varying inclinations. The optimal operation for a condenser was when orienting the evaporator at 30 degrees to the horizontal. The optimal performance for a horizontal evaporator was with a condenser oriented at 30 degrees from the horizontal. Fu [4] also found that varying the condenser length had very little impact on performance while varying the evaporator length had a large impact with a length of 10D yielding poor performance.

Jouhara et al. [5] investigated the heat transfer performance of a thermosyphon with a condenser oriented 12 degrees from the evaporator with the evaporator orientation varying from horizontal to vertical. Water and azeotrope were used as the working fluid. They observed little change in the thermal resistance of the thermosyphon for evaporator inclination angles set at 15

degrees to 90 degrees from the horizontal. However, the thermal resistance of the device was lower when positioned horizontally at low heat flux.

Smith et al. [6] experimentally investigated the effects of varying the evaporator inclination as well as the influence of the bend angle at the adiabatic section, while keeping the condenser vertical. The evaporator orientation was varied from vertical to horizontal (90 degrees to the condenser) in increments of 30 degrees. The temperature transients were used to determine the heat transfer characteristics. With the evaporator vertical as a straight thermosyphon, there was an unfavourable oscillatory behaviour due to the restrictions imposed by the confinement. The addition of a bend in the adiabatic section was found to mitigate these flow oscillations. It was found that failure occurring at low fill volumes could be delayed with bend angles of 30 and 60 degrees. The bend acted as a guide for the return of condensed liquid to cover more surface area effectively and help cool the heater surface under the assistance of gravity. Bend angles of 30 and 60 degrees were also found to lower thermal resistance, improve the maximum power, and result in a steadier operation at low heat flux. A 90-degree bend resulted in higher thermal resistance and failure at lower heat flux. The resistance of the overall thermosyphon appeared independent of the inclination angle of the evaporator except for near failure, where inclination played a significant role.

2.2 Flow regimes

The heat transfer performance within a two-phase thermosyphon is subject to the change in internal flow pattern that can depend on different parameters such as inner diameter, length the of tube, inclination angle, fill ratio, evaporator temperature, type of working fluid, and heat flux [7]. Internal flow patterns have been the subject of many studies, but little has been presented for

thermosyphons with variable geometry. The typical internal flow patterns reported for a vertical evaporator consist of geyser flow, bubbly flow, slug/plug flow, churn flow, and annular flow [9][10][11][12]. An illustration of the flow patterns is presented in Figure 2.1 from [13]. These flow patterns are further described below.

Geyser flow: The flow can be visualized as a large slug of bubbles or coalesced bubble cluster that is gradually formed at the heating section or evaporator and can grow to a similar size of the inner diameter of the thermosyphon. The bubble is suppressed by the upper liquid column. When the disturbance of the interface is greater than the tolerance of the interface, an abrupt vapor eruption would occur until the interface of the vapour and liquid ruptures. This results in the liquid column above the vapour being propelled from evaporator to the condenser. Geyser flow also referred to as intermittent boiling is induced by the interaction between the buoyancy of the vapor bubble and the flow resistance. This usually occurs when the heat input is insufficient to sustain continuous and stable boiling [14][15].

Bubbly flow: Characterized by the development of small bubbles compared to the inner diameter of the thermosyphon relatively similar in size. Occurs at very low liquid and gas velocities. [3][7] [12].

Slug flow: Characterized as bubbles that coalesce into slugs or large vapour bubbles that could span the entire diameter of the thermosyphon. [3][7][12].

Churn flow: Occurs when the continuity of the liquid in the slug between successive Taylor bubbles is constantly disturbed by high local gas concentration in the slug [17]. Increasing the velocity of the slug causes the structure of the flow regime to become unstable. Due to its chaotic nature, its properties are still difficult to understand [18].

Annular flow: When the gas velocity has increased further from churn flow, leading to the gas becoming a continuous phase in the evaporator. The liquid phase is localized on the walls of the thermosyphon as a thin-film adhering to the pipe wall and partly in the form of dispersed droplets in the gas flow as mist. [17]

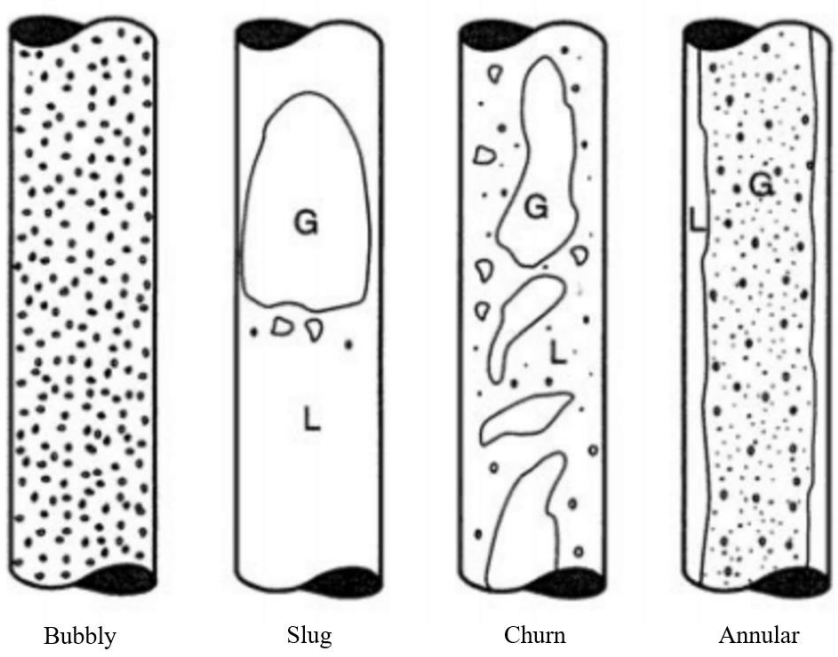

Figure 2.1 Illustration of internal thermosyphon flow regimes from Two-phase flow patterns from [13].

Terdtoon et al. [12] visualized the flow patterns in a straight thermosyphon utilizing a copper condenser and a glass evaporator that was joined at the adiabatic section using a soft O-ring to prevent any leakage. The effect of the Bond number and inclination on the internal flow patterns was documented. A flow pattern map based on the visualizations was developed in terms of the modified Kutateladze number and Reynolds number of vapor as shown in Figure 2.2. The modified

Kutateladze number was stated as $ku^* = ku\frac{d}{Le}\frac{\rho_v}{\rho_l}$ [12]. Grooten et al. [19] investigated the effects of inclination angle on heat transfer characteristics by visualizing the internal flow patterns using a 290 mm long glass thermosyphon. Acetone was used as the working fluid with a filling ratio of 80 percent. Plug flow, classified as a large vapour bubble originating from the middle of the evaporator that rose and disintegrated at the vapour and liquid interface, was observed at all inclinations from 0 to 80 degrees from the vertical for low heat flux below 14 kW/m^2. At higher heat fluxes, pool boiling was observed with fluid returning as annular flow coating the full circumference of the interior wall. The pool boiling at high heat flux was in agreement with the results of Terdoon et al. [12], but the latter did not observe plug flow at low heat flux [19]. A wavy structure was also found in the annular condensate film return [19].

Jouhara et al. [5] investigated the flow patterns in a smooth-walled 1.5 m long copper thermosyphon with an outer diameter of 22 mm and wall thickness of 0.9 mm. Geyser boiling was observed with water as the working fluid at moderate heat fluxes (approximately 0.23 W/cm^2) when the evaporator was positioned vertically. The same was not observed when azeotrope was used as the working fluid. Analyzing the temperatures collected from the wall of the thermosyphon evaporator suggested a pool boiling region and a film evaporation region at moderate heat flux, with the temperatures in the pool region reaching higher values than the film evaporation region. The temperature difference was not present when the thermosyphon was oriented vertically at high heat flux or when oriented horizontally at moderate and high heat flux. There was no temperature difference at either orientation when azeotrope was used as the working fluid.

Smith et al. [6] investigated the heat transfer characteristics of an elbow thermosyphon with the condenser positioned vertically. The internal flow patterns were inferred from the temperature traces collected from the evaporator wall over a period. At low heat flux, there was evidence of

geyser boiling that was reduced by lowering the fill volume or inclining the evaporator. There was also evidence of high oscillations in the evaporator wall temperature suggesting unsteady flooding and droplet entrainment affecting the liquid return to the evaporator. Smith et al 2018 [10][11] used a transparent sapphire thermosyphon to observe the influence of varying the confinement number. Confinement traditionally represents the ratio of the capillary length of the fluid and the channel hydraulic diameter [20]. The advantage of sapphire is it has a comparable thermal conductivity to metals. The main drawback of using materials such as sapphire and glass tubes in the evaporator section is a reduction in nucleation sites as a result of different surface texture. This would highly affect the repeatability of the results for exact same testing conditions but with a copper tube instead. The confinement number was varied by using different working fluids: water, ethanol and HFE-700 developing a new flow regime map in terms of degree of confinement and rate of vapour production [10] shown in Figure 2.3. In part b [11] a flow regime map based on superficial momentum flux was suggested and is shown in Figure 2.4. The tested conditions were found to be under a gravity force dominant regime, leading the two-phase flow behaviour to be very sensitive to confinement effects, as noted by Di Marco [21]. Results for unconfined thermosyphons at low heat fluxes, the conventional nucleate boiling with falling film condensation was noted. Increasing the heat flux resulted in higher vapour production rates and the flow transitioned to a churn type flow. When considering a high confinement and low vapour production, the flow was established as slug/plug flow, and increasing the vapour production rate to relatively high, the flow regime transitions to slug/plug flow. Results using water and ethanol as the working fluid operating a low pressure fell under geyser flow. Keeping the operating conditions of the thermosyphon in churn or bubbly regime allowed for the most stable performance while having a higher heat transfer coefficient.

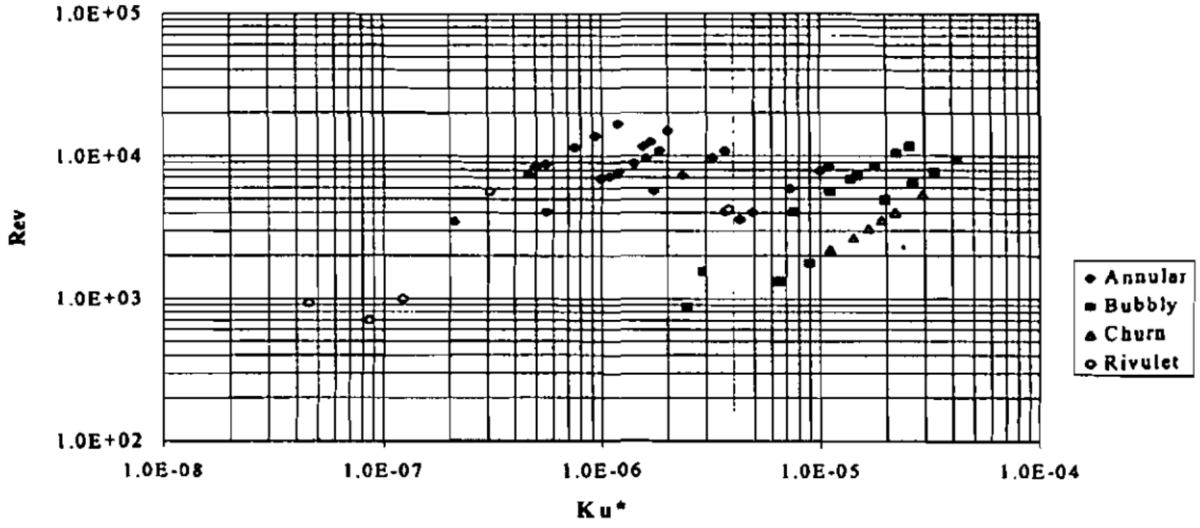

Figure 2.2 Terdoon et al flow regime map with vertical evaporator [12]

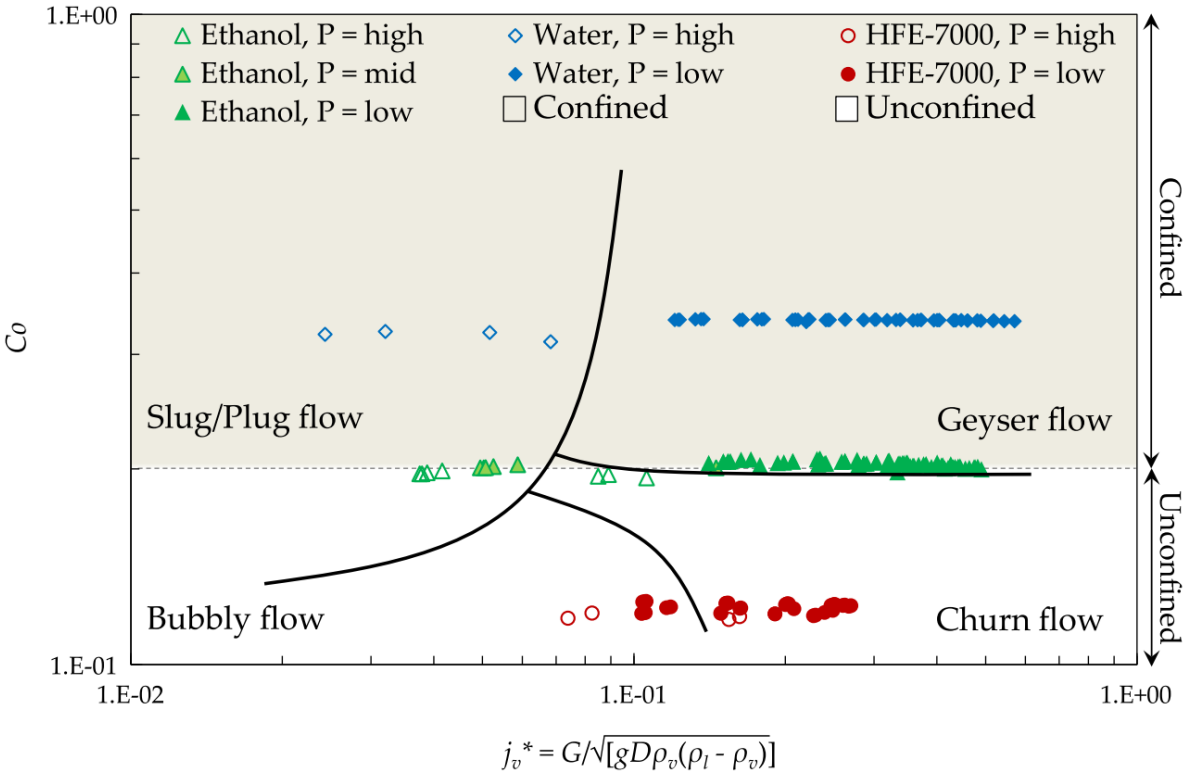

Figure 2.3 Confinement and rate of vapour production of each fluid investigation suggested by Smith et al. [10].

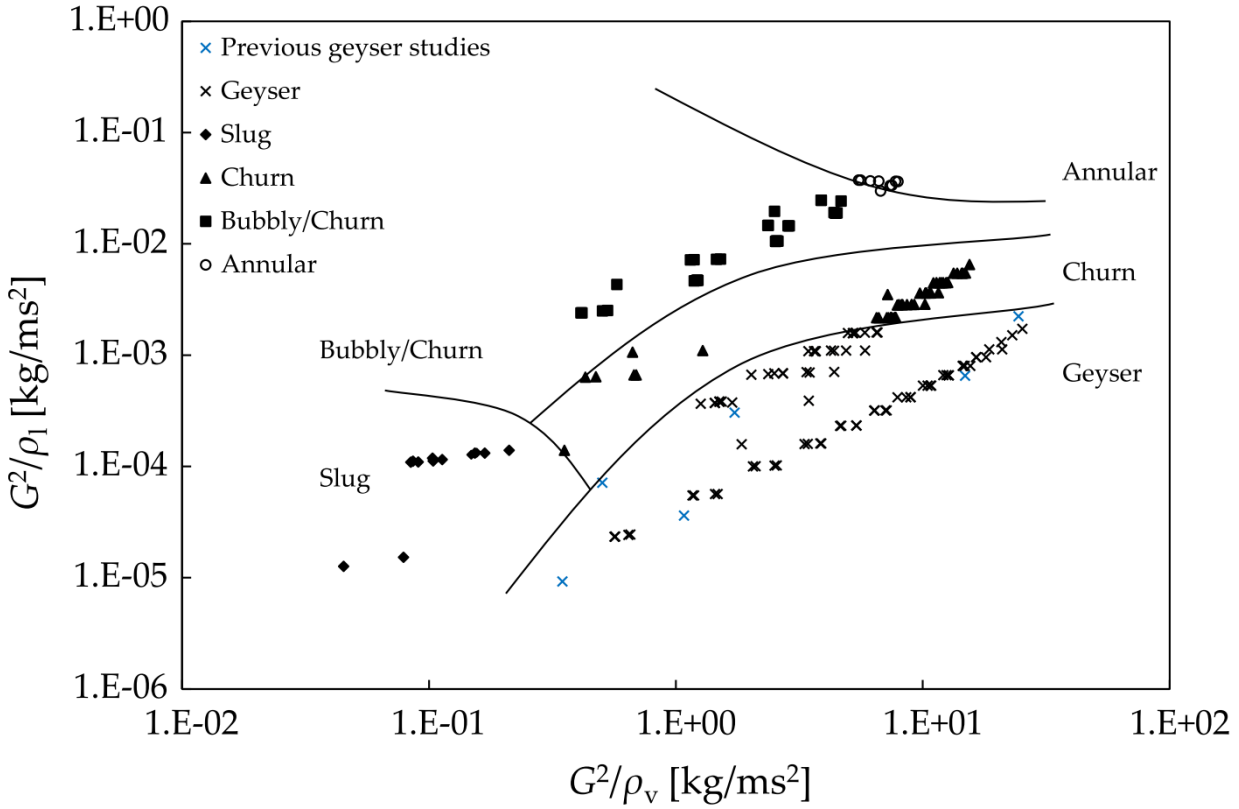

Figure 2.4 Superficial momentum flux flow regime map suggested by Smith et al. [11].

2.3 Evaporator performance

The performance of the evaporator section can be determined by analysing the mean temperature transients along the heating length. The thermal resistance in the evaporator can be modeled as either pool boiling or film evaporation depending on the fluid loading. The performance is often characterized using nucleate pool boiling models as suggested by Rohsenow [22] or using models developed from previous thermosyphon investigations recommended by Imura et al. [23], Padovan et al. [24]and El Genk & Saber [25].

Shiraishi et al. [27] investigated the evaporator and condenser performance of a 1230 mm long straight closed thermosyphon with a 37 mm inner diameter. The two-phase boiling in a closed thermosyphon is considered similar to an open thermosyphon, but at modified operating pressure [27]. Generally, the former operates at reduced pressure while the latter occurs at atmospheric. Thus, the heat transfer process is thought to be the same as that which occurs in an open thermosyphon with a pressure factor added given by: h_p (closed)∝h_p (open).(P/P_Δ)^n [22]. The experimental results taken for this thesis are completed using a closed thermosyphon under reduced pressure. Within the evaporator the heat transfer in the liquid pool and liquid film were considered separately taking into account the flow regime of the liquid film along with the pool section. A flow visualization study completed by Andros and Florschuestz [27] reported four flow regimes: smooth continuous film with surface evaporation, the breakdown of smooth continuous film into series of stable rivulets, a wavy film with unstable rivulets, and a wavy film with bubble nucleation occurring in the unstable rivulets [27].

It is widely accepted that a single or set of correlations is not capable of predicting the boiling heat transfer coefficients in all thermosyphon variants. Jouhara and Robinson [28] compared correlations developed specifically for pool boiling in thermosyphons with correlations that included adjustable constants that depend on the nature of the surface-fluid combination. Correlations were compared to experimental results from a closed 200 mm straight thermosyphon constructed from a 12mm diameter rod with an inner diameter drilled to 6 mm. The working fluids used were water, FC-84, FC-77, and FC-3283. Experimental results were calculated as a single system using the entire length of the evaporator as a result of the transitioning internal flow patterns. The results showed the pool boiling and combined pool boiling and thin-film evaporation correlations provided good predictions. The best agreement was from Labuntsov [29], Rohsenow

[22], and Stephan and Abdelsalam [30] at high thermal resistance, while Kutateladze [31] showed better agreement at lower thermal resistance values. The correlations of Imura et al. [23], and Shiraishi et al. [26] that are thermosyphon based are comparable, but underpredict the experimental values for low resistance or high heat flux cases [29].

2.4 Condenser performance

At startup, the condensation of the vapour in the condenser starts as drop-wise condensation. Eventually, the entire inner wall is covered by a thin liquid film which flows downward by gravity and returns to the evaporator [28]. By assuming the condensate film flow as laminar and the film very thin with respect to the radius of curvature, the condensation heat transfer can be modeled as film condensation on a vertical plate. When the condenser is positioned vertically and with a smooth inner surface, the condensate film is one-dimensional. With small Reynolds number the film flow is also laminar with a vapour side interface. Heat is thought to be transferred by pure conduction across the film, which is subcooled [27]. When the condenser is inclined, the liquid flow field becomes two-dimensional resulting in the streamlines forming curved paths. Rohsenow modified the Nusselt condensing falling film [29] by incorporating a subcooled correction. Hussein et al. [30] and Gross [27] suggested an angle correction to compensate for the variation when considering two-dimensional liquid return. Wang and Ma [31] added a pressure correction as well as an angle correction to the Nusselt model. Guichet and Jouhara[29] provided a critical review of correlations for heat transfer through falling film condensation. Considering previous studies [32][25] using water-filled thermosyphons, Nusselt film condensation model was found to overpredict the heat transfer coefficient at low Reynolds number.

2.5 Limits

The performance of thermosyphons is typically characterized by the heat transfer and thermal transients or temperature profile of the evaporator and condenser region. There are several factors that can contribute to limit the maximum heat flux through a thermosyphon. These include, but are not limited to: (i) dryout limit in the evaporator at low fluid loading, (ii) entrainment or flooding limit which considers the interaction between vapour and liquid, (iii) boiling limit occurring in the film region of the evaporator, (iv) intermittent or geyser limit, and (v) condenser limit or restriction on external heat transfer.

Dry out limit: Occurs as a result of insufficient fluid in the evaporator to sustain steady operation. The cause can be by different operating conditions. Dry out occurs when there is insufficient fluid loading to allow for continuous flow of liquid film returning from the condenser to the evaporator due to the increase in volume of the return film. This can be avoided by ensuring the thermosyphon is initially filled with sufficient working fluid. A method used to predict the required filling ratio of working fluid for smooth thermosyphons was proposed by Shiraishi et al. [33] using modified Cohen and Baley [39] mode to predict maximum heat flux during operation. Nusselt film models were also previously used to determine the maximum fluid loading required given the heat transfer rate [7][37].

Entrainment or flooding limit: Occurs from the interaction between the vapour flow restricting the return of the liquid film from the condenser due to high interfacial shear stresses. This is found to occur with moderate fluid loading levels or when analysis shows the fluid loading is sufficient to support higher heat fluxes. The Wallis [40] model or Kutateladze number is often used to predict flooding [41][42][43]. The Kutateladze number represents the ratio of inertial force to hydrostatic force on a bubble [44].

Boiling limit: With a combination of high flux and high fluid loadings, the boiling in the evaporator can transition from pooling to film boiling. This would lead to lower heat transfer rates and large evaporator temperature. The critical heat flux for smooth walled thermosyphons can be estimated by the model suggested by Grorbis and Savchenkov [45]. The model related the heat flux to the onset of film boiling for a finite diameter thermosyphon [7].

Geyser boiling limit: Occurs when heat flux at the evaporator is insufficient to sustain continuous boiling. Geyser boiling is characterized by relatively large temperature oscillations in the evaporator and condenser. This is found to occur more frequently at higher fill ratios and low operating pressures. Geyser boiling does not necessarily result in a limitation to the performance, but results in high fluctuations in temperature and pressure that could result in damage to the thermosyphon, particularly the condenser end cap as a result of the impact of rising vapor slugs. A method to predict the onset of geyser boiling for water and ethanol was suggested by Lin et al. [46], but is not particularly generalized. Casarosa et al. [48] discussed correlations for heat transfer coefficient during geyser boiling. The effect of geyser boiling can be reduced by an inclination angle of the thermosyphon or inclining towards horizontal orientation. This would allow the vapour slugs to be disrupted by the thermosyphon walls [2][48].

Condenser limit: When the performance or maximum heat flux of the thermosyphon is limited by the ability of the condenser to reject the heat to the colder region. This is essentially a thermal resistance limit but is often referred to the condenser limit.

2.6 Methods to Improve Performance

Several methods that could be considered to enhance the performance of the thermosyphon by either reducing the thermal resistance or by mitigating the failure points or limits. Some of the method include, grooved or textured inner wall surface, the addition of nanofluid or nanoparticles, hydrophobic surfaces to avoid film condensation in favour of dropwise, and hydrophilic surface to promote film evaporation in the heated section.

Grooves or textured surface added to the inner walls of a thermosyphons have multiple benefits including increasing the surface area in contact with the working fluid, improving the heat transfer and reducing the effects of flooding [7]. The performance of grooved thermosyphons typical of those included in the thesis were investigated by Park et al. [49] for a straight thermosyphon with FC-72 as the working fluid and by Han and Cho [50] for straight and spiral grooved thermosyphons with water as the working fluid. Both investigations found grooves to decrease the thermal resistance in the condenser. Park et al. [49] also found increasing the filling ratio reduced the thermal resistance. Han and Cho [50] found the optimal inclination angle for helical grooves to be 25 to 30 degrees and for straight grooves to be 40 degrees with a fill ratio of 30 percent of the evaporator. For vertical thermosyphon the optimal fill ratio was 20 percent.

The use of nanofluids was shown to improve the thermal performance of thermosyphons, primarily in the evaporator section. Nanoparticles increased the thermal conductivity of the working fluid and improved the boiling heat transfer. However, there were also a number of unresolved issues with the use of nanofluids that affect the long-term stability and performance. Liu et al. [51] investigated the effects of using CuO nanoparticles with a nominal diameter of 50 μm in water for a grooved thermosyphon. Macgregor et al. [52] recommends the addition of 5% ethylene glycol in water to be used as the working fluid as results reported more consistent

performance at varying heat flux and ambient temperature while still providing similar heat transfer performance as water only.

2.7 References

[1] Hahne E, Gross U. The influence of the inclination angle on the performance of a closed two-phase thermosyphon. InAdvances in Heat Pipe Technology 1982 Jan 1 (pp. 125-136). Pergamon.

[2] Negishi, K, Sawada, T. (1983) Heat transfer performance of an inclined two-phase closed thermosyphon, *International Journal of Heat and Mass Transfer*, **26**, 1207 – 1213.

[3] Lock, G. S. H. and Fu, J. (1993) Observations of an evaporative elbow thermosyphon, Journal of Heat Transfer, 115, 501-503.

[4] Fu J. The elbow thermosyphon: an experimental investigation of its evaporative behavior.

[5] Jouhara H, Ajji Z, Koudsi Y, Ezzuddin H, Mousa N. Experimental investigation of an inclined-condenser wickless heat pipe charged with water and an ethanol–water azeotropic mixture. Energy. 2013 Nov 1;61:139-47.

[6] Smith, K. Siedel, S. Robinson, A. J., Kempers, R. (2016) The effect of bend angle and filling ration on the performance of a naturally aspirated thermosyphon, *Applied Thermal Engineering*, **101**, 455-467.

[7] Faghri, A. (1995) *Heat pipe science and technology*, Taylor & Francis, Washington, DC.

[8] Peterson, G. P. (1994) *An introduction to heat pipes*, John Wiley & Sons,Inc.,New York.

[9] Sichamnan S, Chompookham T, Parametthanuwat T. A case study on internal flow patterns of the two-phase closed thermosyphon (TPCT). Case Studies in Thermal Engineering. 2020 Apr 1;18:100586.

[10] Smith K, Kempers R, Robinson AJ. Confinement and vapour production rate influences in closed two-phase reflux thermosyphons Part A: flow regimes. Int. J. Heat and Mass Transfer, 2018;119:907-21.

[11] Smith K, Robinson AJ, Kempers R. Confinement and vapour production rate influences in closed two-phase reflux thermosyphons Part B: Heat transfer. International Journal of Heat and Mass Transfer. 2018 May 1;120:1241-54.

[12] Terdtoon P, Chailungkar M, Ritthidej S, Shiraishi M. (1997) Effects of Bond numbers on internal flow patterns of an inclined, closed, two-phase thermosyphon at normal operating conditions, Experimental Heat Transfer, 1997, 10:4, 233-251.

[13] Cheremisinoff NP, Gupta R. Handbook of fluids in motion.

[14] Liu Y, Li Z, Li Y, Kim S, Jiang Y. Experimental investigation of geyser boiling in a two-phase closed loop thermosyphon with high filling ratios. International Journal of Heat and Mass Transfer. 2018 Dec 1;127:857-69.

[15] Chen J, Yang S, Liao S, Cao X. Experimental investigation of effective parameters on geyser periodicity in a vertical heated system. Experimental Thermal and Fluid Science. 2015 Nov 1;68:163-76.

[16] Carey VP. Liquid-vapor phase-change phenomena: an introduction to the thermophysics of vaporization and condensation processes in heat transfer equipment. CRC Press; 2018 Aug 15.

[17] Mokhatab S, Poe WA. Handbook of natural gas transmission and processing. Gulf professional publishing; 2012 Aug 8.

[18] Cheremisinoff NP, Gupta R. Handbook of fluids in motion.

[19] Grooten MH, Van der Geld CW, Van Deurzen LG, Butrymowicz D. A study of flow patterns in a thermosyphon for compact heat exchanger applications. InProc. 5th Int. Conf. on Transport Phenomena in Multiphase Systems, HEAT 2008 (Vol. 2, pp. 323-328).

[20] Kew PA, Cornwell K. Correlations for the prediction of boiling heat transfer in small-diameter channels. Applied thermal engineering. 1997 Aug 1;17(8-10):705-15.

[21] Di Marco P. Influence of force fields and flow patterns on boiling heat transfer performance: a review. Journal of heat transfer. 2012 Mar 1;134(3).

[22] Rohsenow WM. A method of correlating heat transfer data for surface boiling of liquids. Cambridge, Mass. MIT Division of Industrial Cooperation, 1951.

[23] Imura H, Kusuda H, Ogata J-I, Miyazaki T, Sakamoto N. Heat transfer in two-phase closed-type thermosyphons, Japan Society of Mechanical Engineers, Transactions, Series B, 45, 1979 (393), 712-722.

[24] Padovan A, Bortolin S, Rossato M, Filippeschi S, Del Col D. Vaporization heat transfer in a small diameter closed two-phase thermosyphon. Journal of Heat Transfer, 2019 141(9).

[25] El-Genk MS, Saber HH. Heat transfer correlations for small, uniformly heated liquid pools. Int. J. Heat and Mass Transfer, 1998 41(2):261-74.

[26] Shiraishi, M, Kikuchi K, Yamanishi T, Investigation of heat transfer characteristics of a two-phase closed thermosyphon. Journal of Heat Recovery Systems, 1981 vol. 1, no. 4, 287–297.

[27] Andros FE, FE A, LW F. THE TWO-PHASE CLOSED THERMOSYPHON. AN EXPERIMENTAL STUDY WITH FLOW VISUALIZATION.

[28] Jouhara H, Robinson AJ. Experimental investigation of small diameter two-phase closed thermosyphons charged with water, FC-84, FC-77 and FC-3283. Applied thermal engineering. 2010 Feb 1;30(2-3):201-11.

[29] Labuntsov DA. Heat transfer problems with nucleate boiling of liquids. Therm. Eng.(USSR)(Engl. Transl.), v. 19, no. 9, pp. 21-28. 1973 Sep 1.

[30] Stephan K, Abdelsalam M. Heat-transfer correlations for natural convection boiling. International Journal of Heat and Mass Transfer. 1980 Jan 1;23(1):73-87.

[31] Kutateladze, S. S. Heat transfer and hydrodynamic resistance, Energoatomizdat Publishing House, Moscow. 1990

[32] Gross U. Reflux condensation heat transfer inside a closed thermosyphon. International journal of heat and mass transfer. 1992 Feb 1;35(2):279-94.

[33] Shiraishi M, Kikuchi K, Yamanishi T. Investigation of heat transfer characteristics of a two-phase closed thermosyphon. InAdvances in heat pipe technology 1982 Jan 1 (pp. 95-104). Pergamon.

[34] Guichet V, Jouhara H, Condensation, evaporation and boiling of falling films in wickless heat pipes (Two-phase closed thermosyphons): A critical review of correlations, Int. Journal of Thermofluids, 2020 (1-2) 100001.

[35] Hussein HM, Mohamad MA, El-Asfouri AS. Theoretical analysis of laminar-film condensation heat transfer inside inclined wickless heat pipes flat-plate solar collector.

[36] Wang JC, Ma Y. Condensation heat transfer inside vertical and inclined thermosyphons. Journal of Heat Transfer, ASME Journal of Heat Transfer, 1991 113(3) 777-780.

[37] Vasil'Ev LL, Grakovich LP, Khrustalev DK. Limiting characteristics of inclined thermosyphons and heat pipes with excess heat-transfer agent. Journal of engineering physics. 1984 May;46(5):505-10.

[38] Hashimoto, H. and Kaminaga, F., 2002. Heat transfer characteristics in a condenser of closed two-phase thermosyphon: Effect of entrainment on heat transfer deterioration. *Heat Transfer—Asian Research: Co-sponsored by the Society of Chemical Engineers of Japan and the Heat Transfer Division of ASME*, *31*(3), pp.212-225.

[39] Cohen H, Bayley FJ. Heat-transfer problems of liquid-cooled gas-turbine blades. Proceedings of the Institution of Mechanical Engineers. 1955 Jun;169(1):1063-80.

[40] Wallis GB. One-dimensional two-phase flow. Dover Publications; 2020.

[41] Imura H, Sasaguchi K, Kozai H, Numata S. Critical heat flux in a closed two-phase thermosyphon. International journal of Heat and mass transfer. 1983 Aug 1;26(8):1181-8.

[42] Tien CL, Chung KS. Entrainment limits in heat pipes. AIAA Journal, 1979, 17(6) 643-6.

[43] Faghri A, Chen MM, Morgan M. Heat transfer characteristics in two-phase closed conventional and concentric annular thermosyphons, 1989, 111(3) 611-618

[44] Kim Y, Shin DH, Kim JS, You SM, Lee J. Boiling and condensation heat transfer of inclined two-phase closed thermosyphon with various filling ratios. Applied Thermal Engineering. 2018; 145:328-42.

[45] Gorbis ZR, Savchenkov GA. Low temperature two-phase closed thermosyphon investigation. Heat Pipes. 1976:37-45.

[46] Lin TF, Lin WT, Tsay YL, Wu JC, Shyu RJ. Experimental investigation of geyser boiling in an annular two-phase closed thermosyphon. International journal of heat and mass transfer. 1995 Jan 1;38(2):295-307.

[47] Casarosa C, Latrofa E, Shelginski A. The geyser effect in a two-phase thermosyphon. International Journal of Heat and Mass Transfer. 1983 Jun 1;26(6):933-41.

[48] Negishi K. Unstable phenomena in a two-phase closed thermosyphon. In Proceedings of the symposium on mechanics for space flight, 1SAS Report SP 1983 Mar (Vol. 1, pp. 257-263).

[49] Park YJ, Kang HK, Kim CJ. Heat transfer characteristics of a two-phase closed thermosyphon to the fill charge ratio. International Journal of Heat and Mass Transfer. 2002 Nov 1;45(23):4655-61.

[50] Han KI, Cho DH, Park JU. Investigation of boiling heat transfer characteristics of two-phase closed thermosyphons with various internal grooves. KSME international journal. 2003 Nov 1;17(11):1739-45.

[51] Liu ZH, Li YY, Bao R. Thermal performance of inclined grooved heat pipes using nanofluids. International journal of thermal sciences. 2010 Sep 1;49(9):1680-7.

[52] MacGregor RW, Kew PA, Reay DA. Investigation of low Global Warming Potential working fluids for a closed two-phase thermosyphon. Applied thermal engineering. 2013 Mar 1;51(1-2):917-25.

Chapter 3: Heat Transfer in a Vertical Grooved Thermosyphon

Complete citation:

Hammouda, M.G., Ewing, D., Zaghlol, A., Ching, C.Y., Heat Transfer Performance in a Vertical Grooved Thermosyphon, International Journal of Thermofluids (2021). DOI: 10.1016/j.ijft.2021.100107.

Relative Contributions:

M.G. Hammouda: Performed all experiments, interpretation and analysis of the data and wrote the first draft of the manuscript including all figures and text.

D. Ewing: Assisted in the interpretation and discussion of results.

A. Zaghlol: Industry liaison. Provided context from an industry perspective.

C. Y. Ching: Supervisor of M.G. Hammouda and was responsible for the final editing and submission to the journal.

3.1 Abstract

The performance of a grooved copper-water thermosyphon with a modest bend between a vertical evaporator section and inclined condenser section was characterized for a moderate fluid loading. The time-averaged temperature varied significantly along the evaporator for heat fluxes up to 10 W/cm^2 before becoming more uniform at higher heat fluxes. Transients of the measured temperatures show evidence of different flow regimes that were compared to existing flow pattern maps. The evaporator performance for both the pool region, which had the highest temperature, and the film region were not well predicted for heat fluxes up to 10 W/cm^2. The local evaporator performance changed with the change in flow regime, suggesting the need for a flow regime-based performance model. The performance of the condenser appeared to depend on the reduced pressure and was significantly overpredicted by the standard condensation models. A modified model for the condenser was proposed.

3.2 Nomenclature

Bo Bond number $D\sqrt{g[(\rho_l - \rho_v)/\sigma]}$

c_{pl} Liquid specific heat, (J/kg K)

Co Confinement Number $(1/D_i)\sqrt{\sigma/[(\rho_l - \rho_v)g]}$

$C_{s,f}$ Constant in the boiling correlation

D Inner diameter, (m)

g Gravitational acceleration, (m/s^2)

G Superficial mass flux, $Q/h_{fg}A_c$ (kg/m^{2}s)

h_e Evaporator heat transfer coefficient, (W/m^{2}K)

h_{fg} Latent heat, (J/kg)

j_v^* Normalized vapour production rate $G/\sqrt{[gD_i(\rho_l - \rho_v)]}$

k_l Liquid thermal conductivity, (W/m K)

Ku Kutateladze number (eqn 1)

Ku^* Modified Kutateladze number $[Ku(D/L_e)(\rho_v/\rho_l)]$

L_c Condenser length, (m)

L_b Bubble length scale, $\sqrt{\sigma/[g(\rho_l - \rho_v)]}$ (m)

l_o Viscous length scale $(v_l^2/g)^{1/3}$, (m)

M Molecular weight, (kg/kmol)

Nu Nusselt Number hl_o/k

P_{crit} Critical pressure, (Pa)

P_v Vapor pressure, (Pa)

Pr Prandtl number

q_e Wall heat flux in the evaporator, (W/m^2)

Re_f Film Reynolds number Γ/μ_l

Re_v Vapor Reynolds number, $[\rho_v u_v D/\mu_v]$

T_e Evaporator wall temperature, (^{o}C)

T_{AD} Adiabatic wall temperature, (^{o}C)

T_{cond} Condenser wall temperature, (^{o}C)

T_{sat} Saturation temperature, (^{o}C)

u_v Vapor velocity, (m/s)

G Mass flow per unity width $Q/h_{gh}\pi D_i$ (kg/ms)

μ_l Dynamic viscosity of liquid water, (Pa s)

v_l Kinematic viscosity of liquid, (m^2/s)

ρ_l Liquid density, (kg/m^3)

ρ_v Vapor density, (kg/m^3)

σ Surface tension, (N/m)

3.3 Introduction

Passive two-phase heat transfer devices, including thermosyphons [1] and looped devices [2,3], are increasingly being used to cool power electronic devices with high power removal requirements. Multiple thermosyphons are often used in parallel for these applications, but the power removed by each thermosyphon is typically large, which may result in changes in the thermosyphon operation. Measurements for a copper-water thermosyphon with a range of fluid loading and inclinations angles by Kim et al. [4] showed evidence of an inflection in the evaporator heat transfer coefficient near 10 W/cm^2 as the Kutateladze number approached a maximum. The inflection in the heat transfer coefficient was attributed to a partial dry-out of the evaporator associated with an increase in the bubble generation. The evaporator heat transfer coefficient increased after the inflection for heat fluxes up to 25 W/cm^2. The evaporator performance in [4] and other investigations [5][6] is characterized by the evaporator heat transfer coefficient based on the average of the temperatures along the length of the evaporator. Local temperature variations associated with the liquid pool [[5],[7][8]] can affect the ability of thermosyphon based systems to meet power electronics temperature constraints. Shiraishi et al [7] proposed modelling the evaporator temperature distributions using separate correlations for the film and pool regions, where the fluid distribution was determined using film models. Parallel resistance models for the film and pool regions have also been used to estimate average evaporator resistances [[8][9][10]].

The onset of boiling and changes in the flow regime in thermosyphons can affect the performance of the thermosyphon, such as causing geyser boiling instabilities that result in pressure and temperature fluctuations along the thermosyphon [47][13]. The flow patterns observed in thermosyphons with a vertical evaporator section include natural convection, bubbly, geyser or slug flow, churn flow and annular flow [[6][12][16]] depending on the confinement,

aspect ratio and operating conditions of the evaporator. Visualizations for thermosyphons with small fill ratios [6] indicate that these thermosyphons can have similar flow regimes to those with larger fill ratios [[12],[13]]. Flow pattern maps were presented in Terdtoon et al. [[3][15]] based on a modified Kutateladze number and the vapour Reynolds number. More recently Smith et al. [[12][13]] proposed maps based on the confinement number and vapour production rate [12], and based on the superficial momentum fluxes of the vapour and liquid phase [13].

The objective of this investigation was to characterize the heat transfer performance of the pool and film regions in the evaporator section of a larger diameter (15.87 mm) thermosyphon with rifled grooves as in [10] and a moderate water fluid loading over a range of heat fluxes. Transients of the temperatures measured along the evaporator were also used to characterize the nature of the instability and internal flow patterns and the link between the flow pattern and heat transfer performance. Power was applied using heat cartridges inserted in heater blocks attached to a heat spreader plate, typical of power electronic applications. The condenser performance was also characterized and compared to existing correlations. The experimental methodology is outlined in the next section. The results of the experiments are then presented and discussed.

3.4 Experimental Facility

The measurements were performed for a 1 m long rifle grooved copper-water thermosyphon with an outer diameter of 15.87 mm, wall thickness of 0.5 mm, and a nominal groove height of 0.3 mm. The thermosyphon evaporator was embedded in an aluminium heat spreader plate as shown in Figure 3.1. The plate had a length of 310 mm, width of 40.7 mm and a nominal thickness (into the page) of 20 mm. Mounting flanges for the heating plates were included on each side. The axis

of the thermosyphon was at an angle of 3° relative to the plate surface in this device. The experiments were performed with he evaporator oriented vertically or with the heat spreader plate oriented 3° from vertical. The thermosyphon was heated using two 254 mm long cartridge heaters inserted in aluminium heating plates on each side of the heat spreading plate, centred along the length and width of the plate. The electrical power to the heaters was measured using a power transducer with an uncertainty of 0.5%. The 200 mm adiabatic section between the evaporator and condenser sections had a bend of 8°. The thermosyphon was cooled using water from a chiller with a flow rate of 1.2 L/min passing through a water jacket with an internal length of 346 mm. The water flow rate through the jacket was measured using a turbine flow meter with an uncertainty of 0.1%, while the water temperature at the inlet and outlet were measured using T-type thermocouples calibrated against an RTD accurate to 0.01ºC. The effect of bias error was reduced by correcting for the temperature difference measured before the experiments. There was a second approximately 20 mm adiabatic section between the condenser section and the thermosyphon tip.

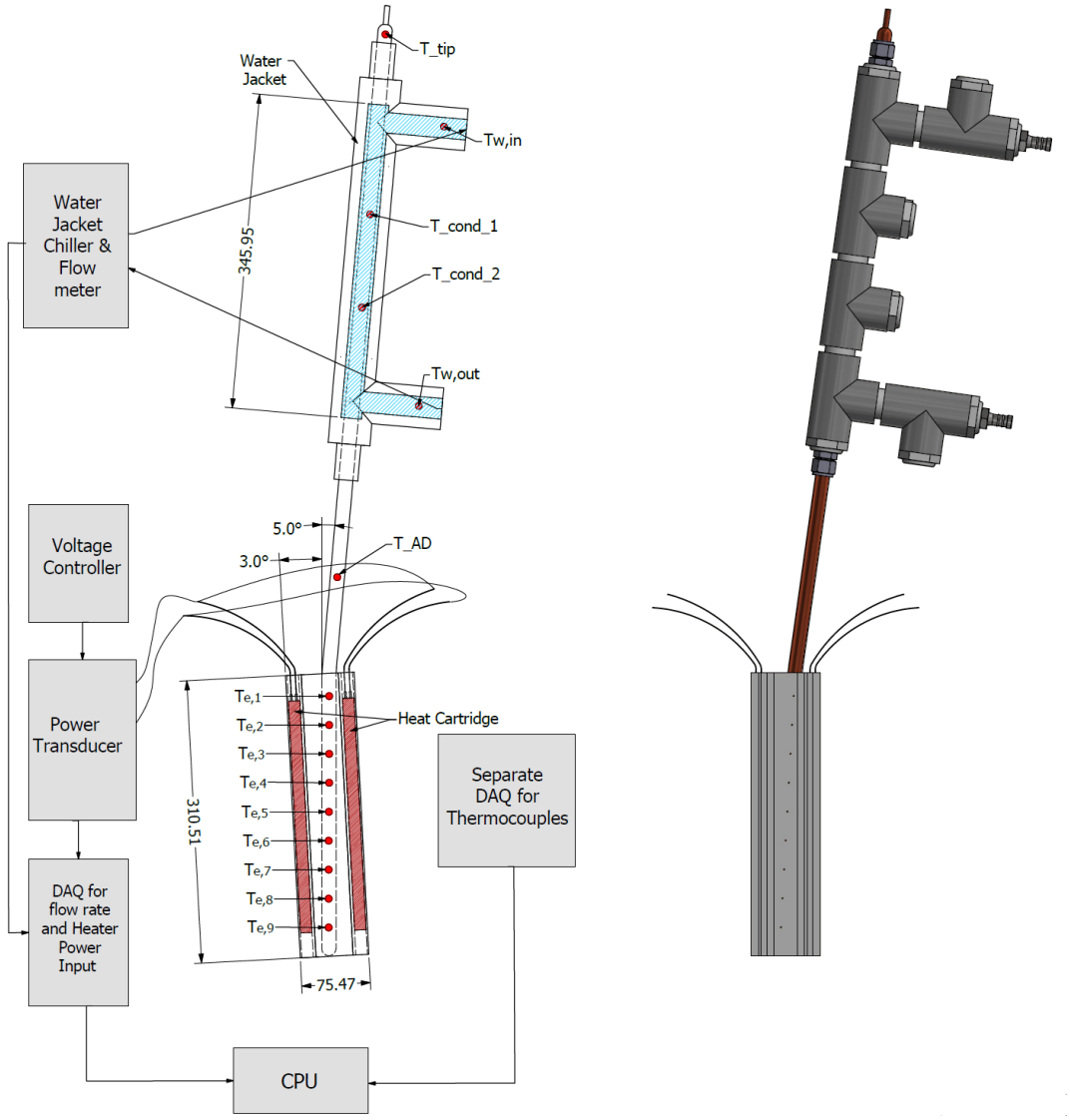

Figure 3.1. Schematic of the experimental facility

The temperature of the evaporator surface was measured using nine T-type thermocouples embedded into the heat spreader plate to the outer surface of the thermosyphon. These thermocouples were positioned along the central axis of the thermosyphon. The wall temperature in the adiabatic sections was measured using one thermocouple between the evaporator and condenser sections and one thermocouple in the adiabatic tip section. The condenser section wall

temperature was measured using two thermocouples positioned evenly along the condenser section. These thermocouples were also calibrated against a RTD accurate to 0.01°C before the experiments using a water bath for temperatures from 4 to 90°C and an oil bath for temperatures from 60 to160°C. The output of the thermocouples was sampled using a thermocouple A/D board. A separate A/D board was used to sample the output from the power and water flow rate transducers. The data in both cases was recorded at 2 samples per second.

The experiments were performed for a thermosyphon with a fluid loading of 17 cm^3 of deionized water that corresponded to approximately 35% of the interior volume of the thermosyphon within the heat spreader plate. Experiments were performed for three different cooling water inlet temperatures; 10°C, 20°C, and 35°C. These temperatures were maintained to ±0.1°C by the chiller. The power to the heater cartridges was increased in increments of 125W up to 1625W. Data were recorded throughout the experiments. The thermosyphon performance at each power was characterized using data from the period after the system had reached steady state at that power, that typically required between 30 and 35 minutes after the power was adjusted. The facility was fully insulated to limit the heat transfer to the surrounding air during the experiments. The heat transfer to the cooling water during the steady state periods agreed with the power input to the heaters to within ±5% for most measurements reported here as shown in Figure 3.2. The wall temperature measured in the adiabatic tip region was below the temperature measured in the adiabatic section between the evaporator and condenser at low powers suggesting some possible effect of non-condensable gases, but the temperatures agreed at higher powers. Thus, the wall temperature measured in the adiabatic section between the evaporator and condenser sections was considered to be the saturation temperature here.

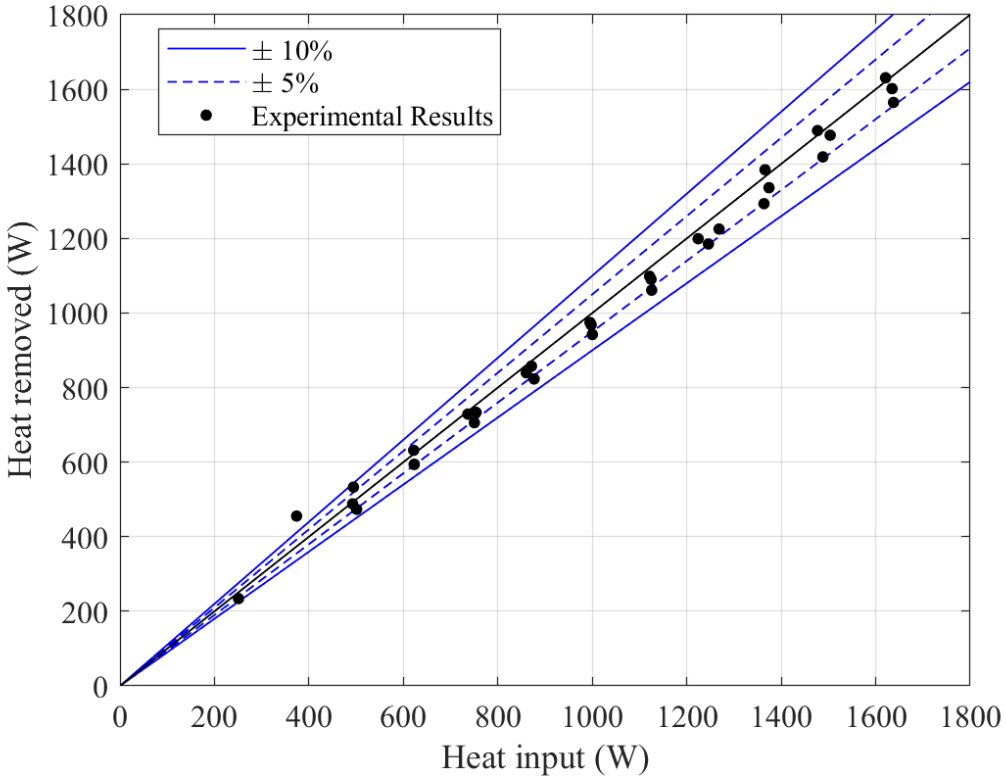

Figure 3.2. Comparison of the heat input and heat removed by the cooling water

3.5 Results and Discussion

Typical profiles of the time averaged wall temperature along the evaporator relative to the saturation temperature for the cooling water temperature of 20°C are shown in Figure 3.3. The results at moderate heat transfer rates show two distinct regions typically associated with the pool and film regions [7][8]. The difference between the temperature on the wall and the saturation temperature at the bottom of the evaporator or the pool region were much higher than those in the upper portion of the evaporator or the film region. The temperature difference in the pool region increased when the power was increased from 500W to 625W but decreased when the power was increased beyond 625W. The temperature difference in the film region did not change significantly when the power was increased from 500W to 875W, but subsequently increased when the power

was increased to 1375W, with a substantial increase between 1125W and 1375W. The temperature distribution was relatively uniform along the evaporator at 1375W with the highest temperature near the middle of the evaporator. There was little change in the temperature along the entire length of the evaporator when the power was increased from 1375W to 1625W.

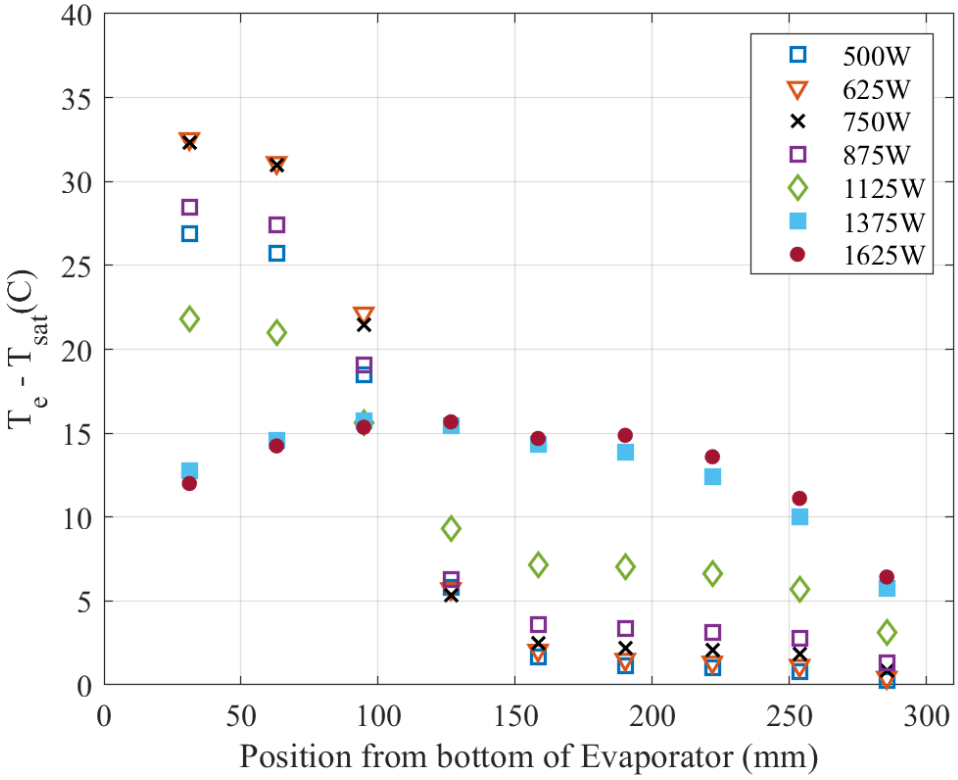

Figure 3.3. Profiles of the evaporator wall temperature relative to the saturation temperature for the inlet cooling water temperature of 20°C.

The variation in the temperature profile along the evaporator can be characterized by the difference between the maximum local time averaged temperature and average of these temperatures along the length of the evaporator. The change in this temperature difference with heat transfer rate for the different inlet cooling water temperatures in Figure 3.4 shows that the difference between the maximum temperature and average temperature increased with increasing

power to a maximum value at 500W or 625W. The largest temperatures at these powers occurred in the pool region in all the cases. The maximum difference was similar when the inlet cooling water temperature was 10°C and 20°C but was substantively smaller for 35°C. The difference between the local maximum and average temperature along the evaporator decreased when the power transferred through the thermosyphon increased beyond 625W until it reached a plateau, where the temperature distribution along the evaporator was relatively uniform. This occurred at lower powers as the inlet cooling water temperature increased. The largest temperature occurred at the lowest measurement location in the pool region until the temperature distribution became more uniform in all cases as it did in Figure 3.3. The change in temperature profile along the length of the evaporator with heat transfer rate appeared to be due to a change in the flow pattern within the evaporator section from pool natural convection or boiling to a more dynamic or developed flow regime.

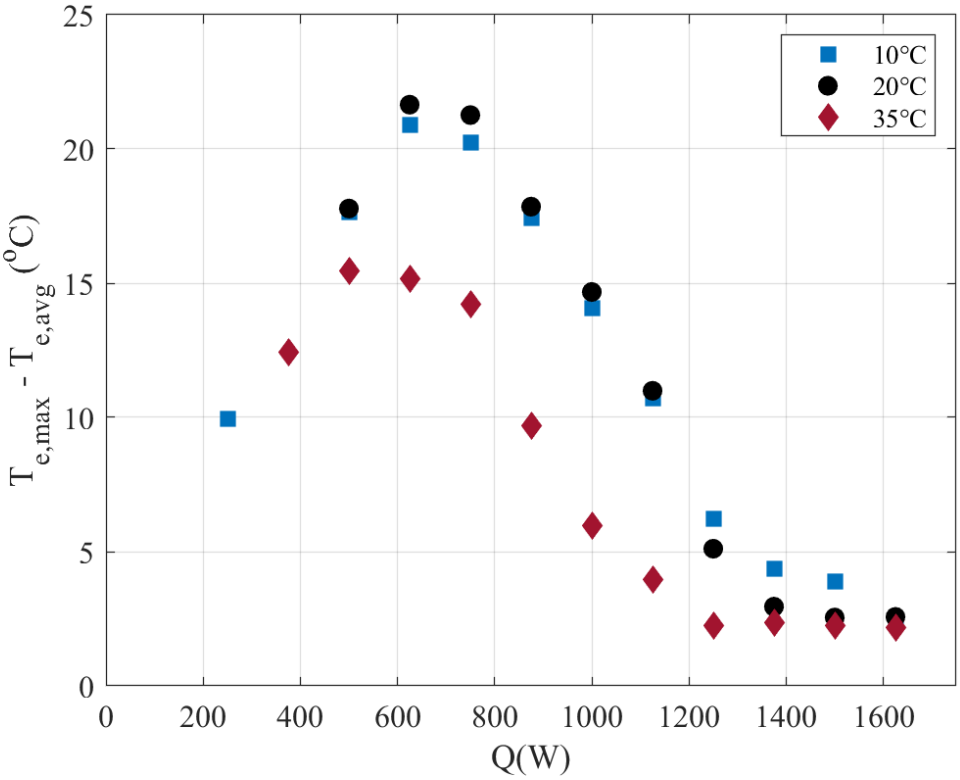

Figure 3.4. Change in the maximum evaporator wall temperature relative to the average temperature along the length with heat transfer rate.

The flow regime present in the evaporator was characterized by examining transients of the evaporator wall temperatures during the steady state period. Typical results for the cooling water temperature of 20°C are shown in Figure 3.5. The temperature traces at low heat transfer rates, such as 500W (or 4 W/cm^2) in Figure 3.5(a), show little evidence of fluctuations. Temperature fluctuations for this cooling water temperature were not observed until a heat transfer rate of 625W (or 5.1 W/cm^2) in Figure 3.5(b), where there were short duration decreases in the evaporator wall temperature in the pool region accompanied by an increase in the saturation temperature and the wall temperature in the film region. The short decreases were followed by prolonged periods where the wall temperature in the pool region increased while the saturation temperature decreased. The

nature of the fluctuations was similar for powers up to 1125W (or 9.1 W/cm^2) in Figure 3.5(c) for this cooling water temperature, but the time between consecutive temperature fluctuations decreased with increasing power, as did the difference between the maximum mean temperature and average of these temperature as in Figure 3.4. The transients of the wall temperatures differed at 1250W (or 10.1 W/cm^2) shown in Figure 3.5(d) where the fluctuations in the pool region (at 30 mm and 94 mm) appeared to be in phase with the saturation temperature and not the fluctuations in the film region. The amplitude of wall temperature fluctuations decreased substantially for powers of 1375 W (or 11.2 W/cm^2) and 1650 W (or 13.5 W/cm^2) in Figure 3.5(e) and (f). The time scale appeared to decrease as the input power increased. The mean temperature was more uniform along the evaporator in these cases with the maximum temperature near the middle of the evaporator. Comparing the temperature transients with those from Smith et al. [12] and Grooten et al. [16] suggest that the onset of fluctuations in Figure 3.5(b) reflects a change from natural convection to bubbly or slug flow. The frequency of the bubble or slugs increase with power input in Figure 3.5(c). The decrease in the magnitude of the fluctuations for power inputs of 1375W and greater suggest a churn type flow [13]. The flow pattern at 1250W or in Figure 3.5(d) is unclear but it may be associated with change from slug flow to a more developed boiling regime in the pool region while bubbly or slug flow was observed in the film region.

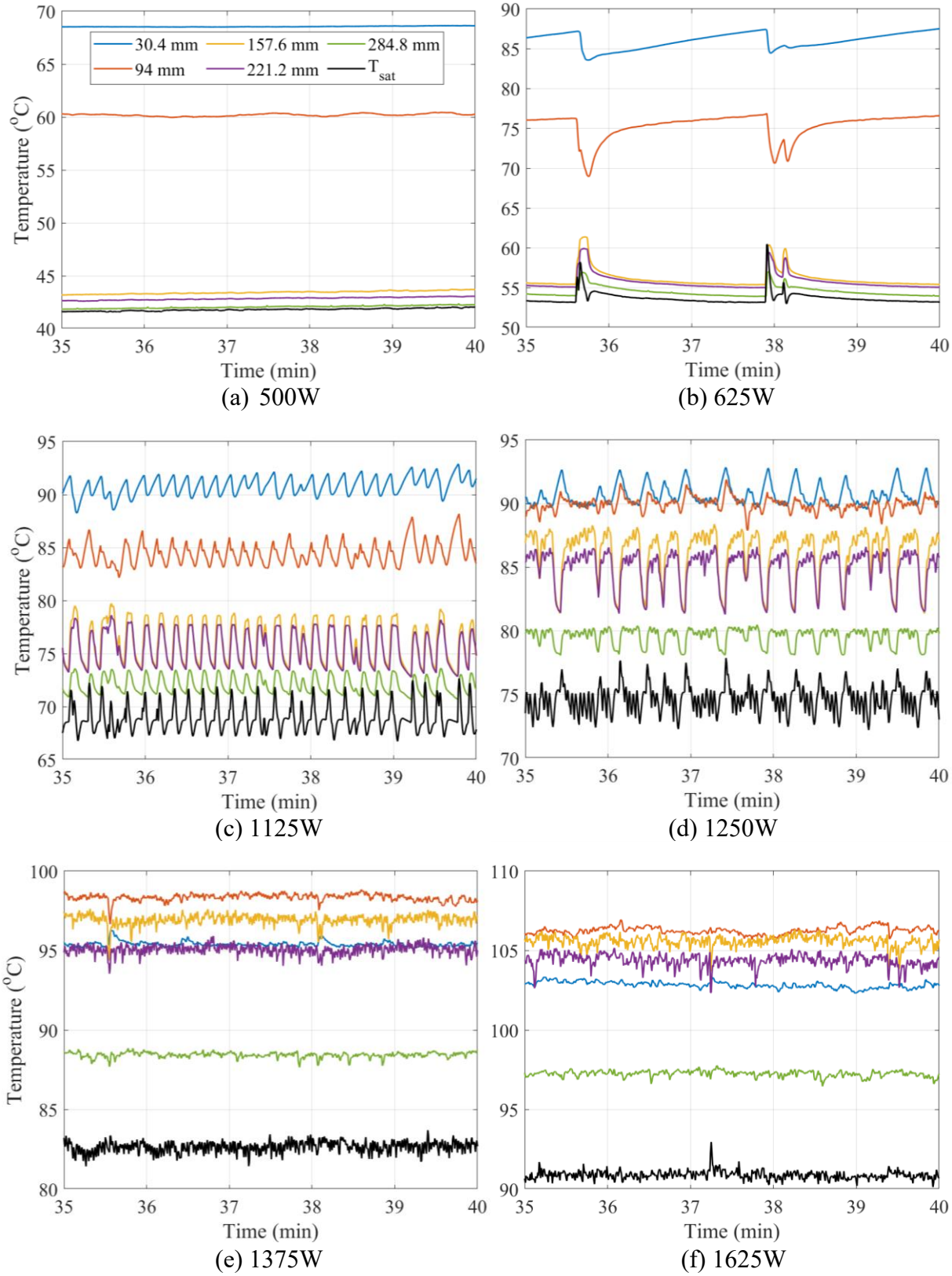

Figure 3.5. Transient wall temperatures across the length of the evaporator with condenser cooling water 20°C for heat transfer from 500W to 1625W.

The cases considered here fell well outside the range of modified Kutateladze number for bubbly or churn flows in the flow pattern maps that Terdtoon et al. [3],[15] developed using R123 as the working fluid (see *Figure 3.14*). A comparison of the proposed flow regimes, as classically defined in [17], with the flow regime maps proposed in Smith et al. [12][13] are shown in Figure 3.6. Figure 3.6(b) plots the flow regimes based on the confinement number and vapour production rate determined using the expression $j_v^* = G/\sqrt{[gD\rho_v(\rho_l - \rho_v)]}$[12]. The Confinement number (Co) was below 0.2 for all cases here and thus the results were in the unconfined region of the Confinement and rate of production map [12]. The measurement conditions all fell well into the churn region of this map and thus, it did not capture the different flow regimes observed here. The map based on the superficial momentum flux proposed in [13] in Figure 3.6(b) show that the natural convection regime of the present measurements fell under the geyser region on this map. The cases that appear to be bubble/slug flow here fell under churn flow, and the results that appear to be churn flow fell under bubbly/churn flow in [13] but seem to be following a similar trend to the map. The results here were largely beyond the range of parameters considered in Smith et al. suggesting there may be a need to further consider the boundaries in this approach at large superficial vapour momentum flux.

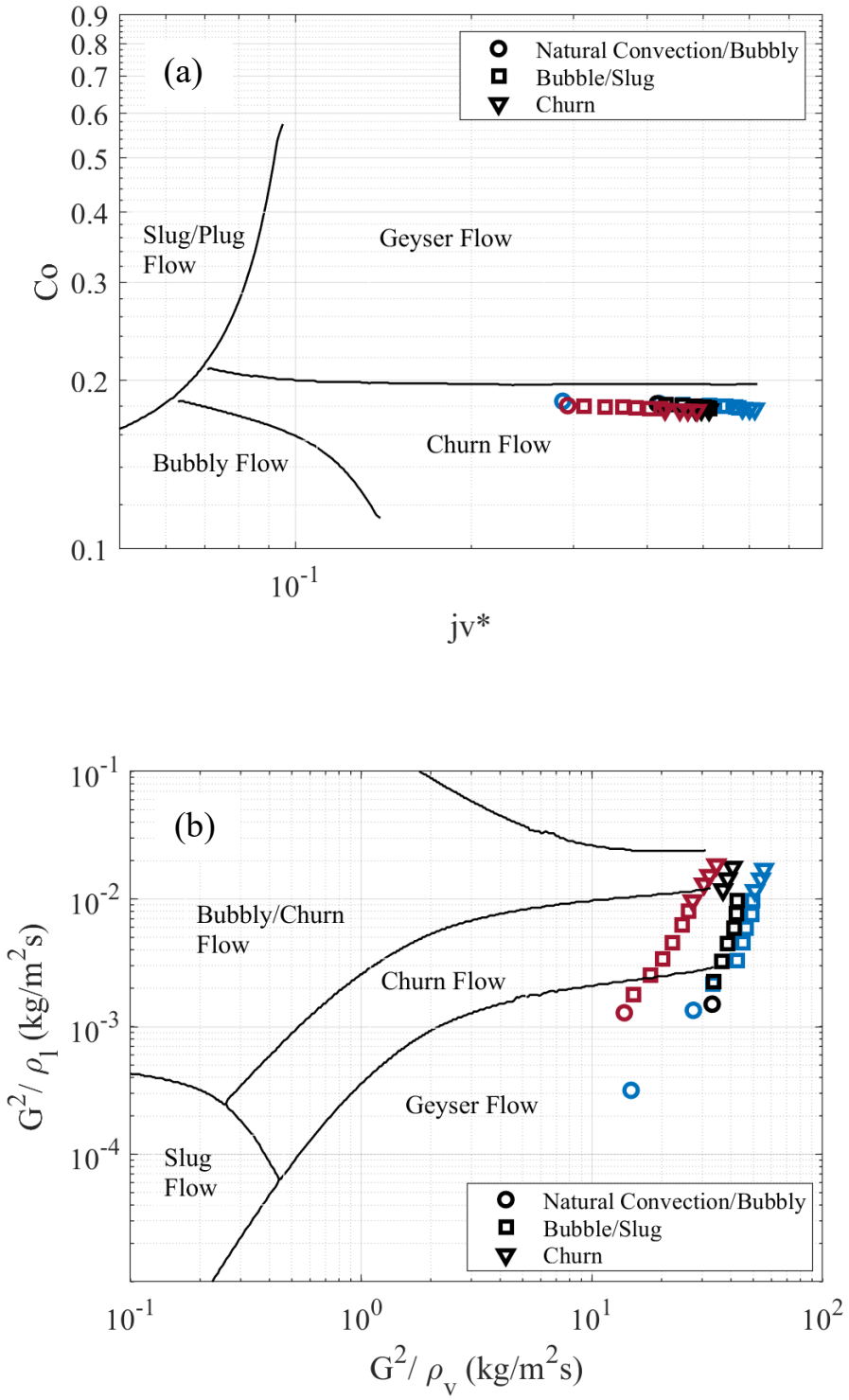

Figure 3.6. Comparison of flow regimes with the flow maps of Smith et al. [12][13]: (a) vapor production rate vs confinement number and (b) superficial momentum flux coordinates at condenser cooling water temperature of [Blue] 10°C, [Black] 20°C and [Maroon] 35°C.

The role of the onset of a flooding or entrainment limit in the change of flow regime was characterized by examining the change in the Kutateladze number given by [3]

$$Ku = \frac{q_e}{h_{fg}\left[\sigma g \rho_v^2 (\rho_l - \rho_v)\right]^{1/4}} \quad (1)$$

with the heat flux and saturation temperature as shown in Figure 3.7. The Kutateladze number increased with heat flux throughout for the lowest and highest cooling water temperatures. There was a decrease in the Kutateladze number at 11.2 W/cm^2 for the cooling water temperature of 20°C where the flow regime changed to churn flow, but the Kutateladze number subsequently increased suggesting the performance was not limited by the vapor flow holding up the returning liquid flow from the condenser or entraining droplets from this flow. The presence of an internal groove structure is thought to mitigate the latter [19]. The comparison of the Kutateladze numbers with typical correlation given in Table 3.1 show that the experimental results were approaching the critical value proposed by Imura et al. [3] but were still well below the correlation proposed by Faghri et al. [21]. The change in Kutateladze number with saturation temperature in Figure 3.7(b) shows there were inflections in the profiles for all the cooing water temperatures that appears to correspond to the changes in the flow regime.

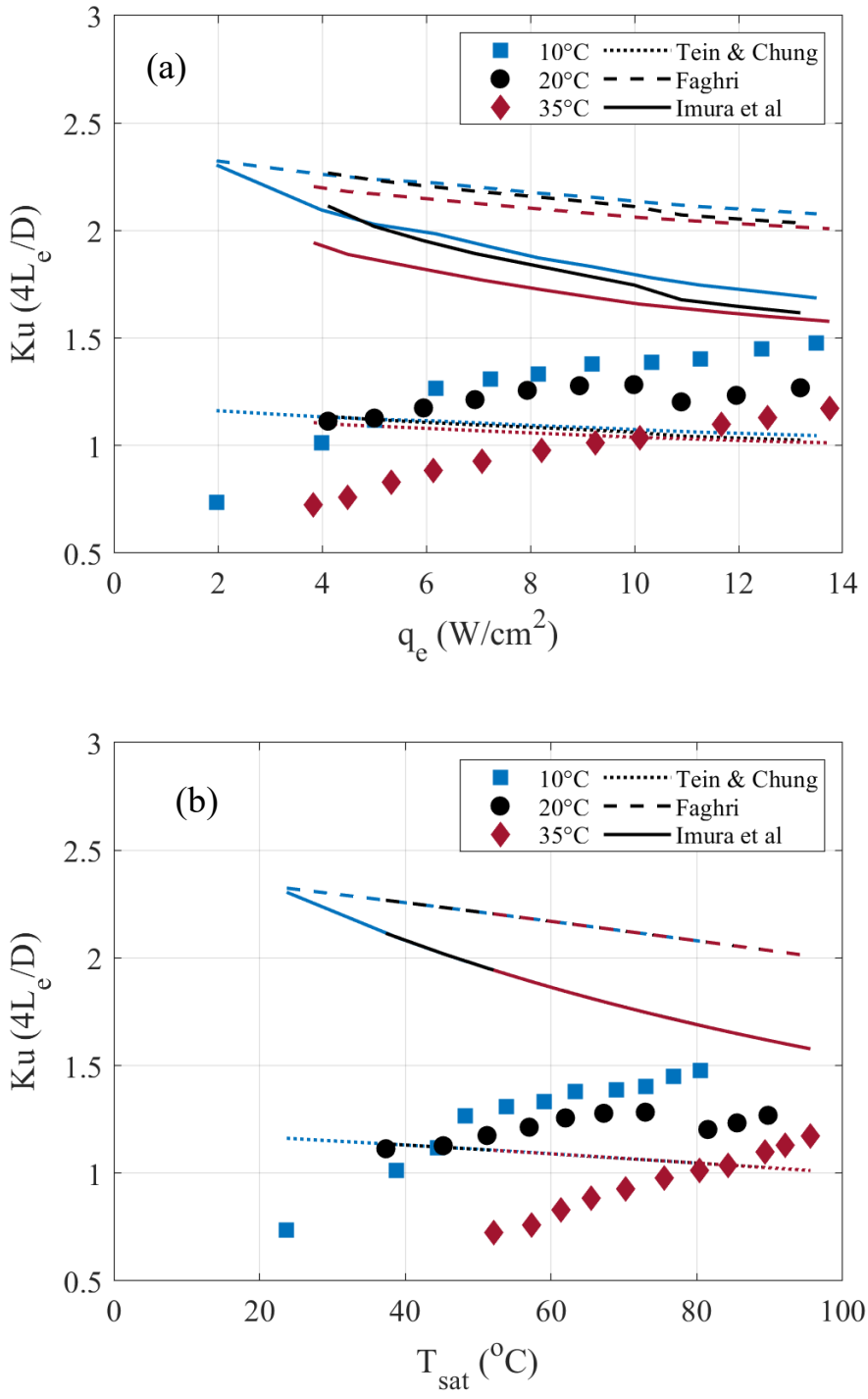

Figure 3.7. Variation of Kutateladze number with (a) evaporator wall heat flux and (b) saturation temperature for the different cooling water inlet temperatures.

The change in the heat transfer coefficient of the evaporator section, based on the average of the mean temperature along the length of the evaporator, with the nominal heat flux are shown in Figure 3.8. The heat flux is based on the heater length. The uncertainty in the heat transfer coefficient was estimated to be in the range of ±2.8% at the higher powers to ±5.6% at the lower powers. The results are compared with correlations for heat transfer coefficient of the evaporator by Imura et al [23] and Padovan et al [5] (Table 3.2) and the Rosenhow pool boiling correlation [22] (Table 3.2) as in [4], with $C_{s,f}$ = 0.128 and n = 1 for water and polished copper [29]. The measurements are in reasonable agreements with prediction from the correlation proposed by Imura et al. [23] but are substantively larger than those for small diameter or confined thermosyphons considered by Padovan et al. [5]. The results show though that the heat transfer coefficient of the evaporator has a plateau between 7 and 10 W/cm^2 similar to the results in Kim et al. [4] that was not predicted by the correlations. The heat transfer coefficient subsequently increased for heat fluxes greater than 10 to 11 W/cm^2 with the change in flow pattern to the churn type flow and the more uniform temperature distribution in the evaporator. The initial increase in heat transfer coefficient was more rapid here than the results for the smooth walled thermosyphon in [4]. The results for the lower fill ratio of 0.25 in [4] showed a more pronounced plateau than that in the results here or for the fill ratio of 0.5 in [4].

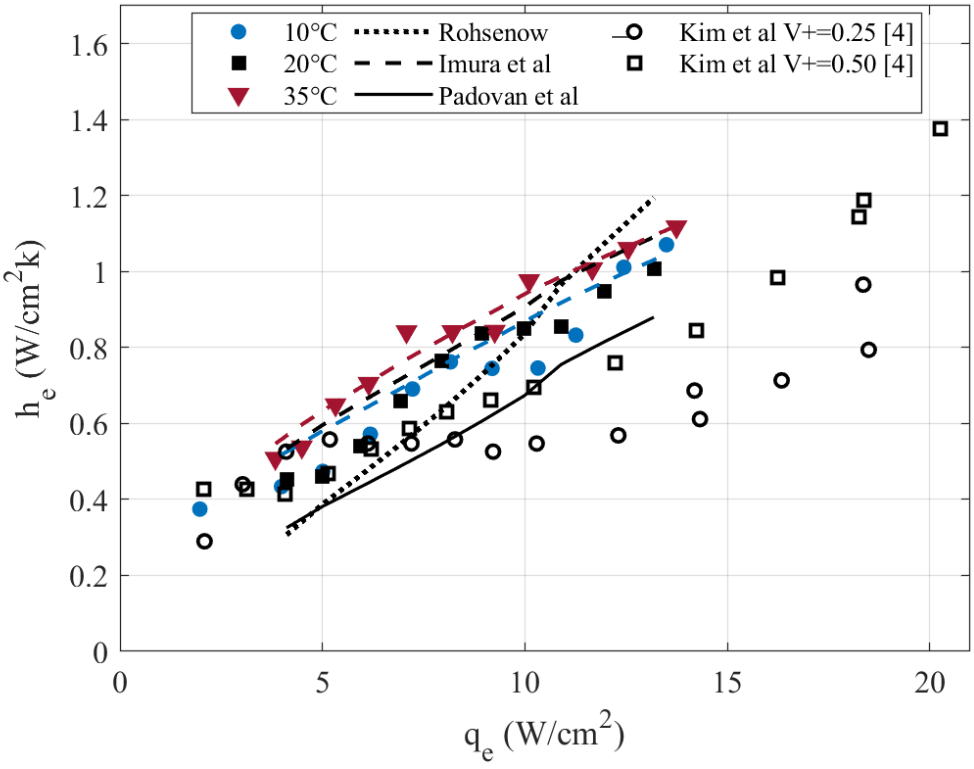

Figure 3.8. Change in the average evaporator heat transfer performance with heat flux. Correlations results are for the inlet cooling water temperature of 20°C except for Imura et al. where the inlet cooling water temperature is denoted with line colours corresponding to the symbols.

The change in the average heat transfer coefficients for the pool and film regions [7] with heat flux is shown in

Figure 3.9. The heat transfer coefficient for the pool region was determined from the average of the two temperatures at 31 mm and 63 mm from the bottom, while the heat transfer coefficient for the film region was determined from the average of the four temperatures from 157 mm to 254 mm from the bottom. The heat transfer coefficient for the pool region was initially approximately constant before increasing with heat flux from approximately 4 to 6 W/cm^2 near the transition to bubbly or slug flow. The increase was initially greater for the higher cooling water temperatures.

The change in the coefficient appeared to have an inflection near 10 W/cm^2 in these cases with the change in the flow regime. The results up to 10 W/cm^2 were overpredicted by a number of the pool and thermosyphon boiling correlations (presented in Table 3.2) used to predict the performance of thermosyphons [30] and the natural convection (NC) correlation proposed in El Genk and Saber [26]. Other correlations, such as the geyser boiling correlation of Casarosa et al. [47], intersect the data at lower heat fluxes but overpredict the data at low heat fluxes. The same was found for a number of other correlations from [30] not presented. The El Genk and Saber [26] nucleate boiling (NB) correlation appears to be in best agreement with the data above 10 W/cm^2 for this operating condition. The performance at the low heat fluxes was in best agreement with the piece-wise heat transfer regime correlation model of Shabgard et al [27]. The model did not predict the approximately constant heat transfer coefficient at low heat fluxes and overpredicted the heat transfer coefficient at moderate heat fluxes. This resulted in an underprediction in the large pool superheat observed at moderate heat fluxes, typical of water boiling at low pressures [31], as shown in Figure 3.10. This appears to be due in part to differences in the transition to the slug regime here and the two-phase region proposed in the model. The presence of the groove structure may enhance the single-phase natural convection and delay the onset of this transition. Differences also occurred at higher heat fluxes, but this type of flow regime based model appears needed to model the changes in heat transfer performance observed here.

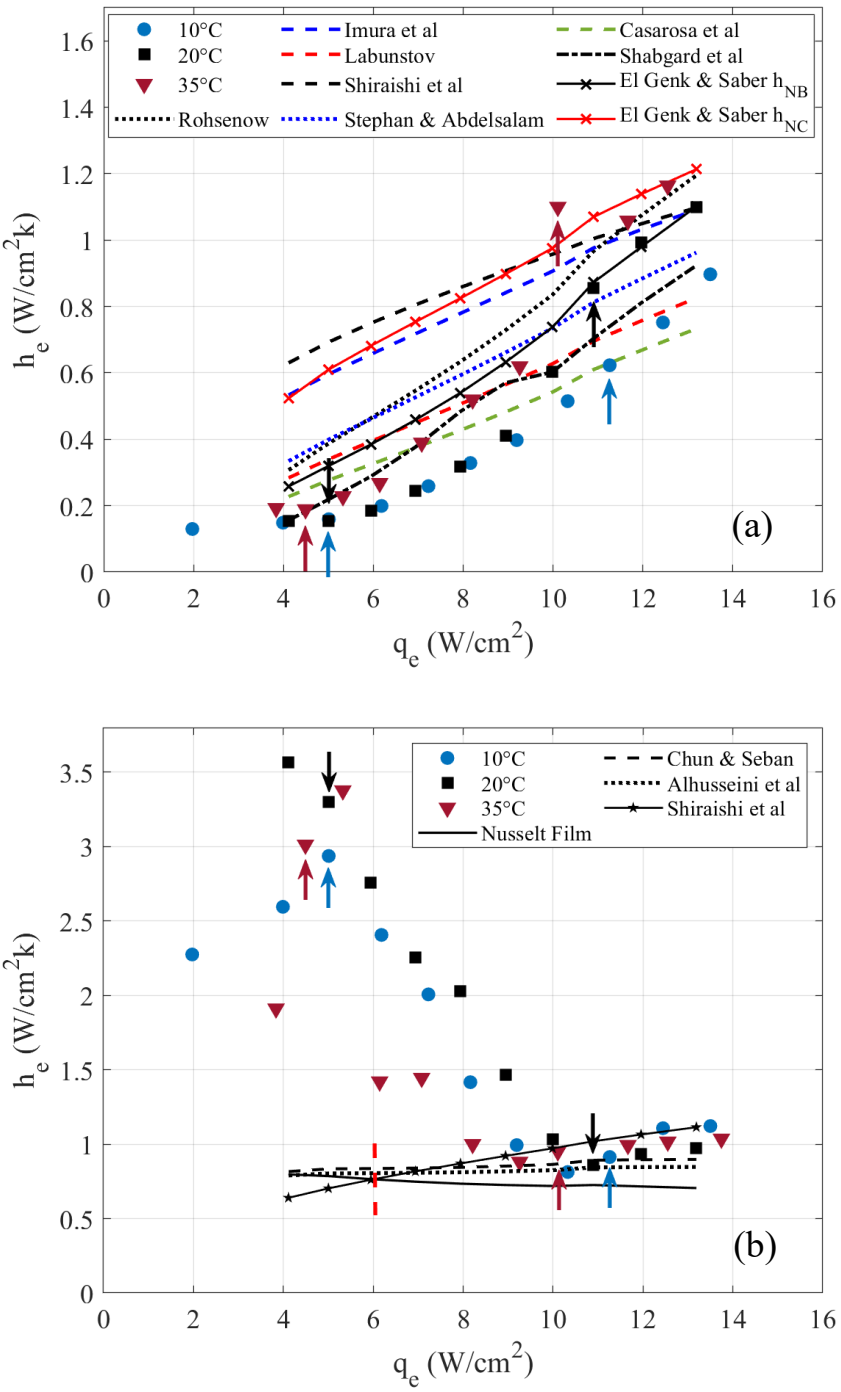

Figure 3.9. Change in the heat transfer coefficient for the (a) pool and (b) film regions. Correlations are for the inlet cooling water temperature of 20°C. Arrows indicate flow regime change.

The results for the film region show that the heat transfer coefficient was initially much larger than the coefficient predicted with the Nusselt type film evaporation model [7][32] or the Chun and Seban [32] or the Alhusseini et al. [33] correlation for wavy flow (Table 3.3) at low and moderate heat fluxes suggesting that the groove structure enhances the film evaporation. The heat transfer coefficient decreases significantly at heat fluxes above 5 to 6 W/cm^2 where the flow regime transitioned to bubbly or slug flow. This reduction may be due to an increase in the fluid within the groove structure due to intermittent two-phase flow from the pool. The heat transfer coefficient approached the wavy film correlations before there was an increase in the coefficient as the flow regime appeared to transition to churn flow. Shiraishi et al [7] proposed modelling the film heat transfer coefficient using their boiling correlation when its value exceeded the value predicted by the evaporation models. Although the results at the high heat fluxes appear similar to the thermosyphon boiling correlations proposed in Shiraishi et al [7], the transition here appears after the intersection of the evaporation and boiling curves and appears to more closely correspond to the transition in the flow regime.

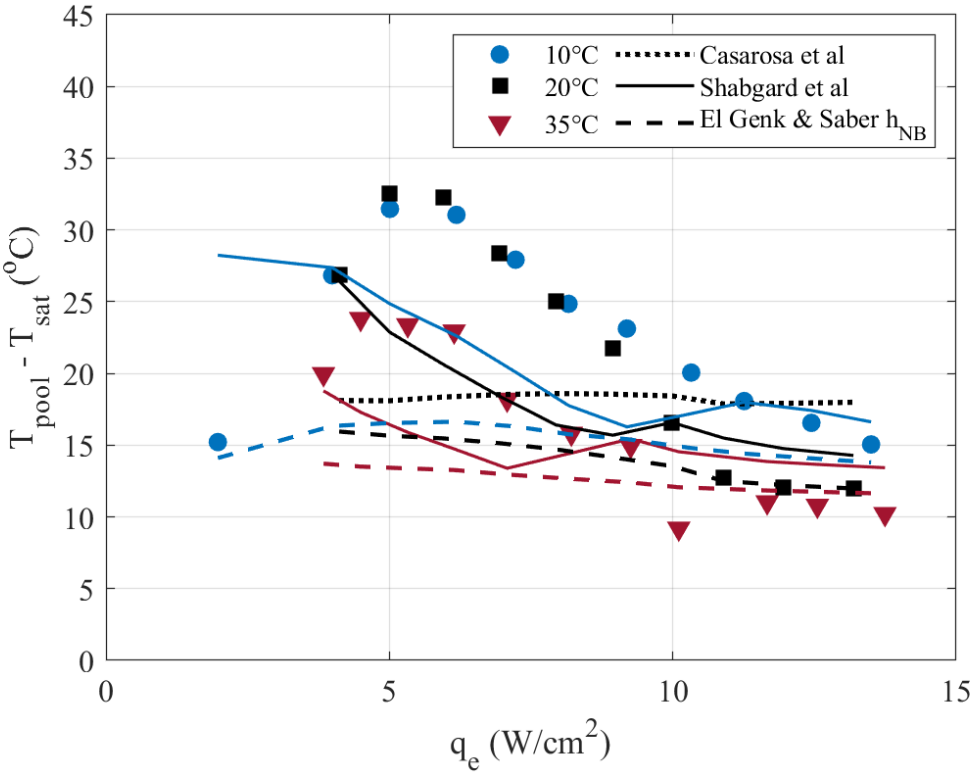

Figure 3.10. Change in the wall superheat in the pool region with evaporator heat flux. Correlations are for the inlet cooling water temperature denoted with line colours corresponding to the symbols.

The performance of the condenser was characterized based on the difference between the saturation temperature and the average of two wall temperatures measured along the length of the condenser section. The change in the condenser heat transfer coefficient with heat flux and the resulting Nusselt number $(h_c(\nu_l^2/g)^{1/3}/k_l)$ with the film Reynolds number (Γ/μ) are shown in Figure 3.11. The Nusselt number is defined as the ratio of convection heat transfer to conduction heat transfer [34]. Representing results as Nusselt number allows for a dimensionless comparison for heat transfer rate.

The heat transfer coefficients are substantially lower than the predictions from the Nusselt film condensation model, consistent with the measurement for a grooved vertical thermosyphon with water as a working fluid in [10]. This differed from the results for grooved thermosyphons with refrigerants [10][35] where a significant heat transfer enhancement was observed or methanol [10] where little effect was observed. The effect of the inclination has not been included in the prediction but would be expected to result in a 5 to 10 percent increase in the predicted value [37],[38]. The Nusselt number decreased with increasing Reynolds number unlike the results in [9][39] or the results for the semi-empirical pressure correction in the Wang and Ma correlation [37]. The results appeared to follow a trend similar to the predictions from the Rohsenow model [2] (in Table 3.4) that included a reduced pressure correction $1.51\ (P_v/P_{crit})^{0.14}$ and a subcooling correction to the Nusselt film condensation model. The change in heat transfer coefficient normalized by the heat transfer coefficient for the Nusselt film model with the subcooling correction with the reduced pressure are shown in Figure 3.12. The results show that the ratio approximately varied with $(P_{sat}/P_{crit})^{0.14}$ as in the Rohsenow model and not a higher power such as $P_{sat}^{0.37}$ found in Wang and Ma [37]. The modified correlation given by

$$h = \left\{0.954 * \left(\frac{P_v}{P_{crit}}\right)^{0.14}\right\} * 0.943 \left\{\frac{\rho_l(\rho_l-\rho_v)g{k_l}^3}{\mu_l L_c(T_{sat}-T_w)}\left[i_{lv} + {}^3/_8\, C_{pl}(T_{sat}-T_w)\right]\right\}^{1/4} \qquad (3)$$

with the properties evaluated at $T_w + 0.31(T_{sat} - T_w)$ as in the Rohsenow model [2], were in reasonable agreement with the experimental results as shown in Figure 3.13.

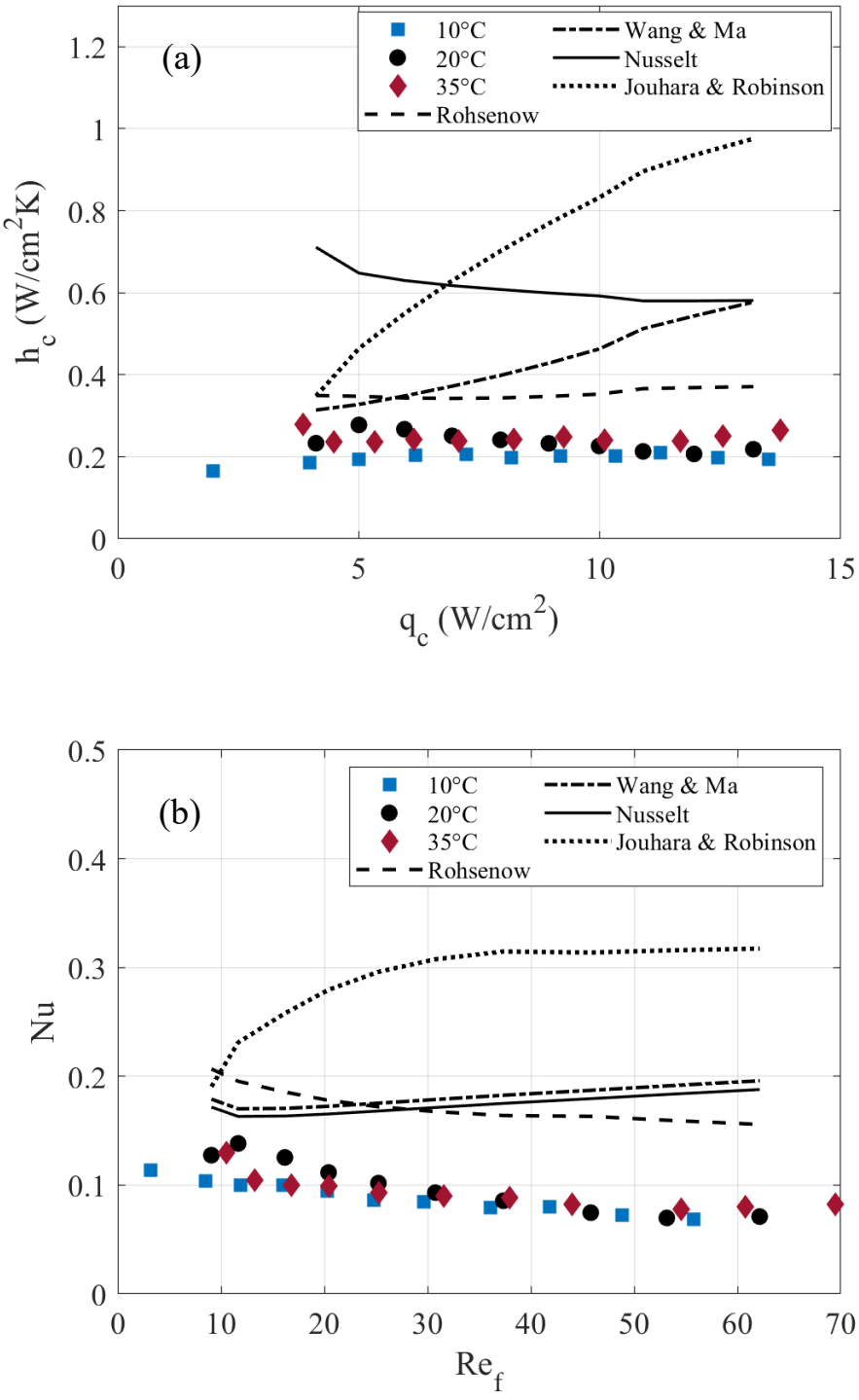

Figure 3.11. Change in the (a) condenser heat transfer performance with heat flux and (b) the resulting Nusselt number with film Reynolds number.

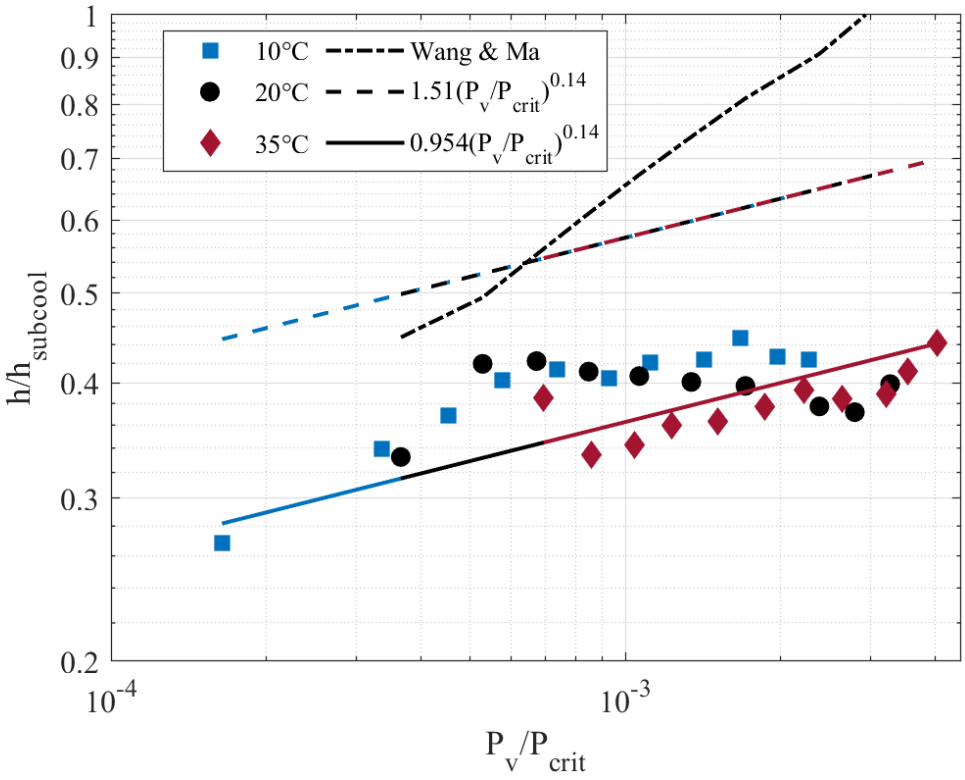

Figure 3.12. Effect of the reduced pressure on the condenser performance

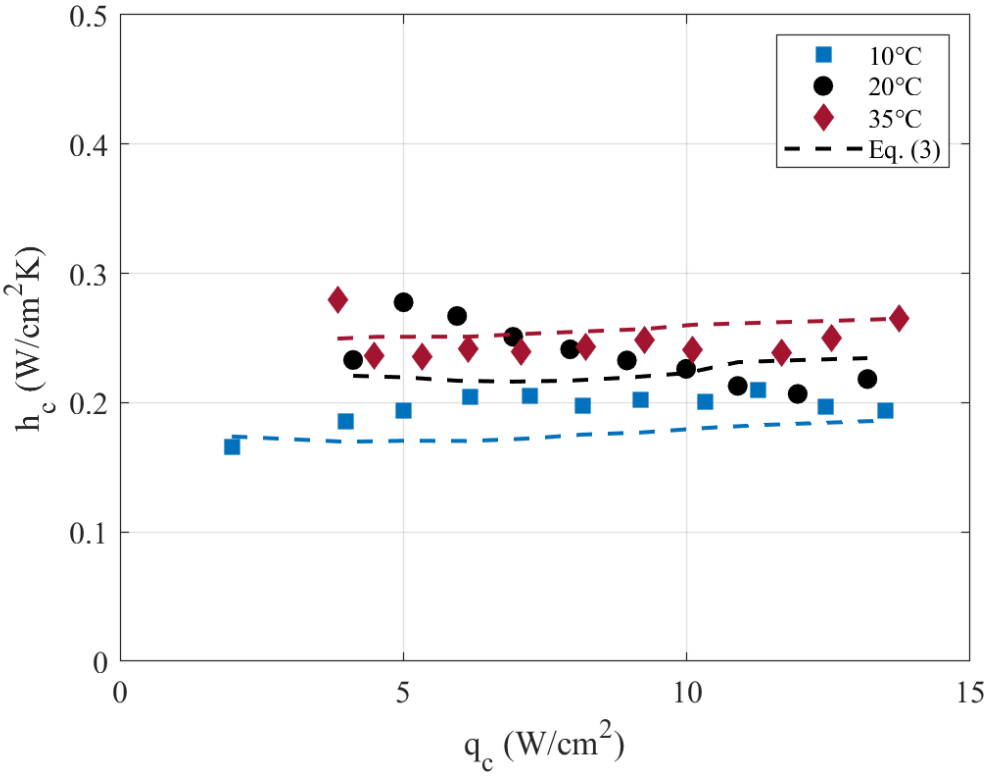

Figure 3.13. Comparison of the condenser performance with proposed correlation (equation 3).

3.6 Conclusion

Measurements were performed to characterize the heat transfer performance of a grooved copper-water thermosyphon with a 310 mm long vertical section embedded into a plate that was heated over the central 254 mm. The condenser was 346 mm and near vertical and the fluid loading occupied approximately 35 percent of the embedded length. Tests were performed for heat transfer rates from 250W (2 W/cm^2) up to 1625W (13.5 W/cm^2). The average temperature varied significantly along the evaporator at moderate heat transfer rates showing the existence of a pool and film region. The temperature profile along the evaporator became more uniform with increasing heat transfer. Increasing the operating temperature or the condenser cooling water also improved the uniformity of the evaporator temperature profile. Transients of the evaporator wall

temperatures show evidence of bubbly, slug and churn flow patterns. The flow regime map based on the confinement and vapour production values proposed by Smith et al. [12] was unable to predict the flow regimes. The map based on the liquid and vapor momentum flux in Smith et al. [13] showed more promise though there were differences in the boundaries. The heat transfer coefficient in both the pool and film region of the thermosyphon was found to be influenced by the internal flow pattern. The flooding or boiling limits in the thermosyphon was examined through the change in Kutateladze number with heat flux and saturation temperature. There was no evidence that the performance was limited by the flooding and boiling limits. The condenser heat transfer was lower than those predicted by the Nusselt film condensation model, but consistent with those for a grooved vertical thermosyphon. A modified Rohsenow model proposed here was able to accurately predict the condenser performance.

Table 3.1

Flooding/Entrainment Limit

Imura et al. [3]	$Ku = 0.16\langle 1 - exp\left[-\left({}^{D}/_{L_e}\right)\left({}^{\rho_v}/_{\rho_l}\right)^{0.13}\right]\rangle$
Tien and Chung [20]	$Ku = \dfrac{3.2tanh^2\left(0.5Bo^{1/4}\right)}{4\left({}^{L_e}/_{D}\right)\left[1+(\rho_v-\rho_l)^{1/4}\right]^2}$
Faghri et al. [21]	$Ku = \dfrac{3.2tanh^2\left(Bo^{1/4}\right)}{4\left({}^{L_e}/_{D}\right)\left[1+(\rho_v-\rho_l)^{1/4}\right]^2}$

Table 3.2

Nucleate pool boiling, thermosyphon pool, and thermosyphon evaporator correlations

Rohsenow [22]	$h = \left(\frac{\mu_l h_{fg}}{L_b}\right)^{0.33} \frac{c_{pl}}{C_{s,f} h_{gh} Pr_l^n} q^{2/3}$
Imura et al. [23]	$h = 0.32\left(\frac{p_l{}^{0.65} k_l{}^{0.3} C_{pl}{}^{0.7} g^{0.2}}{p_v{}^{0.25} h_{fg}{}^{0.4} \mu_l{}^{0.1}}\right)\left(\frac{P_v}{P_{atm}}\right)^{0.3} q^{0.4}$
Shiriashi et al [7]	$h = 0.32\left(\frac{p_l{}^{0.65} k_l{}^{0.3} C_{pl}{}^{0.7} g^{0.2}}{p_v{}^{0.25} h_{fg}{}^{0.4} \mu_l{}^{0.1}}\right)\left(\frac{P_v}{P_{atm}}\right)^{0.23} q^{0.4}$
Padovan et al [5]	$h = 231 p_r^{023} M^{-0.93} (Bo^2)^{0.14} q^{0.41}$
Labunstov [29]	$h = 0.075\left[1 + 10\left(\frac{\rho_v}{\rho_l - \rho_v}\right)^{0.67}\right]\left(\frac{k_l^2}{v_l \sigma (T_{sat} + 273.15)}\right)^{0.33} (q)^{0.67}$
Stephan and Abdelsalam [25]	$Nu = 0.246 * 10^7 X_1^{0.673} X_4^{-1.58} X_3^{1.26} X_{13}^{5.22}$ $X_1 = \frac{(qd)}{(k_l T_{sat})}, X_3 = \frac{\left((c_p) T_{sat} d^2\right)}{\alpha_l^2}, X_4 = \frac{((h_{fg}) d^2)}{\alpha_l^2}, X_{13} = \frac{(\rho_l - \rho_v)}{\rho_l},$ $d = 0.146\beta b, \;\; b = \left[\frac{2\sigma}{g(\rho_l - \rho_v)}\right]^{1/2}$ $Note: c_p \; in \left(\frac{kJ}{kg\,K}\right), \;\; h_{fg} \; in \left(\frac{kJ}{kg}\right), \qquad \beta = 45° \; for \; water$
El Genk and Saber [26]	
Natural Convection (NC)	$h = \left(\frac{k_l}{D_i}\right) 0.475 Ra^{0.35} \left(\frac{L_b}{D_i}\right)^{0.58}$
Nucleate Boiling (NB)	$h = (1.0 + 4.95\psi) h_{ku} \quad ; \qquad h_{ku} = 6.95x10^{-4} \left(\frac{k_l}{l_m}\right) Pr_l^{0.35} \left(\frac{q L_b}{\rho_v h_{fg} v_l}\right)^{0.7} \left(\frac{P L_b}{\sigma}\right)^{0.7}$ $\psi = \left(\rho_v / \rho_l\right)^{0.4} \left[\left(\frac{p v_l}{\sigma}\right)\left(\frac{\rho_l^2}{\sigma g (\rho_l - \rho_v)}\right)^{0.25}\right]^{0.25}$
Casarosa [47]	$h = 2.925 P_v{}^{0.18} q^{2/3}$
Shabgard et al [27]	$h = \left(1 - \frac{X}{10^6}\right)^{0.75} h_{sc} + \left(\frac{X}{10^6}\right)^{0.75} h_{TC} \qquad X < 10^6$ $h = h_{TC} = 4\left(\frac{k_l}{D_i}\right)(ArFr^{0.5})^{1/3} Pr_l^{0.5} \left(\frac{Bo}{10}\right)^n$ [28] $\qquad 10^6 \le X \le 2 \times 10^6$ $n = 1/2 \text{ for } Bo \le 10$ $n = 1/6 \; for \; Bo > 10$ $h = \left(\frac{10}{8} - \frac{X}{8x10^6}\right)^{0.75} h_{TC} + \left(\frac{X}{8x10^6} - \frac{2}{8}\right)^{0.75} h_{NB} \qquad 2 \times 10^6 < X < 10^7$ $h = h_{NB} = 0.32\left(\frac{p_l{}^{0.65} k_l{}^{0.3} C_{pl}{}^{0.7} g^{0.2}}{p_v{}^{0.25} h_{fg}{}^{0.4} \mu_l{}^{0.1}}\right)\left(\frac{P_v}{P_{atm}}\right)^{0.3} q^{0.4}$ [23] $\qquad X > 10^7$

$$X = \Psi(RaPr_l)^{0.35}\left(\frac{P_v L_b^2 q_e^{"}}{\sigma \rho_v h_{fg} v_l}\right)^{0.7},\ \Psi = \left(\frac{\rho_v}{\rho_l}\right)^{0.4}\left[\frac{P_v v_l}{\sigma}\left(\frac{\rho_l^2}{\sigma g(\rho_l - \rho_v)}\right)^{0.25}\right]^{0.25} \quad [26]$$

$$h_{sc} = \begin{cases} 0.75\left(\frac{k_l}{L_p}\right)Ra^{0.2}, & 10^5 < Ra < 10^{13} \\ 0.645\left(\frac{k_l}{L_p}\right)Ra^{0.22}, & 10^{13} < Ra < 10^{16} \end{cases}$$

Table 3.3

Film evaporation correlations

Inverse Nusselt [32]	$h = \left(\frac{4}{3}\right)^{1/3}\left(\frac{k^3 g}{v^2}\right)^{1/3}\left(\frac{4\Gamma}{\mu}\right)^{-1/3}$
Chun and Seban [32]	$h = 0.606\left(\frac{k^3 g}{v^2}\right)^{1/3}\left(\frac{\Gamma}{\mu}\right)^{-0.22}\ when\ \left(\frac{4\Gamma}{\mu}\right) > 2.43\left(\frac{\mu^4 g}{\rho\sigma^3}\right)^{-1/11}$
Alhusseini et al. [33]	$h = \left(\frac{k^3 g}{v^2}\right)^{1/3} 2.65\left(\frac{4\Gamma}{\mu}\right)^{-0.158}\left(\frac{\mu^4 g}{\rho\sigma^3}\right)^{0.0563}$

Table 3.4

Condensing falling film heat transfer models

Nusselt [2]	$h = h_{Nusselt} = 0.943\left(\frac{\rho_l(\rho_l - \rho_v)h_{fg}k_l^3 g}{\mu_l(T_{sat} - T_w)L_c}\right)^{1/4}$
Rohsenow [2]	$h = 1.51\left(\frac{P_v}{P_{crit}}\right)^{0.14} * 0.943\left\{\frac{\rho_l(\rho_l - \rho_v)g{k_l}^3}{\mu_l L_c(T_{sat} - T_w)}\left[h_{fg} + {}^3/_8\, C_{pl}(T_{sat} - T_w)\right]\right\}^{1/4}$
	properties evaluated at $T_w + 0.31(T_{sat} - T_w)$
Wang and Ma [37]	$h = h_{Nusselt}P_v^{0.37}\left(\frac{L_c}{R}\right)^{\frac{cos\beta}{4}}[0.41 - 0.72\psi - (62.7\psi^2 - 14.5\psi - 7.1)\beta/1000]$
	$\psi = V_f/V_{tot} \quad \beta - from\ horizontal\ (^o)\ \ P_v\ (bar)$
Jouhara and Robinson [9]	$h = 0.85\left(\frac{4\Gamma}{\mu}\right)^{0.1} exp\left[-6.7x10^{-5}\left(\frac{\rho_l}{\rho_v}\right) - 0.14\right]h_{Nusselt}$

3.7 Appendix

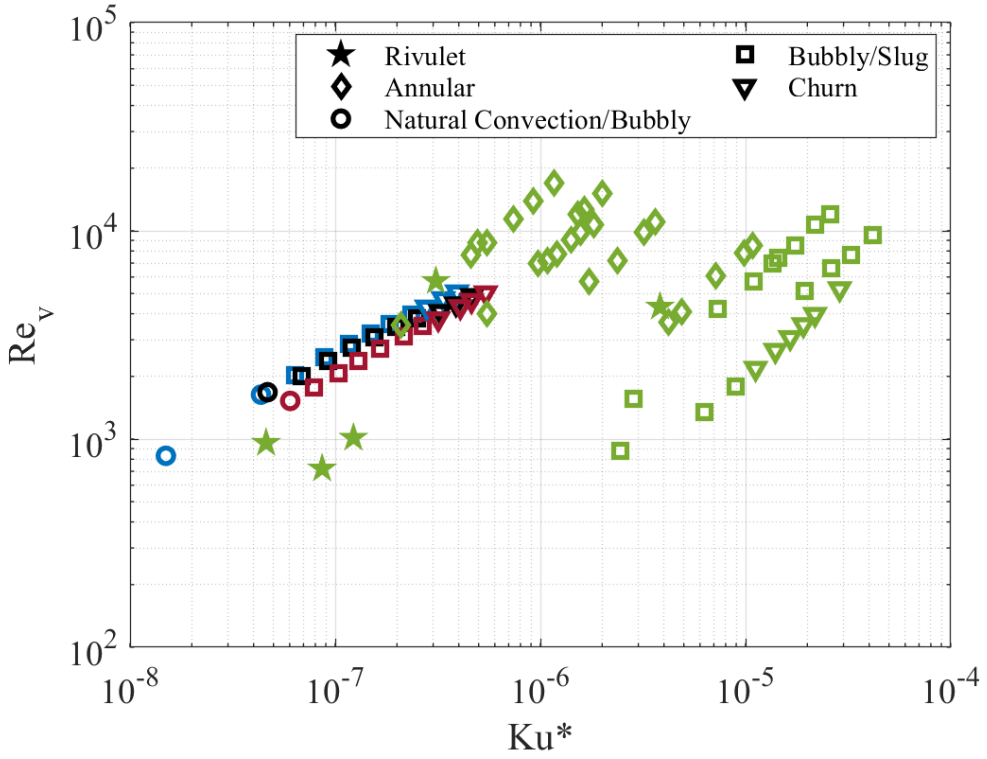

Figure 3.14. Comparison of flow regimes with the flow map of Terdtoon et al. [15, 16] at condenser cooling water temperature of [Blue] 10°C, [Black] 20°C and [Maroon] 35°C. The data of Terdtoon et al. are in [Green].

Acknowledgments

The support from the Natural Sciences and Engineering Research Council (NSERC) of Canada and the Ontario Centres of Excellence (OCE) is gratefully acknowledged. Funding was also provided by MERSEN Canada Inc.

3.8 References

[1] Park YJ, Kang HK, Kim CJ. Heat transfer characteristics of a two-phase closed thermosyphon to the fill charge ratio. Intl Journal of Heat and Mass Transfer. 2002; 45(23):4655-61.

[2] Vasiliev L, Lossouarn D, Romestant C, Alexandre A, Bertin Y, Piatsiushyk Y, Romanenkov V. Loop heat pipe for cooling of high-power electronic components. Intl Journal of Heat and Mass Transfer. 2009; 52(1-2):301-8.

[3] Agostini F, Gradinger T, Cottet D. Compact gravity driven and capillary-sized thermosyphon loop for power electronics cooling. Journal of Thermal Science and Engineering Applications. 2014; 6(3).

[4] Kim Y, Shin DH, Kim JS, You SM, Lee J. Boiling and condensation heat transfer of inclined two-phase closed thermosyphon with various filling ratios. Applied Thermal Engineering. 2018; 145:328-42.

[5] Padovan A, Bortolin, S, Rossato, M, Filippeschi S, Del Col D. Vaporization heat transfer in a small diameter closed two-phase thermosyphon, J. of Heat Transfer, 141, 091811-1.

[6] Robinson AJ, Smith K, Hughes T, Filippeschi S. Heat and mass transfer for a small diameter thermosyphon with low fill ratio. Intl Journal of Thermofluids. 2020; 1:100010.

[7] Shiraishi M, Kikuchi K, and Yamanishi T Investigation of heat transfer characteristics of a two-phase closed thermosyphon, J. of Heat Rec Systems, 1981; 1 287-297.

[8] Jafari D, Di Marco P, Filippeschi S, Franco A. An experimental investigation on the evaporation and condensation heat transfer of two-phase closed thermosyphons. Exptl Thermal and Fluid Science, 2017; (88) 111-23.

[9] Jouhara H, Robinson AJ. Experimental investigation of small diameter two-phase closed thermosyphons charged with water, FC-84, FC-77 and FC-3283. Applied Thermal Engineering. 2010; 30(2-3):201-11.

[10] MacGregor RW, Kew PA, Reay DA. Investigation of low global warming potential working fluids for a closed two-phase thermosyphon. Applied Thermal Engineering. 2013; 51(1-2): 917-25.

[11] Casarosa C, Latrofa E, Shelginski A. The geyser effect in a two-phase thermosyphon. Intl Journal of Heat and Mass Transfer. 1983; 26(6):933-41.

[12] Smith K, Kempers R, Robinson AJ. Confinement and vapour production rate influences in closed two-phase reflux thermosyphons Part A: flow regimes. Intl Journal of Heat and Mass Transfer. 2018; 119:907-21.

[13] Smith K, Robinson AJ, Kempers R. Confinement and vapour production rate influences in closed two-phase reflux thermosyphons Part B: heat transfer. Intl Journal of Heat and Mass Transfer. 2018; 120:1241-54.

[14] Terdtoon P, Chailungkar M, Ritthidej S, Shiraishi M. (1997) Effects of Bond number on internal flow patterns of an inclined, closed, two-phase thermosyphon at normal operating conditions, Experimental Heat Transfer. 1997; 10:4, 233-251.

[15] Terdtoon P, Chailungkar M, Shiraishi M. Effects of aspect ratios on internal flow patterns of an inclined closed two-phase thermosyphon at normal operating condition, Heat Transfer Engineering. 1998, 19:4, 75-85.

[16] Grooten MH, Van der Geld CW, Van Deurzen LG, Butrymowicz D. A study of flow patterns in a thermosyphon for compact heat exchanger applications. In Proc. 5th Int. Conf. on Transport Phenomena in Multiphase Systems, HEAT 2008 (Vol. 2, pp. 323-328).

[17] Carey VP. Liquid-vapor phase-change phenomena: an introduction to the thermophysics of vaporization and condensation processes in heat transfer equipment. CRC Press; 2018 Aug 15.

[18] Imura H, Sasaguchi K, Kozai H, Numata S. Critical heat flux in a closed two-phase thermosyphon. Int. Journal of Heat and Mass Transfer. 1983; 26(8):1181-1188.

[19] Faghri, A. Heat Pipe Science and Technology, 1995 Taylor and Francis, New York.

[20] Tien CL, Chung KS. Entrainment limits in heat pipes. AIAA Journal. 1979; 17(6): 643-646.

[21] Faghri A, Chen MM, Morgan M. Heat transfer characteristics in two-phase closed conventional and concentric annular thermosyphons. 1989; 111(3) 611-618

[22] Rohsenow WM. A method of correlating heat transfer data for surface boiling of liquids. Cambridge, Mass. *MIT Division of Industrial Cooperation*, 1951

[23] Imura H, Kusuda H, Ogata J-I, Miyazaki T, Sakamoto N. Heat transfer in two-phase closed-type thermosyphons, Japan Society of Mechanical Engineers, Transactions, Series B, 45, 1979 (393), 712-722.

[24] Labuntsov DA. Heat transfer problems with nucleate boiling of liquids. Therm. Eng.(USSR)(Engl. Transl.). 1993; v. 19, no. 9, pp. 21-28. 1973 Sep 1.

[25] Stephan K, Abdelsalam M. Heat-transfer correlations for natural convection boiling. International Journal of Heat and Mass Transfer. 1980 Jan 1;23(1):73-87.

[26] El-Genk MS, Saber HH. Heat transfer correlations for small, uniformly heated liquid pools. Int. Journal of Heat and Mass Transfer. 1998; 41(2):261-74.

[27] Shabgard H, Xiao B, Faghri A, Gupta R, Weissman W. Thermal characteristics of a closed thermosyphon under various filling conditions, Int. Journal of Heat and Mass Transfer, 2014, 70, 91-102.

[28] Gross U. Pool boiling heat transfer inside a two-phase thermosyphon correlation of experimental data. Proceedings of the 9th International Heat Transfer Conference, Jerusalem, Israel, 1990, pp. 57-62.

[29] Vachon RI, Nix GH, Tanger GE. Evaluation of Constants for the Rohsenow Pool-Boiling Correlation. ASME. J. Heat Transfer. 1968; 90(2): 239–246.

[30] Guichet V, Almahmoud S, Jouhara H, Nucleate pool boiling heat transfer in wickless heat pipes (two-phase closed thermosyphons): A critical review of correlations, Thermal Science and Engineering Progress, Volume 13, 2019, 100384.

[31] McGillis WR, Carey VP, Fitch JS, Hamburgen WR. Boiling binary mixtures at subatmospheric pressures. In IEEE Proceedings of Intersociety Conference on Thermal Phenomena in Electronic Systems. 1992; (pp. 127-136).

[32] Chun KR, Seban RA. Heat transfer to evaporating liquid films, ASME Journal Heat Transfer. 1971; 391-396.

[33] Alhusseini AA, Tuzla K, Chen JC. Falling film evaporation of single component liquids, Int. Journal of Heat and Mass Transfer, 1998; 41(12), 1623-1632.

[34] Astakhov VP. Environmentally friendly near-dry machining of metals. InMetalworking Fluids (MWFs) for Cutting and Grinding 2012 Jan 1 (pp. 135-200). Woodhead Publishing.

[35] Park YJ, Kang HK, Kim CJ, Heat transfer characteristics of a two-phase closed thermosyphon to the fill charge ratio, International Journal of Heat and Mass Transfer, 45 (23), 2002.

[36] Guichet V., Hussam J. Condensation, evaporation and boiling of falling films in wickless heat pipes (two-phase closed thermosyphons): A critical review of correlations, International Journal of Thermofluids, 2020; 1–2, 100001.

[37] Wang JC, Ma Y. Condensation heat transfer inside vertical and inclined thermosyphons. Journal of Heat Transfer. 1991;113(3):777-80.

[38] Hussein H.M.S., Mohamad M.A., El-Asfouri A.S., Theoretical analysis of laminar-film condensation heat transfer inside inclined wickless heat pipes flat-plate solar collector, Renewable Energy. 2001; 23, Issues 3–4, 525-535.

[39] Hashimoto H, Kaminaga F. Heat transfer characteristics in a condenser of closed two-phase thermosyphon: Effect of entrainment on heat transfer deterioration. Heat Transfer—Asian Research: Co-sponsored by the Society of Chemical Engineers of Japan and the Heat Transfer Division of ASME. 2002; 31(3):212-25.

Chapter 4: Heat Transfer and Hysteresis Characteristics in an Elbow Thermosyphon

Complete citation:

Hammouda, M.G., Ewing, D., Zaghlol, A., Ching, C.Y., Heat Transfer and Hysteresis Characteristics in an Elbow Thermosyphon, Thermal Science and Engineering Progress (Submitted).

Relative Contributions:

M.G. Hammouda: Performed all experiments, interpretation and analysis of the data and wrote the first draft of the manuscript including all figures and text.

D. Ewing: Assisted in the interpretation and discussion of results.

A. Zaghlol: Industry liaison. Provided context from an industry perspective.

C. Y. Ching: Supervisor of M.G. Hammouda and was responsible for the final editing and submission to the journal.

4.1 Abstract

Measurements were performed to characterize the performance of a grooved copper-water elbow thermosyphon with a fluid loading of 30%, typical of thermosyphons used for power electronic devices. The evaporator section was vertical, while the condenser section was inclined at an angle 8 degrees to the horizontal. The performance of the device, characterized for incrementally increasing and decreasing heat transfer rates, shows a significant hysteresis in the evaporator performance at moderate heat transfer rates or fluxes (between 2 and 8 W/cm2). The difference was due to changes in the upper portion or film region of the evaporator. Transients of the temperature suggest a change to a more dynamic flow regime in the evaporator at a heat flux of approximately 6 W/cm2. The transition occurred at similar heat fluxes for both the increasing and decreasing heat transfer rates. The improved performance in the upper or film region was observed after the dynamic regimes, suggesting it may be due to the wetting of the internal structure during this process. The effect was reduced with increasing operating temperature.

Keywords: Elbow thermosyphon; Evaporator performance; Performance hysteresis;

4.3 Nomenclature

Bo Bond number $D\sqrt{g[(\rho_l - \rho_v)/\sigma]}$

c_{pl} Specific heat of cooling water, (J/kg K)

$C_{s,f}$ Function of surface Fluid (0.013)

D Inner diameter of thermosyphon, (m)

g Gravitational acceleration, (m/s^2)

h_{fg} Latent heat of water, (J/kg)

h_e Heat transfer coefficient of evaporator pool, (W/m^{2}K)

h_f Heat transfer coefficient of falling film, (W/m^{2}K)

k_l Thermal conductivity of water, (W/m K)

Ku Kutateladze number

L_c Condenser length, (m)

L_b Bubble length scale $\sqrt{\sigma/[g(\rho_l - \rho_v)]}$ (m)

l_o Viscous length scale $(v_l^2/g)^{1/3}$ (m)

M Molecular weight, (kg/kmol)

Nu Nusselt Number $(h_c/k_l)(v_l{}^2/g)^{1/3}$

P_{crit} Critical vapour pressure of water, (pa)

Pr Prandtl number

P_{sat} Internal saturation pressure, (pa)

q_e Evaporator wall heat flux, (W/m^2)

Ra Rayleigh number $(\beta g D^4 q_e/k_l \alpha_l v_l)$

Re_{fb} Falling film boiling Reynolds number $(q"L_b\rho_l)/(h_{fg}\rho_v\mu_l)$

Re_f Reynolds Number $Q/\pi D h_{fg} \mu_l$

T_e Nominal temperature across length of evaporator, (°C)

T_{AD} Temperature at adiabatic section, (°C)

$T_{w.in}$ Temperature at water jacket inlet, (°C)

$T_{w,out}$ Temperature at water jacket outlet, (°C)

T_{cond} Average condenser wall temperature, (°C)

T_{sat} Saturation Temperature, (°C)

Γ Mass flow per unity width $Q/h_{gh}\pi D_i$ (kg/ms)

μ_l Dynamic viscosity of liquid water, (Pa s)

v_l Kinematic viscosity of liquid, (m^2/s)

ρ_l Density of liquid water, (kg/m^3)

ρ_v Density of saturated water vapour, (kg/m^3)

σ Surface tension of water, (N/m)

α_l Thermal diffusivity, ($m^2\ s^{-1}$)

β Thermal expansion coefficient, (K^{-1})

4.4 Introduction

Thermosyphons are two phase heat transport systems that operate by evaporating liquid working fluid from a hot region and condensing the vapor in a lower temperature region. The condensed liquid is returned to the evaporator section by gravity alone, unlike in wicked heat pipes[1]. The performance of a thermosyphon is dependent on several factors including the length of the thermosyphon sections, the fill ratio, the diameter or bubble confinement, and inclination angle of the thermosyphon[1]-[3]. The performance of the evaporator section in the thermosyphon is often characterized using nucleate pool boiling models[4], or thermosyphon specific models [5]-[7] as discussed in[9], while the condenser performance is typically modeled using film condensation models[10]. For smaller fluid loadings, the presence of a liquid pool and film region can affect the performance along the evaporator[11][12]. The effect of this can be modelled using separate models for the pool and film regions to predict the temperature distribution along the thermosyphon as in [11] or by estimating the resistance using a parallel resistance model[13]. Visualizations of the flow within the thermosyphons [14]-[19] show that a range of flow regimes can occur within the evaporator that can affect the heat transfer throughout the evaporator section and thus may not be well modelled in this separated manner.

The aforementioned investigations of thermosyphons have largely focused on straight thermosyphons. The geometry and orientation of thermosyphons can be changed to better fit specific applications, such as incorporating a bend along the midsection to allow the condenser and evaporator to be mounted at different orientations. The performance of elbow thermosyphons with a vertical evaporator and horizontal condenser, and horizontal evaporator and vertical condenser was considered in[20]. The thermosyphon with vertical evaporator and horizontal condenser performed the better of the two, though neither performed as well as a straight vertical

thermosyphon. The performance of a 90 degree elbow thermosyphon with a range of orientations, geometries and fluid loading was also considered in[21]. The optimal fluid loading was found to be 25-50%. Thermosyphons with short evaporator lengths (<10D) appeared to have poorer performance than devices with longer evaporator lengths. This was attributed to more dynamic boiling for the longer evaporators [21] as in straight thermosyphons[12]. The performance of elbow thermosyphons with a vertical condenser and the evaporator at different angles was also considered in[22]. Bend angles of 30 and 60 degrees were found to improve performance in terms of both thermal resistance and failure and mitigate oscillations due to geyser boiling.

The objective of this study was to investigate the performance of an elbow thermosyphon, typically of that used in power electronics applications to transport heat from a vertical plate to a plate-fin heat exchanger. The evaporator was vertical with a nominal heated length of approximately 10D. The condenser was oriented 8 degrees from the horizontal with a midsection bend of 82 degrees between the evaporator and condenser sections. Measurements were performed for water as the working fluid with a fill ratio of 30% under varying heat loads. The experimental methodology is presented in the next section. This is followed by a presentation of the results and finally the conclusions.

4.5 Experimental Facility

Measurements were performed for an internally grooved copper-water elbow thermosyphon with a vertical evaporator section and a condenser section at 8 degrees to the horizontal as shown in Figure 4.1. The thermosyphon has a 15.87 mm outer diameter and 0.5 mm wall thickness. The internal grooves had a height of 0.3 mm from the inner wall. The evaporator section of the thermosyphon was mounted in an aluminum heat spreader plate (61.7 mm wide, 52.8 mm thick, and 255.8 mm high).

Heat was applied to the heat spreader plate using a 140 mm long heating block (61.7 mm wide and 25.4 mm thick) with four embedded cartridge heaters. The cartridge heaters were wired in parallel and connected to a power transducer. The power to the heaters was controlled by a Variac (voltage regulator) and measured using a power transducer with an uncertainty of ±0.5%. The heating block was positioned on the heat spreader plate so that the bottom of the block was aligned with the bottom of the embedded thermosyphon. The heating block was attached to the heat spreader plate using bolts at each corner with thermal paste applied between the mating surfaces. Ten sheathed 0.5mm T-type thermocouples were inserted through holes drilled in the heat spreader plate to the outer wall of the thermosyphon evaporator. Five additional thermocouples were inserted at the mating surface between the heating block and heat spreader plate to the center of the heater block through 1 mm holes machined into the face of the heater block.

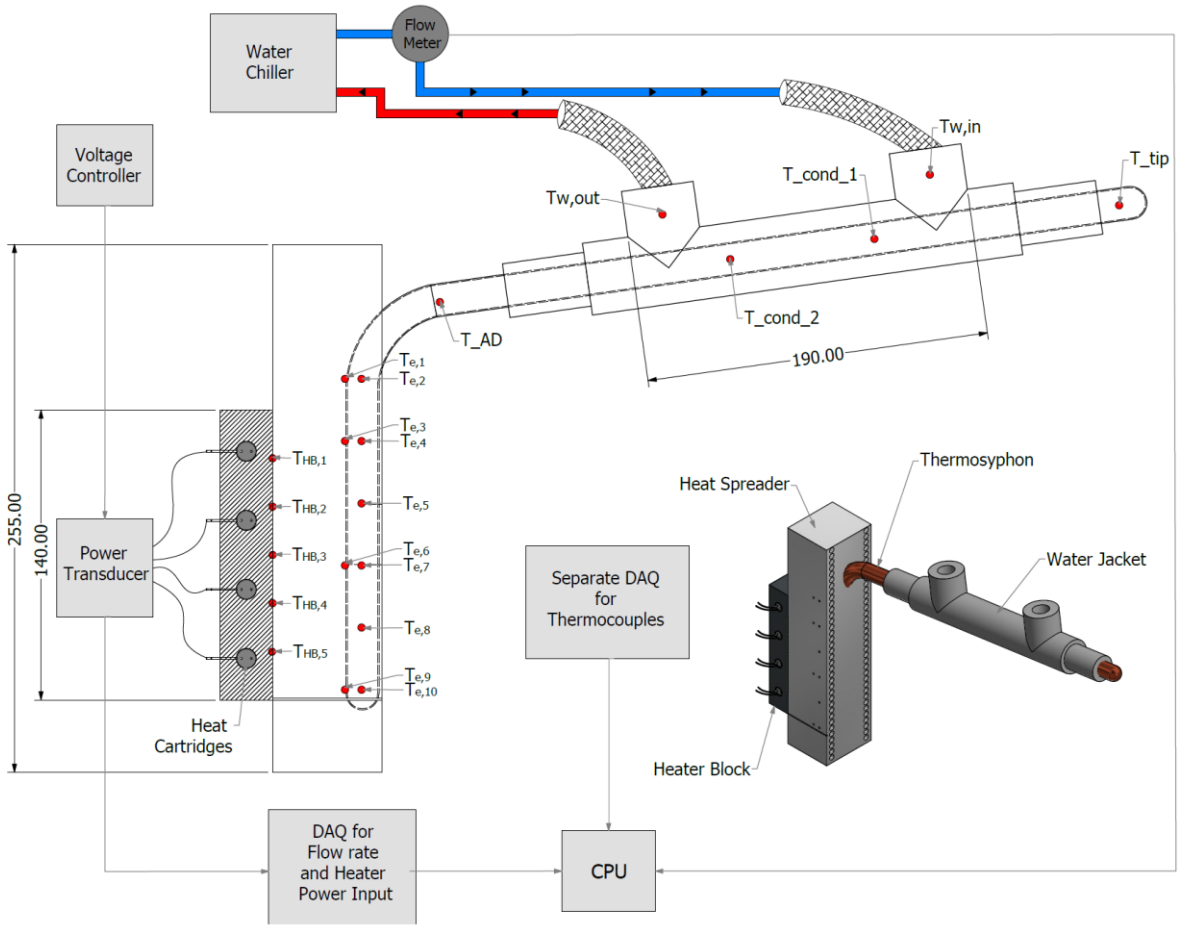

Figure 4.1. Schematic of the experimental facility

Heat was removed from the condenser section using a water jacket with an effective cooling length of 190 mm. The water jacket was constructed using threaded PVC pipe fittings (ID of 18.85 mm). Cooling water for the jacket at a flow rate of 1.2 L/min was supplied from a dedicated chiller that could control the inlet temperature to within ± 0.5°C. The flow rate was recorded using a turbine flowmeter with an uncertainty of ±0.5%, while the inlet and outlet water temperatures were measured using sheathed 0.5 mm T-type thermocouples. Two thermocouples were attached to the outer wall of the condenser section. One was located 4 cm from the water inlet and the other 4 cm from the outlet. The temperature in the adiabatic sections of the thermosyphon were measured using sheathed 0.5 mm

T-type thermocouples; one near the tip of the thermosyphon after the water jacket and one between the heat spreader plate and condenser section. All thermocouples were calibrated in a water bath and an oil bath using an RTD with an uncertainty of 0.01°C. The water bath was operated from 4°C to 95°C and the oil bath from 60°C to 160°C. The uncertainty in the temperature measurements was estimated as ±0.1°C. The outputs from the thermocouples and from the flow meter and power transducer were recorded using two A/D converters at a rate of 2 samples per second.

The experiments were performed using 7 mL of distilled water as the working fluid. This volume corresponded to the inner volume of the thermosyphon over approximately 30% of the heater plate length. The experiments were initiated by flowing water from the chiller through the water jacket on the condenser section with no heat input until the temperature of the thermosyphon reached a steady state. Power was then applied to the heaters. The system was operated until the temperature along the thermosyphon reached a steady state for at least 10 minutes before the power setting was changed and the process repeated. Measurements were performed for power inputs from 40W to 750W with inlet water temperatures of 10°C, 20°C and 35°C. Experiments were performed by two heating methods for each water temperature; one where the power was increased in increments from 40W to 750W, and second where the power was initially set to 850W and then decreased in decrements from 750W to 40W. The system was fully insulated during the measurements to minimize heat transfer to the ambient. The power input into the heaters and the heat removed from the condenser section evaluated by

$$Q_{out} = \rho_l c_{pl}\left(T_{w,out} - T_{w,in}\right) \tag{1}$$

agreed to within ±5% above 200W and within ±10% otherwise, as shown in Figure 4.2.

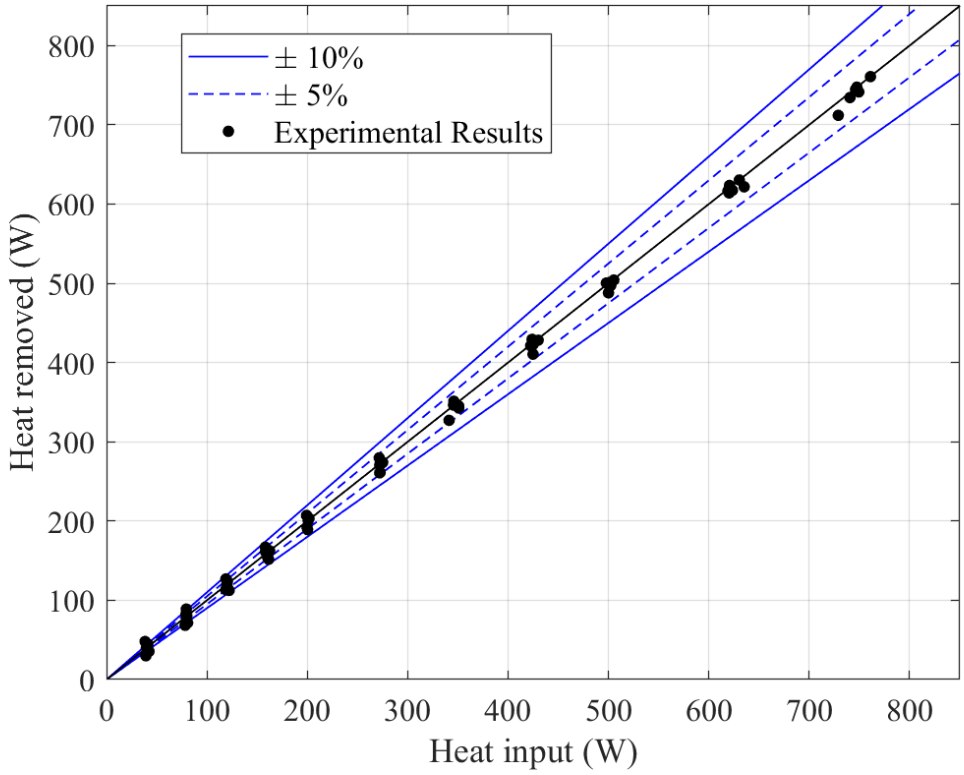

Figure 4.2. Energy balance between the heat input and heat removed.

4.6 Results and Discussion

The performance of the evaporator and condenser sections was characterized by considering the temperature differences between the sections and the saturation temperature estimated from the thermocouple reading in the adiabatic section between the sections. Distributions of the time averaged temperature on the thermosyphon evaporator relative to the saturation temperature are shown in Figure 4.3. The temperature at the bottom of the thermosyphon evaporator, that typically corresponds to the pool region [11] was consistently at a higher temperature than the upper section in both the experiments where the applied power was increased (left column in Figure 4.3) and those where it was decreased (right column). The temperatures in the bottom region of the evaporator show evidence

of a change in the operation in the thermosyphon, particularly in the experiments when the power was increased. In these cases, the temperature at the bottom of the thermosyphon decreased at powers near 425W before subsequently increasing. This transition occurs at higher powers as the cooling water temperature and operating pressure increased and was less evident for the highest water temperatures.

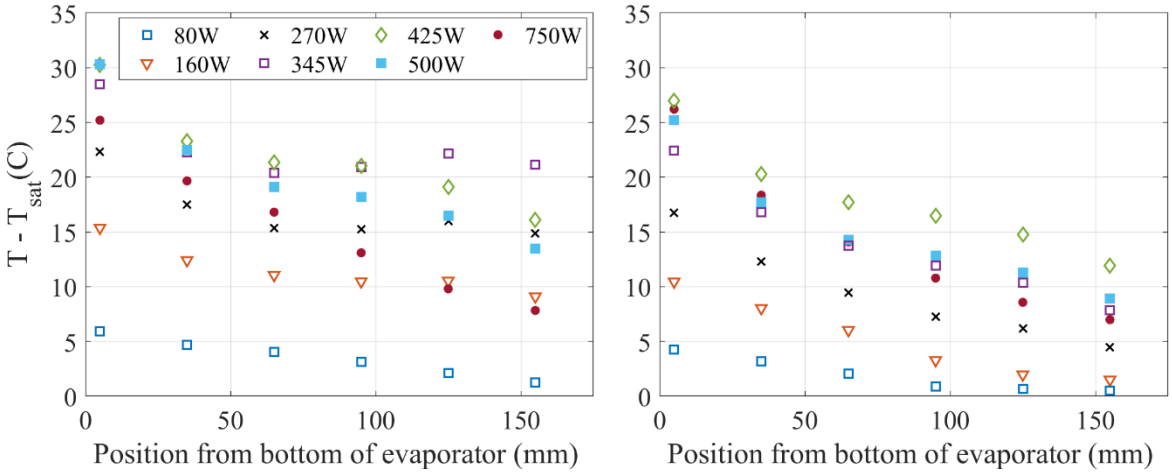

(a) 10°C

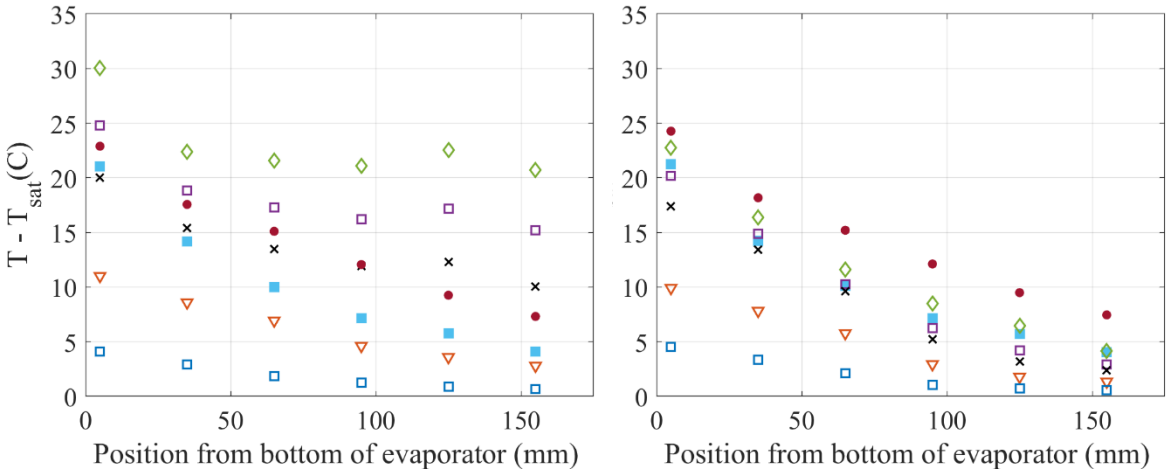

(b) 20°C

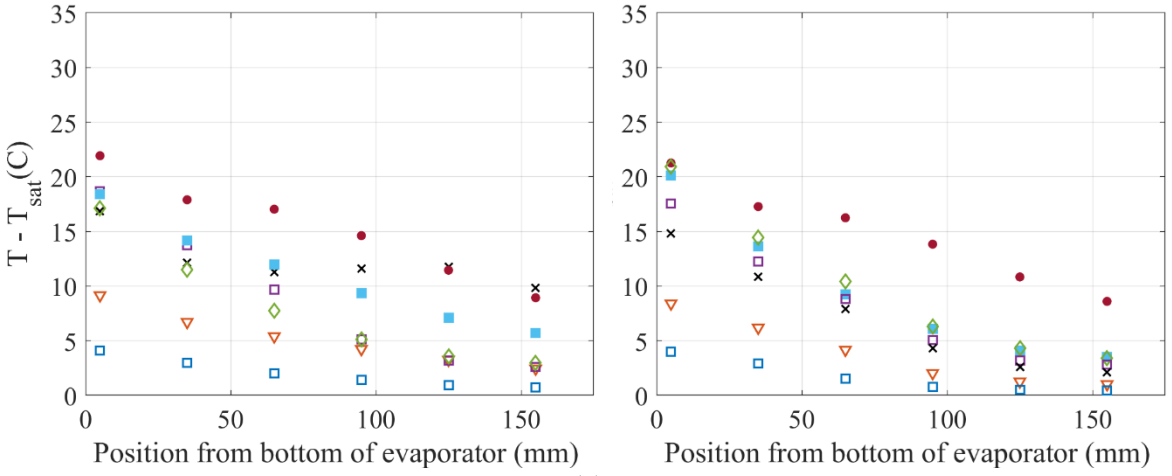

(c) 35°C

Figure 4.3 Variation in the time average temperature along the evaporator during increasing (left) and decreasing (right) power for cooling water temperatures of (a) 10°C, (b) 20°C, and (c) 35°C.

The temperature profiles in the upper portion of the evaporator section, typically associated with the film region [11] also showed a substantial change with heat transfer rate and the method of varying the heat transfer rate. The temperature on the upper section initially increased with the increasing power input before substantively decreasing at heat transfer rates of 425W and or 500W, depending on the temperature of the cooling water. The temperature in this region subsequently increased for a power input of 750W when the cooling water was 20°C and 35°C, but not for 10°C where the initial decrease occurred at a higher power. The nature of the temperature profile in the upper region also changed at this transition in the experiments where the power was incremented from a relatively uniform distribution at low powers to one where the wall temperature decreases along the length of the evaporator for the higher powers in the experiments. In the experiments where the power was decremented, the temperature profiles show a decrease in temperature along the length of the upper region for all powers. The temperature in this region initially increased as the power was decremented for the 10°C cooling water before subsequently decreasing. This was not the case for the water temperatures of 20°C and 35°C where the temperature in the upper region initially decreased before varying little for heat transfer rates between 500W and 270W and decreasing again.

The average heat transfer performance characterized by the entire length of the evaporator is shown Figure 4.4, along with typical correlations for the thermosyphon performance given in Table 4.1. Here, the evaporator surface area is based on the inside diameter of the thermosyphon and the heating block length, while the nominal evaporator temperature is the spatial average of the temperature along the length of the heater block. The uncertainty in the heat transfer coefficient was estimated to be in the range ±2.8% at the higher powers to ±5.6% at the lower powers. The results show an initial decrease in the heat transfer coefficient followed by an increase in the heat transfer coefficient that are typically associated with a film evaporation mode and boiling in the

film and pool, respectively[1]. The performance of the evaporator at low heat fluxes is better than the results for a smooth wall vertical evaporator for water from Kim et al.[25], similar to the results for a grooved thermosyphon with FC-72 in[26]. The performance at low heat fluxes was also greater than results seen in Hammouda et al. [27] with a vertical evaporator (14.87 mm inner diameter) and a condenser angled 8 degrees from vertical. The results at low and moderate heat fluxes show evidence of a significant hysteresis for the lower cooling water temperatures, with the average heat transfer coefficient in the experiments where the power was increased falling well below the results in the experiments where the power was decreased. The results for the lowest cooling water temperature also fell well below the results for the higher water temperature in this range even when the heat power input was decreased indicating that the operating temperature had a significant impact on the performance at moderate heat fluxes. The heat transfer coefficient for the higher cooling water temperatures, such as 20°C, appear to follow the trend of the Imura et al. [5] correlation until reaching a plateau near 8 W/cm^2, similar to the results for a fluid loading of 0.5 in [25]. The results here appear to plateau at a lower heat transfer coefficient than in Hammouda et al. [27]for a similar grooved thermosyphon with a longer evaporator and an 8 degree bend between the evaporator and condenser.

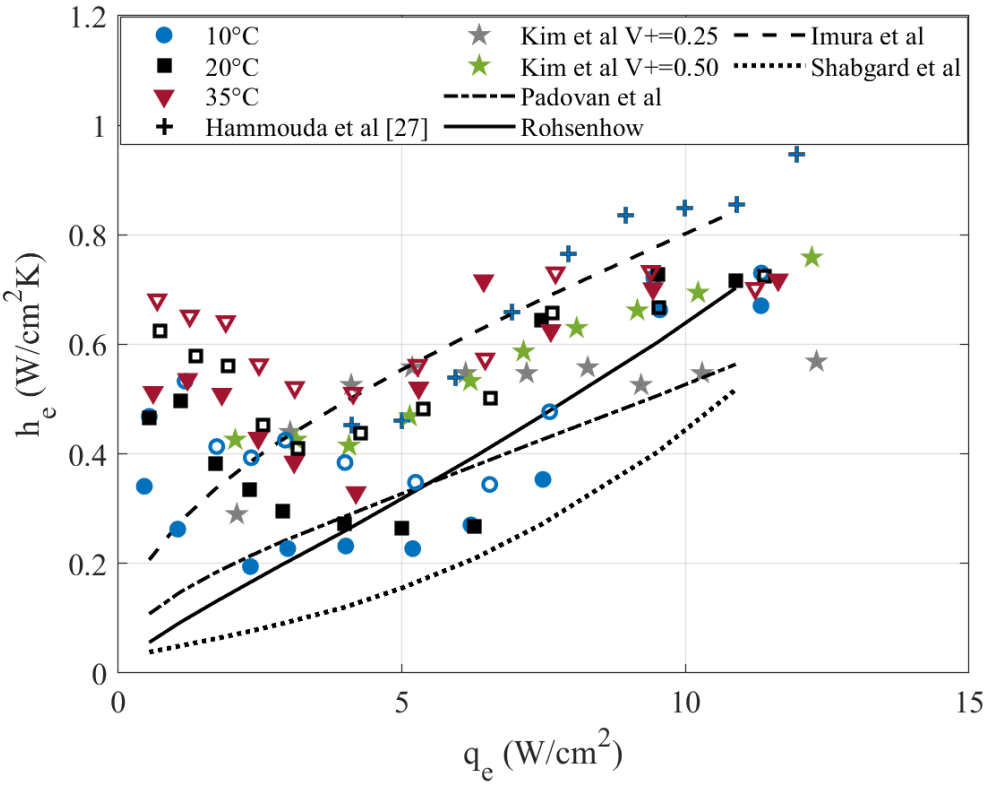

Figure 4.4. Comparison of the experimental evaporator performance with typical correlations. (filled symbols for increasing power and open symbols for decreasing power)

The flow regime in the evaporator section was characterized by examining temperatures over a duration of 5 mins collected at the outer wall of the evaporator at quasi steady state period as in [27]. Typical transients for experiments where the power was incremented and decremented for the cooling water temperature of 20°C are presented in Figure 4.5. The results show no noticeable temperature fluctuations for heat transfer rate of 425 W ($q_e$of 6.5 W/cm^2) when the power was incremented and only intermittent fluctuations when the power was decremented. The results for powers of 350W ($q_e$of 5.3 W/cm^2) and below were steady when the power was decremented, suggesting a small hysteresis in the boiling. This was typical for all cooling water temperatures. The steady temperatures at low powers suggest a natural convection mode in the evaporator. The temperature traces for power of 500W (q_e of 7.6 W/cm^2) show nearly periodic fluctuations in the

temperature near the bottom of the thermosyphon in the pool region. The temperature measured at the adiabatic section (or saturation temperature) had fluctuations that are out of phase with the temperature at the bottom of the pool so that the difference between the pool temperature and the saturation temperature are varying, suggesting a varying heat transfer coefficient. The temperatures located in the upper film region (95mm and 125mm) appear to be in phase with the saturation temperature. The temperature traces for a power of 750W (q_e of 11.5 W/cm^2) have more irregular and greater amplitude fluctuations everywhere but at 35mm near the nominal top of the pool. The results also suggest changes in mode, such as near 31.5 minutes, where fluctuations in the temperature traces largely cease. The onset of this mode is associated with a rapid decrease in the temperature at the bottom of the evaporator and a rapid increase in the temperatures in the upper or film region resulting in more uniformity along the evaporator. The steady temperatures persist for approximately 5 minutes followed by a sudden change back to the original mode. The results for the experiments where the power is decremented show similar patterns in fluctuations for powers greater than 500W.

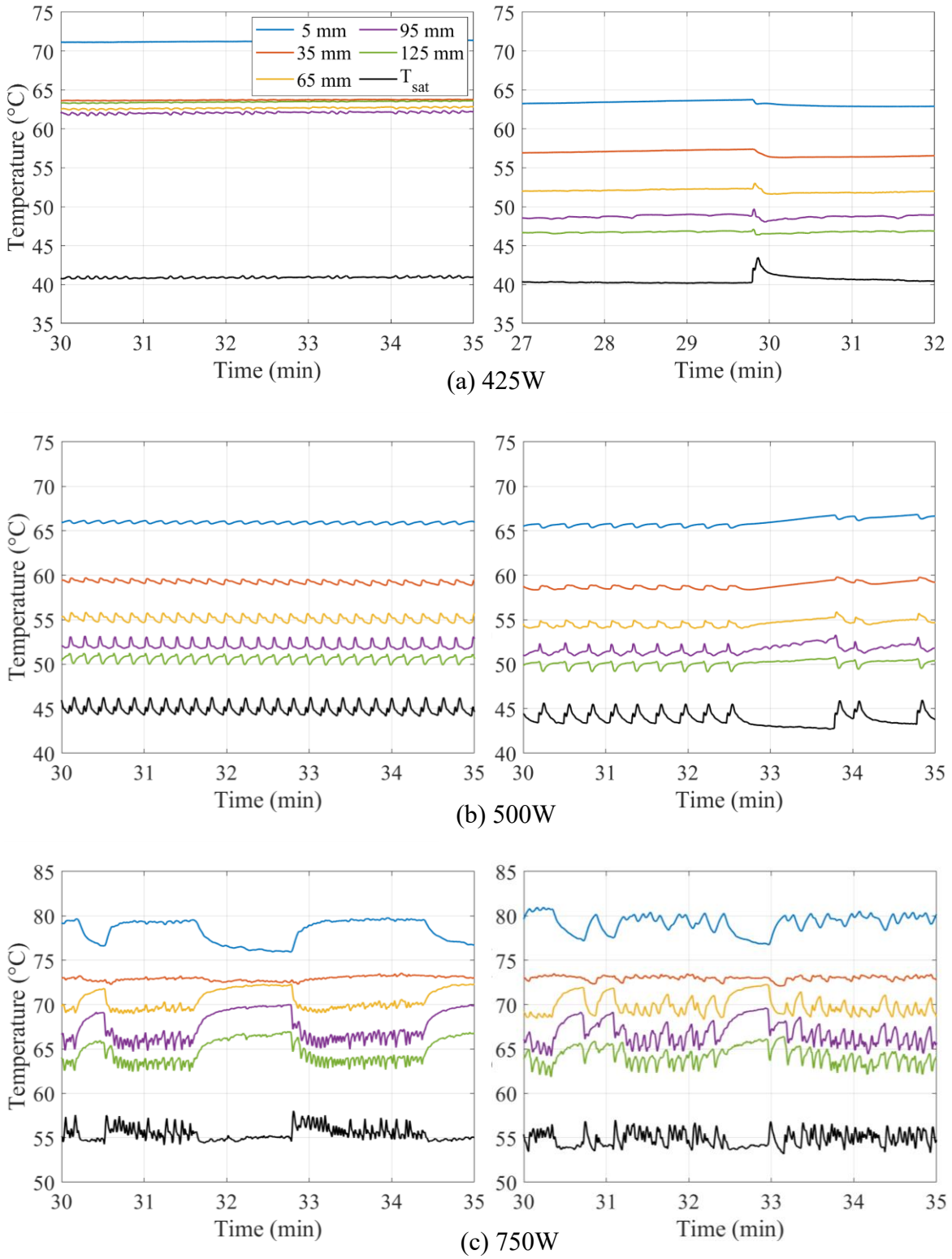

Figure 4.5. Transients of the evaporator surface and adiabatic temperatures at heat input of (a) 425W, (b) 500W and (c) 750W during the experiments with increasing (left) and decreasing (right) power and cooling water temperature of 20°C.

The flow regimes determined from the temperature traces are plotted on the flow map based on the superficial momentum fluxes G^2/ρ proposed in Smith et al. [19] in Figure 4.6 with typical flow regimes similarly deduced in Hammouda et al.[27]. The values of G^2/ρ_v and G^2/ρ_l are based on the total heat transfer rate into the evaporator. The results where the temperature traces had little to no fluctuations (425W in Figure 4.5 (a)*)* are labeled as natural convection; the periodic fluctuations (500W in Figure 4.5 (b)) as bubble/slug, and the more irregular patterns with occurrences of more uniform evaporator temperature (750W in Figure 4.5 (c)) as slug/churn. The results show majority of the cases identified as pool natural convection or bubbly fall within the geyser flow region defined by Smith et al[19]. The confinement number here was typically 0.178 to 0.184, below the value of 0.2 suggested for confined thermosyphons in Smith et al.[18]. The results at the highest heat transfer rates fall near the slug/churn boundary consistent with the observations of the temperature fluctuations. Thus, this aspect of the map appears to predict the flow regime for the elbow-type thermosyphon. The flow regime transitions are different from those in [27] for a longer evaporator suggesting that the length to diameter ratio may play a role in the flow regime as suggested by Terdtoon et al.[14]. The results here did not fall within the range of the bubble or churn flow in the maps proposed in Terdtoon et al. [14] nor were they well predicted by the Confinement number vapor production map in Smith et al. [18] similar to the results in [27].

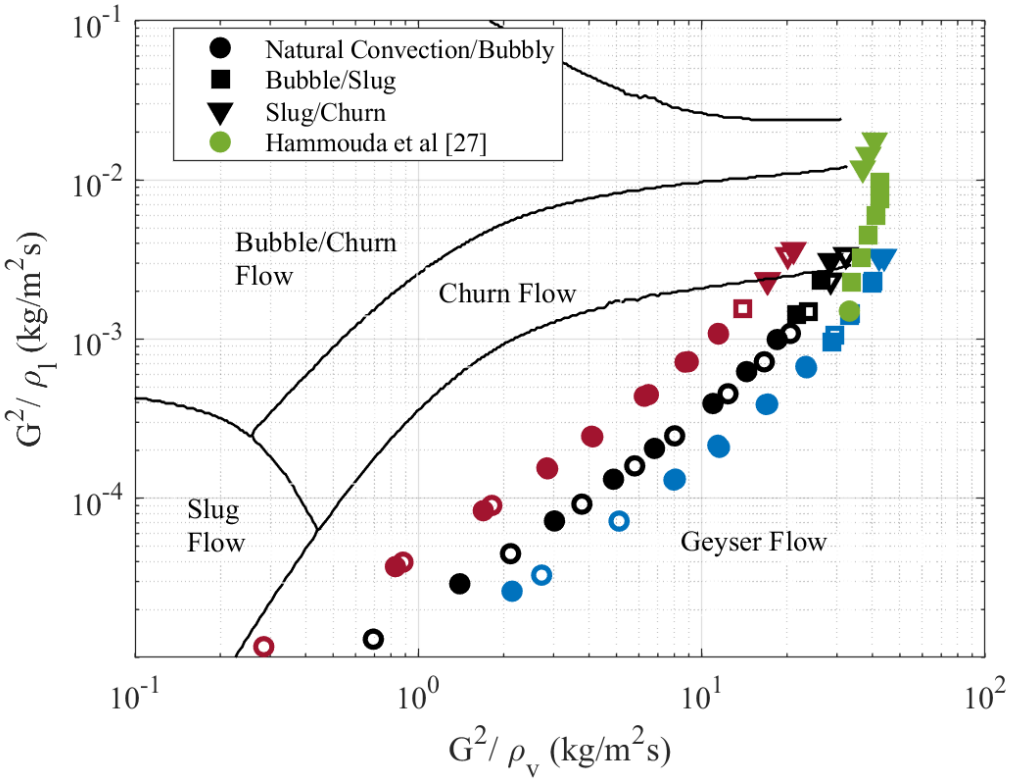

Figure 4.6. Flow regime map for the elbow thermosyphon with cooling water temperature of [BLUE] 10°C, [BLACK] 20°C and [MAROON] 35°C and [GREEN] data from Hammouda et al. [27] at 20°C cooling water temperature with flow regimes and boundaries proposed in Smith et al [19] (filled symbols for increasing power and open symbols for decreasing power).

The change in the Kutateladze number, which is typically used to predict flooding and entrainment limits or boiling limits in thermosyphons, is plotted against the saturation temperature in Figure 4.7 along with typical correlations for the critical value given in Table 4.2. The Kutateladze number given by

$$\boldsymbol{Ku} = \frac{\boldsymbol{q_e}}{\boldsymbol{h_{fg}\rho_v^{1/2}[\sigma g(\rho_l-\rho_v)]^{1/4}}} \tag{3}$$

has been multiplied by the length to diameter ratio so that it reflects the flux based on the cross-sectional area. The experimental results with increasing and decreasing power overlapped for all three cooling water temperatures, not showing any evidence of a hysteresis. The Kutateladze number

increased with the saturation temperature in all cases suggesting that a flooding and entrainment or boiling limit has not yet been reached. The results for the cooling water temperature of 10°C exceeded the limit predicted by Tein and Chung [35] but was below the correlations from Faghri et al [36] for water and Imura et al. [37] that are given in Table 4.2. The experimental results appear to be approaching a plateau, similar to the results in Kim et al. [25]. The results here did not appear to show inflections in the change in Kutateladze number with the saturation temperature observed in[27].

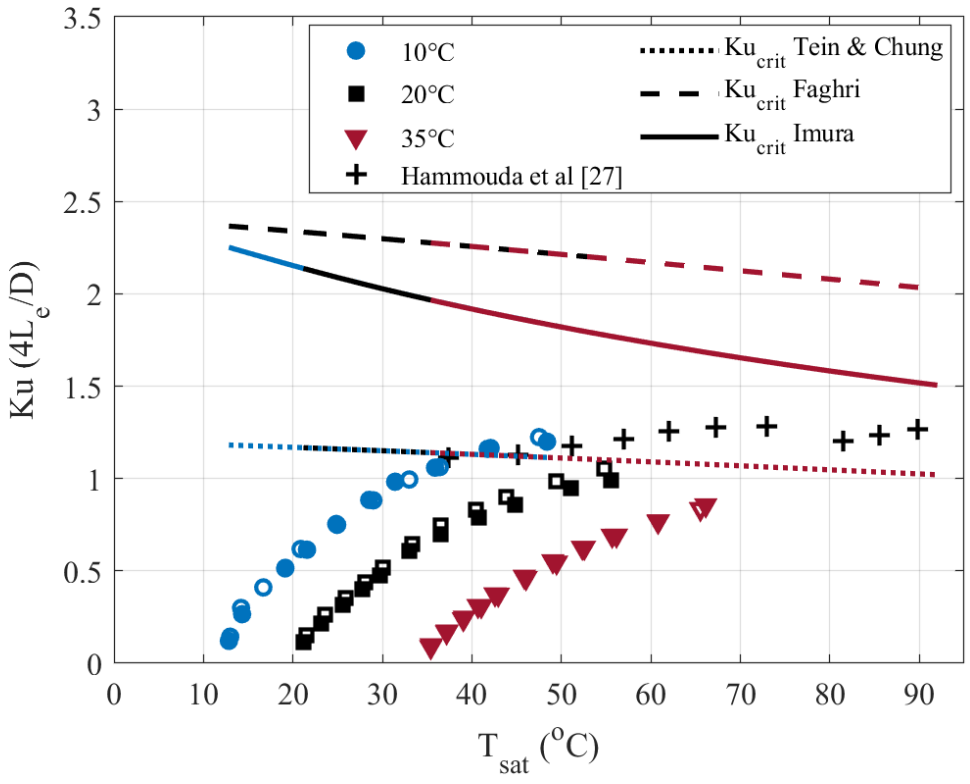

Figure 4.7. Variation of Kutateladze number with saturation temperature for three cooling water temperatures (filled symbols for increasing power and open symbols for decreasing power)

The performance of the evaporator in the pool and film regions was characterized using boiling curves that compare the change in nominal heat flux with the average superheat in each region as shown in Figure 4.8. The results for the pool region were based on the temperature

difference at the lowest point, while the results for the film region were based on the average of the temperature differences from 65 to 125mm from the bottom of the thermosyphon. The results for the pool region in Figure 4.8 (a) are compared to the predictions for boiling and natural convection correlations summarized in Table 4.1 and Table 4.3, respectively. The wall superheat in the pool region was approximately proportional to the nominal heat flux up to 4 to 6 W/cm^2, consistent with the steady temperature traces for this range of heat flux. The wall superheat then decreased with a further increase in heat flux similar to the results in Hammouda et al. [27] and typical of boiling of water at low pressures[28] . There was some evidence of the effect of the delay in the onset of boiling for the lower cooling water temperatures consistent with the observations from the temperature transients, but much of the overshoot in the superheat was observed both when the power was increased and decreased. Thus, the decrease in superheat appears associated with the intermittent or slug boiling regime[28][29]. The experimental superheats fell well above the natural convection correlation proposed in El Genk and Saber [7] at all but the lowest heat fluxes and thus this model was not able to predict the overshoot in the wall temperature. The piece-wise model proposed by Shabgard et al. [8] appeared to be able to predict the overshoot/inflection in temperature superheat. This model overpredicts the wall superheat at low heat fluxes, unlike in Hammouda et al. [27], but this may be due in part to wall conduction effects that would make the heat flux in the pool region of the evaporator smaller than the nominal value. The single phase natural convection correlation in [8] results in a larger heat transfer coefficient than the natural convection correlation for open thermosyphons from Imura and Kozai [33]. The wall superheat for the higher nominal heat fluxes were similar to the predictions for geyser boiling from the correlation of Casarosa et al.[30], and was much higher than the superheat observed in [27] that better agreed with the values predicted by the El Genk and Saber [7] nucleate boiling correlation.

The change in the superheat for the upper or film region (Figure 4.8 (b)) shows evidence of two different behaviors; one that is consistent with film evaporation at low heat fluxes and one with substantively better performance at higher heat fluxes. The results at lower heat fluxes show a significant hysteresis that was responsible for much of the hysteresis in the overall performance in Figure 4.4, unlike previous results where the hysteresis in the overall evaporator performance is typically attributed to the delay in the onset of boiling in the pool region[23][24]. The average wall superheat in the film region was larger than that for the film evaporation model [10] given in Table 4.4 for heat fluxes up to approximately 4 W/cm^2 particularly for the 10°C cooling water temperature when the heat transfer was increased. The difference was more modest for cooling water temperatures of 20°C and 35°C when the heat transfer rate was decreased, but the results were well below the results for a similar grooved thermosyphon with a slight bend between the evaporator and condenser in Hammouda et al. [27] (measured with an increasing heat transfer rate) suggesting that the presence of the elbow bend had a significant affect on the performance of the evaporator even in those cases. The difference for the cooling water temperature of 20°C was large when the heat transfer was increased causing the hysteresis at this cooling temperature. The wall superheat was smaller than predicted by the film evaporation model at high heat transfer rates. The transition between 4-6 W/cm^2 was below the criteria for the transition to laminar wavy region in Chun and Seban [34] and appeared instead to correspond with the transition to the slug flow regime. The wall superheat was initially approximately constant approaching the results in [28] before increasing and approaching the correlation of Shiraishi et al [11], suggesting a boiling or dynamic regime in the film region as in[27].

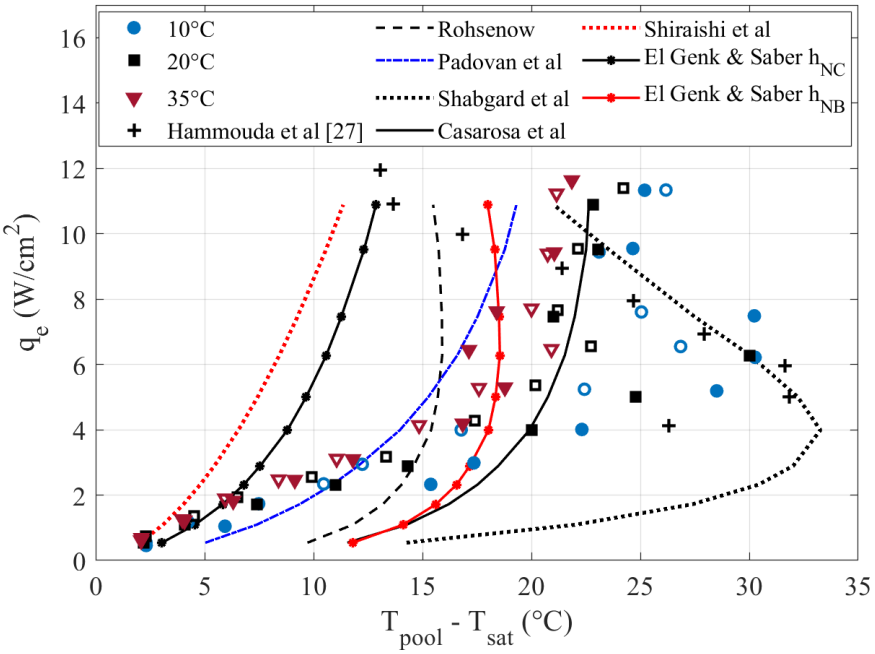

(a)

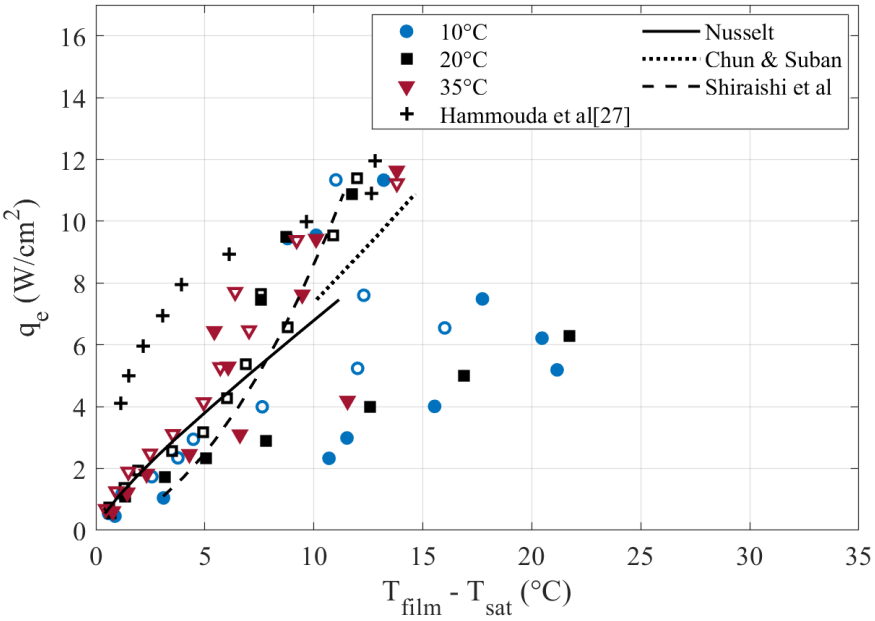

(b)

Figure 4.8. Comparison of the nominal performance in the (a) pool and (b) film regions with typical correlations.

The performance of the condenser was characterized using the heat transfer coefficient based on the cooling water jacket length and are shown in Figure 4.9. The results are presented in terms of the film Nusselt number ($\boldsymbol{h_c\left(\nu_l^2/g\right)^{1/3}/k_l}$) and the nominal film Reynolds number ($\boldsymbol{\Gamma/\mu}$). The results are compared with predictions from correlations for condensation in inclined or horizontal tubes in Table 4.5. The results for the lower cooling water temperature were in good agreement with the results for the correlations for the horizontal condenser and the correlation with the angle correction from Gross[32]. The results for the higher cooling water temperatures were below this result with one case for the moderate cooling water temperature agreeing with each of these results. The angle correction models of Hussein et al. [38]and Wang and Ma [39] (without the pressure correction) fall between the lower and higher cooling water temperatures. A re-examination of the raw experimental data showed that the lower performance cases were performed with the cooling water and falling film in co-flowing mode, while the high performance results were performed with the cooling water flow and the condensing film in a counterflow mode affecting the condensation of the film. There may be a pressure or subcooling correction needed in this case but not to the extent observed for the near vertical condenser in [27].

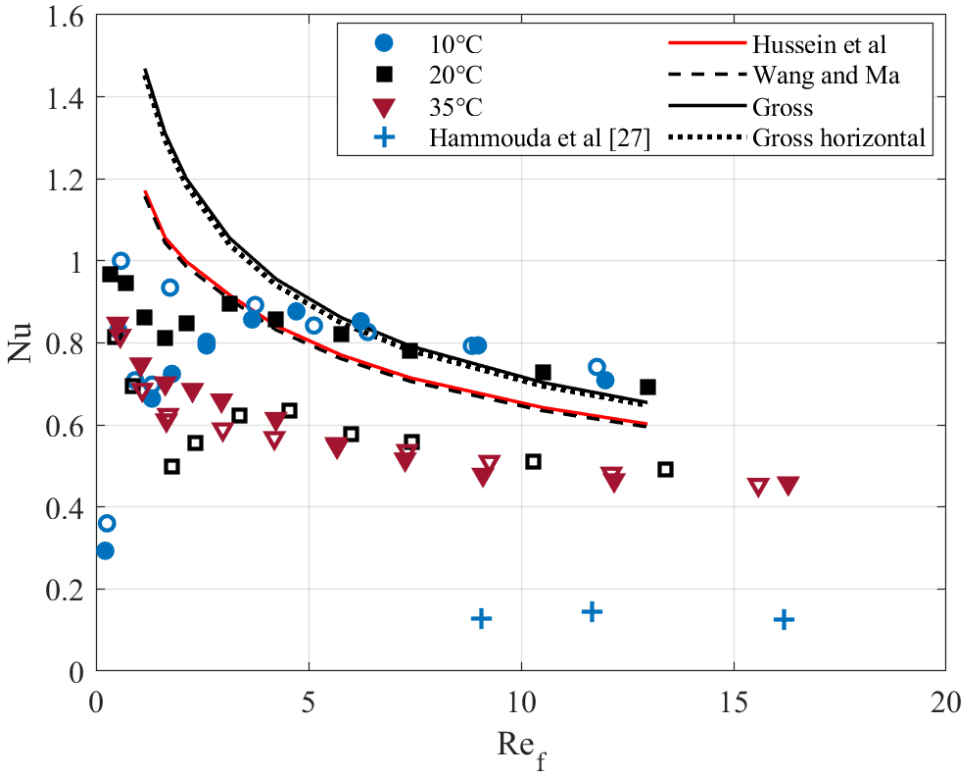

Figure 4.9. Comparison of the experimental condenser performance with predictive models (filled symbols for increasing power and open symbols for decreasing power).

4.7 Summary and Conclusions

Measurements were performed to characterize the performance of a grooved copper-water elbow thermosyphon, where the evaporator was vertical, and the condenser was 8 degrees from the horizontal. The experiments were performed for heat inputs of 40W to 750W, corresponding to heat flux rates of 0.6 W/cm^2 to 11.5 W/cm^2, for a fill ratio of 30%. The temperature profiles along the evaporator and transients of the temperatures show evidence of flow regime changes with a natural convection and perhaps pool boiling at the lower heat fluxes, slug flow at moderate heat fluxes, and slug churn flow at the highest heat fluxes. The transition to the latter was in agreement with the flow map of Smith et al[18]. The other two regimes fell in the geyser flow

regime that was not observed in the experimental results. The results showed evidence of a modest hysteresis in the onset of the more dynamic flow modes that affected the heat transfer in the pool region. A much larger hysteresis was found in the performance of the upper film region of the evaporator, with much better performance after the initiation of the churn type flow that appears to be due to better wetting of the evaporator wall area.

The local heat transfer performance of the evaporator was characterized for both the pool and film regions. In the pool region, the overshoot in the wall temperature could be predicted by the piece-wise single- and two-phase convection model proposed by Shabgard et al. [8]. This overpredicted the wall superheat at low heat fluxes but this may be due to wall conduction reducing the heat flux into the pool region. At higher heat fluxes, the results followed similar trends to the correlation by Casarosa et al[30]. In the film region, a Nusselt [10] model overpredicted the heat transfer performance at low to mid heat flux when the heat transfer rate was increased. There was better agreement when the heat transfer rate was decreased for the higher operating temperature after churn flow was established. The results were in better agreement with Shiraishi et al. [11] model for the more dynamic flow regimes. The condenser performance was in agreement with the correlation proposed by Gross [32] when the cooling water in the water jacket was counter flow to the thermosyphon, while performance was lower for a co-flowing cooling water.

Table 4.1

Nucleate pool boiling heat transfer correlations

Rohsenow [4]	$h_{e=}\frac{{q_e}^{2/3}}{\frac{C_{s,f}h_{fg}}{C_{pl}}\left(\frac{L_b}{h_{fg}\mu_l}\right)^{0.33}Pr_l^1}$ for water and $C_{s,f}=0.013$
Imura et al[5]	$h_e = 0.32\left(\frac{{p_l}^{0.65}{k_l}^{0.3}{C_{pl}}^{0.7}g^{0.2}}{{p_v}^{0.25}{h_{fg}}^{0.4}{\mu_l}^{0.1}}\right)\left(\frac{P_v}{P_{atm}}\right)^{0.3}{q_e}^{0.4}$
Padovan et al. [6]	$h_e = 231p_r^{023}M^{-0.93}(Bo^2)^{0.14}{q_e}^{0.41}$
El Genk and Saber [7]	$h_{NB} = (1.0 + 4.95\gamma)h_{ku}$
	$h_{ku} = 6.95x10^{-4}\left(\frac{k_l}{l_m}\right)Pr_l^{0.35}\left(\frac{q_e l_m}{\rho_v h_{fg} v_l}\right)^{0.7}\left(\frac{Pl_m}{\sigma}\right)^{0.7}$
	$\gamma = \left({\rho_v}/{\rho_l}\right)^{0.4}\left[\left(\frac{pv_l}{\sigma}\right)\left(\frac{\rho_l^2}{\sigma g(\rho_l-\rho_v)}\right)^{0.25}\right]^{0.25}$
Shiriashi et al [11]	$h = 0.32\left(\frac{{p_l}^{0.65}{k_l}^{0.3}{C_{pl}}^{0.7}g^{0.2}}{{p_v}^{0.25}{h_{fg}}^{0.4}{\mu_l}^{0.1}}\right)\left(\frac{P_v}{P_{atm}}\right)^{0.23}q^{0.4}$
Casarosa et al. [30]	$h_e = 2.925{P_v}^{0.18}q_e^{2/3}$

Table 4.2

Flooding/Entrainment Limit

Tien and Chung [35]	$Ku = \frac{3.2tanh^2\left(0.5Bo^{1/4}\right)}{4\left({L_e}/{D}\right)\left[1+(\rho_v-\rho_l)^{1/4}\right]^2}$
Faghri et al. [36]	$Ku = \frac{3.2tanh^2\left(Bo^{1/4}\right)}{4\left({L_e}/{D}\right)\left[1+(\rho_v-\rho_l)^{1/4}\right]^2}$
Imura et al. [37]	$Ku = 0.16\langle 1 - exp\left[-\frac{\left({\rho_v}/{\rho_l}\right)^{0.13}}{\left({L_e}/{D}\right)}\right]\rangle$

Table 4.3

Natural convection heat transfer correlations

El Genk and Saber [7]	$\left(\frac{hD_i}{k_l}\right)_{NC} = 0.475Ra^{0.35}\left({}^{L_b}/_{D_i}\right)^{0.58}$
Shabgard et al. [8]	$h_p = \left(1-\frac{X}{10^6}\right)^{0.75} h_{sc} + \left(\frac{X}{10^6}\right)^{0.75} h_{TC}$
	$h_{sc} = \begin{cases} 0.75\left(\frac{k_l}{L_p}\right)Ra^{0.2}, & 10^5 < Ra < 10^{13} \\ 0.645\left(\frac{k_l}{L_p}\right)Ra^{0.22}, & 10^{13} < Ra < 10^{16} \end{cases}$
	$h_{TC} = 4\left(\frac{k_l}{D_i}\right)(ArFr^{0.5})^{1/3}Pr_l^{0.5}\left(\frac{Bo}{10}\right)^n$ (Gross [31])
	$n = {}^1/_2 \; for \; Bo \le 10$
	$n = {}^1/_6 \; for \; Bo > 10$
	$X = \Psi(RaPr_l)^{0.35}\left(\frac{P_v L_b^2 q_e^{"}}{\sigma\rho_v h_{fg} v_l}\right)^{0.7}$
	$\Psi = \left(\frac{\rho_v}{\rho_l}\right)^{0.4}\left[\frac{P_v v_l}{\sigma}\left(\frac{\rho_l^2}{\sigma g(\rho_l-\rho_v)}\right)^{0.25}\right]^{0.25}$

Table 4.4

Film boiling heat transfer correlations

Nusselt [10]	$h = \left(\frac{4}{3}\right)^{1/3}\left(\frac{k^3 g}{v^2}\right)^{1/3}\left(\frac{4\Gamma}{\mu}\right)^{-1/3}$
Chun and Seban [34]	$h = 0.606\left(\frac{k^3 g}{v^3}\right)^{1/3}\left(\frac{\Gamma}{\mu}\right)^{-0.22}$
	$when \;\; \left(\frac{4\Gamma}{\mu}\right) > 2.43\left(\frac{\mu^4 g}{\rho\sigma^3}\right)^{-1/11}$

Table 4.5

Condensing falling film heat transfer models

Gross [32] Inclined Condenser	$Nu = \left(\left(f_p Nu_l\right)^2 + (Nu_t)^2\right)^{1/2}$
	$Nu_l = 0.925 Re_\varphi^{-1/3}$
	$Nu_t = 0.044 Pr_l^{2/5} Re_\varphi^{1/6}$
	$f_p = \dfrac{1}{1 - 0.63\left(P/P_{crit}\right)^{3.3}}$
	$Re_\varphi = Ref_\varphi, \quad f_\varphi = 2.87\left(\dfrac{d}{Lsin\varphi}\right)$
	$\varphi = 0\ for\ vetical\ tube$
Horizontal Condenser	$Nu = 0.651\left(L/D\right)^{1/3} Re^{-1/3}$
Hussein et al. [38] with angle correction	$\dfrac{Nu}{Nu_{Nusselt}} = \left(\dfrac{1}{0.943}\right)\left(\dfrac{L_c}{D_i}\right)^{\frac{cos\beta}{4}} (0.997 - 0.334(cos\beta)^{0.108})$
	$\beta = angle\ from\ the\ horizontal$
Wang and Ma [39] with angle correction	$\dfrac{h}{h_{Nusselt}} = \left(\dfrac{L_c}{R_i}\right)^{\frac{cos\beta}{4}} (0.54 + 5.86 \times 10^{-3}\beta)$

Acknowledgements

The support from the Natural Sciences and Engineering Research Council (NSERC) of Canada and the Ontario Centres of Excellence (OCE) is gratefully acknowledged. Funding was also provided by MERSEN Canada Inc.

4.8 References

[1] Faghri A. Heat Pipe Science and Technology. Global Digital Press, 1995.

[2] Jafari D, Franco A, Filippeschi S, Di Marco P. Two-phase closed thermosyphons: A review of studies and solar applications. Renewable and Sustainable Energy Reviews, 2016 (53) 575-593.

[3] Gedik E. Experimental investigation of the thermal performance of a two-phase closed thermosyphon at different operating conditions, Energy and Buildings, 2016 (127) 1096-1107.

[4] Rohsenow WM. A method of correlating heat transfer data for surface boiling of liquids. Cambridge, Mass. MIT Division of Industrial Cooperation, 1951.

[5] Imura H, Kusuda H, Ogata J-I, Miyazaki T, Sakamoto N. Heat transfer in two-phase closed-type thermosyphons, Japan Society of Mechanical Engineers, Transactions, Series B, 45, 1979 (393), 712-722.

[6] Padovan A, Bortolin S, Rossato M, Filippeschi S, Del Col D. Vaporization heat transfer in a small diameter closed two-phase thermosyphon. Journal of Heat Transfer, 2019 141(9).

[7] El-Genk MS, Saber HH. Heat transfer correlations for small, uniformly heated liquid pools. Int. J. Heat and Mass Transfer, 1998 41(2):261-74.

[8] Shabgard H, Xiao B, Faghri A, Gupta R, Weissman W. Thermal characteristics of a closed thermosyphon under various filling conditions. Int. J. Heat and Mass Transfer, 2014 70:91-102.

[9] Guichet V, Almahmoud S, Jouhara H, Nucleate pool boiling heat transfer in wickless heat pipes (two-phase closed thermosyphons): A critical review of correlations, Thermal Science and Engineering Progress, 2019 (13) 100384.

[10] Guichet V, Jouhara H, Condensation, evaporation and boiling of falling films in wickless heat pipes (Two-phase closed thermosyphons): A critical review of correlations, Int. Journal of Thermofluids, 2020 (1-2) 100001.

[11] Shiraishi, M, Kikuchi K, Yamanishi T, Investigation of heat transfer characteristics of a two-phase closed thermosyphon. Journal of Heat Recovery Systems, 1981 vol. 1, no. 4, 287–297.

[12] Jafari D, Di Marco P, Filippeschi S, Franco A. An experimental investigation on the evaporation and condensation heat transfer of two-phase closed thermosyphons. Exptal Thermal and Fluid Science, 2017 (88) 111-23.

[13] Jouhara H, Robinson AJ. Experimental investigation of small diameter two-phase closed thermosyphons charged with water, FC-84, FC-77 and FC-3283. Applied Thermal Engineering, 2010 30(2-3), 201-11.

[14] Terdtoon P, Chailungkar M, Ritthidej S, Shiraishi M. (1997) Effects of Bond numbers on internal flow patterns of an inclined, closed, two-phase thermosyphon at normal operating conditions, Experimental Heat Transfer, 1997, 10:4, 233-251.

[15] Terdtoon P, Chailungkar M, Shiraishi M. Effects of aspect ratios on internal flow patterns of an inclined closed two-phase thermosyphon at normal operating condition, Heat Transfer Engineering, 1998, 19:4, 75-85.

[16] Grooten MH, Van der Geld CW, Van Deurzen LG. A study of flow patterns in a thermosyphon for compact heat exchanger applications. Fifth Int. Conference on Transport Phenomena In Multiphase Systems, 2008 (pp. 1-7).

[17] Jouhara H, Ajji Z, Koudsi Y, Ezzuddin H, Mousa N. Experimental investigation of an inclined-condenser wickless heat pipe charged with water and an ethanol–water azeotropic mixture. Energy, 2013 61:139-47.

[18] Smith K, Kempers R, Robinson AJ. Confinement and vapour production rate influences in closed two-phase reflux thermosyphons Part A: flow regimes. Int. J. Heat and Mass Transfer, 2018;119:907-21.

[19] Smith K, Robinson AJ, Kempers R. Confinement and vapour production rate influences in closed two-phase reflux thermosyphons Part B: Heat transfer. Int. J. Heat and Mass Transfer. 2018, 120:1241-54.

[20] Lock GS, Fu J. Observations on an evaporative, elbow thermosyphon. ASME Journal of Heat Transfer, 1993 115(2) 501-503.

[21] Fu J. The elbow thermosyphon: an experimental investigation of its evaporative behavior. 1993, MASc Thesis, University of Alberta, Canada

[22] Smith K, Siedel S, Robinson AJ, Kempers R, The effect of bend angle and fill ratio on the performance of a naturally aspirated thermosyphon, Applied Thermal Engineering, 2016 (101) 455-467.

[23] Wadowski T, Akbarzadeh A, Johnson P, Hysteresis in thermosyphon-based heat exchangers and introduction of a novel triggering system for low-temperature difference heat-recovery applications, Heat Recovery Systems and CHP, 1991 11(6),523-531.

[24] Li H, Akbarzadeh A, Johnson P, The thermal characteristics of a closed two-phase thermosyphon at low temperature difference, Heat Recovery Systems and CHP, 1991 11(6), 533-540.

[25] Kim Y, Shin DH, Kim JS, You SM, Lee J, Boiling and condensation heat transfer of inclined two-phase closed thermosyphon with various filling ratios, Applied Thermal Engineering, 2018 (145) 328-342.

[26] Park Y-J, Kang HK, Kim CJ, Heat transfer characteristics of a two-phase closed thermosyphon to the fill charge ratio, Int. J. Heat and Mass Transfer, 2002, 45(23), 4655-4661.

[27] Hammouda M, Ewing D, Zaghlol A, Ching CY, Heat transfer performance in a vertical grooved thermosyphon, Int. J. Thermofluids, 2021 (in Press).

[28] McGillis WR, Fitch JS, Hamburgen WR, Carey VP (1992) Boiling Binary Mixtures at Subatmospheric Pressures, Western Research Laboratory Technical Note TN-23, preprint of 10.1109/ITHERM.1992.187750.

[29] Niro A, Beretta GP, Boiling regimes in a closed two-phase thermosyphon, Int. J. Heat and Mass Transfer, 1990, 33 (10), 2099-2110.

[30] Casarosa C, Latrofa E, Shelginski A, The geyser effect in a two-phase thermosyphon, Int. J. Heat and Mass Transfer, 1983, 26 (6), 933-941

[31] Gross U. Pool boiling heat transfer inside a two-phase thermosyphon correlation of experimental data. InInternational Heat Transfer Conference Digital Library 1990. Begel House Inc.

[32] Gross U. Reflux condensation heat transfer inside a closed thermosyphon, Int. J Heat and Mass Transfer, 1992 35(2):279-94.

[33] H. Imura and H. Kozai, Experimental investigation of natural convection heat transfer in an open thermosyphon, Bulletin of JSME, 29(250), 1188-1194

[34] Chun KR, Seban RA, Heat transfer to evaporating liquid films, ASME Journal Heat Transfer, 1971 391-396.

[35] Tien CL, Chung KS. Entrainment limits in heat pipes. AIAA Journal, 1979, 17(6) 643-6.

[36] Faghri A, Chen MM, Morgan M. Heat transfer characteristics in two-phase closed conventional and concentric annular thermosyphons, 1989, 111(3) 611-618

[37] Imura H, Sasaguchi K, Kozai H, Numata S. Critical heat flux in a closed two-phase thermosyphon. Int. J. Heat and Mass Transfer, 1983 26(8):1181-1188.

[38] Hussein HM, Mohamad MA, El-Asfouri AS. Theoretical analysis of laminar-film condensation heat transfer inside inclined wickless heat pipes flat-plate solar collector. Renewable Energy. 2001 Jul 1;23(3-4):525-35.

[39] Wang JC, Ma Y. Condensation heat transfer inside vertical and inclined thermosyphons. Journal of Heat Transfer, ASME Journal of Heat Transfer, 1991 113(3) 777-780.

Chapter 5: Conclusion and Recommendations

Experiments were performed to characterize the thermal performance of two different shaped copper-water thermosyphons typically used in thermal management of power electronics applications. The first thermosyphon had a 310 mm long vertical evaporator and 385 mm long condenser, with the condenser inclined at 5 degrees to the vertical. The second thermosyphon had a shorter evaporator with a length of 140 mm and a 190 mm long condenser bent at an angle of 8 degrees from the horizontal. The nominal diameter of both thermosyphons was 14.87 mm and the internal surface was rifle grooved with a nominal height of 0.3 mm. The fill ratios of the two thermosyphons were 35 and 30 percent, respectively. Tests were performed for power inputs from 500W (4 W/cm^2) to 1625 W (13 W/cm^2) for the first thermosyphon and 40W (0.5 W/cm^2) to 750W (11 W/cm^2) for the second thermosyphon. To compare the effects of varying ambient temperatures, both thermosyphons were tested with cooling water flowing at 10°C, 20°C, and 35°C with a flow rate of 1.1L/min. Temperature measurements taken along the evaporator and condenser were used to characterize the evaporator and condenser performance. The unsteady operation of the thermosyphons was characterized from the transients in the temperature along the thermosyphons. The two - phase flow patterns in the evaporator were inferred from these transient temperature measurements and compared to existing flow maps. For the elbow thermosyphon, measurements were made while the power was incremented as well as when the power was decremented to study any hysteresis effects.

For the slight bend thermosyphon, the average temperature varied significantly along the evaporator at moderate heat fluxes of 4 to 5 W/cm^2 indicating the presence of a pool and film region. The temperature variation was in the range 5 to 35°C from the bottom of the evaporator to the top at a condenser cooling water temperature of 20°C. The temperature profile became more uniform as the heat flux and condenser cooling water temperature was increased. The flow patterns within the evaporator, inferred from the transients in the temperature along the evaporator, show evidence of bubbly, slug, and churn flow. The internal flow patterns were plotted on the flow regime maps proposed by Smith et al. [1][2]. The map based on the confinement and vapour production values of [1] did not capture the transition locations witnessed in the current study and suggesting all heat fluxes were in the churn flow regime when evidence of bubbly flow and slug was found. The flow regime map based on superficial momentum flux also did not agree with the current results from the temperature transients but seem to capture the transition locations and follow a similar trend. The average evaporator heat transfer coefficient initially increased with heat flux and then approached a plateau at 7 W/cm^2 followed by an increase with heat flux after 10 W/cm^2. The pool and film regions in the evaporator were later studied by considering the heat transfer performance of the two regions separately. The heat transfer in the pool region increased linearly with heat flux. Operation with the 35°C cooling water displayed the higher heat transfer performance throughout the heat flux range. The heat transfer performance in the film region with the 10°C displayed a sudden increase in heat transfer from 2 W/cm^2 reaching a maximum at 5 W/cm^2. This was followed by a sudden decrease in heat transfer before seeing a slow linear increase at 10.3 W/cm^2. The condenser heat transfer showed a steady performance with little change with heat transfer. A modified Rohsenow correlation [2] for the condenser heat transfer was proposed (Equation 3 from Chapter 3) that agreed to within 90 percent of the data. The

flooding or boiling limits were investigated by examining the change in the Kutateladze number and comparing it to correlations in the literature. The experimental results were approaching the critical value proposed by Imura et al. [3] but the thermosyphon performance was not limited by the flooding or boiling limit.

The measurements in the elbow thermosyphon also showed a change in the flow patterns in the evaporator, with natural convection at the low heat fluxes transitioning to pool boiling and slug flow at moderate heat fluxes and slug churn flow at the higher heat fluxes. The transition from slug flow to churn flow was in agreement with the flow regime map of Smith et al. [2]; however, the other two regimes were in the regime identified as geyser flow which was not observed in the current experimental results. There was a hysteresis in the performance of the thermosyphon, much of which can be attributed to the performance of the upper film region of the evaporator with a much smaller effect in the pool region. The evaporator heat transfer coefficient initially decreased with heat flux and then increased with a further increase in the heat flux typical of a film evaporation mode and boiling in the film and pool. The evaporator performance at low heat fluxes was greater than that in the thermosyphon with the slight bend. The performance of the pool and film regions was characterized by comparing the nominal heat flux with the average superheat in each region. The condenser heat transfer performance was characterized using the Nusselt number and compared to condensation heat transfer correlations that included an angle correction. The experimental results with cooling water running in counter-flow over the condenser followed the correlations suggested by Gross [5] for both the horizontal condenser and the correlation with an angle correction.

5.1 Recommendations for future studies

Based on the present study, the following are recommended for future studies:

1. The flow regimes in the current study are inferred from the transients in the temperature measurements. A visualization section to visually confirm the flow regimes and boiling dynamics will be useful to better understand the heat transfer mechanisms.
2. Complete testing with internal instrumentation for measuring the saturation temperature.
3. Investigate the effects of varying fill ratios with varying geometries.
4. Investigate the effects varying condenser angle, while keeping the lengths of the evaporator and condenser constant.
5. Characterize the performance with different working fluids, and the use of nanofluids.
6. Examine the effect of using a screen mesh within the evaporator section.
7. Develop methods to mitigate the instabilities and extend the stable operating range of the thermosyphons considered.
8. Investigate the effects of lower operating temperatures (below 10°C) on the performance and stability of both elbow thermosyphon and slight bend thermosyphon.

5.2 References

[1] Smith K, Kempers R, Robinson AJ. Confinement and vapour production rate influences in closed two-phase reflux thermosyphons Part A: flow regimes. Int. J. Heat and Mass Transfer, 2018;119:907-21.

[2] Smith K, Robinson AJ, Kempers R. Confinement and vapour production rate influences in closed two-phase reflux thermosyphons Part B: Heat transfer. International Journal of Heat and Mass Transfer. 2018 May 1;120:1241-54.

[3] Guichet V., Hussam J. Condensation, evaporation and boiling of falling films in wickless heat pipes (two-phase closed thermosyphons): A critical review of correlations, International Journal of Thermofluids, 2020, 1–2, 100001.

[4] Imura H, Sasaguchi K, Kozai H, Numata S. Critical heat flux in a closed two-phase thermosyphon. Int. J. Heat and Mass Transfer, 1983 26(8):1181-1188.

[5] Gross U. Reflux condensation heat transfer inside a closed thermosyphon, Int. J Heat and Mass Transfer, 1992 35(2):279-94.